# The physics of fast $Z$ pinches

D. D. Ryutov

*Lawrence Livermore National Laboratory, Livermore, California 94551*

M. S. Derzon

*Sandia National Laboratories, Albuquerque, New Mexico, 87185*

M. K. Matzen

*Sandia National Laboratories, Albuquerque, New Mexico, 87185*
*(Received 27 May 1999)*

The spectacular progress made during the last few years in reaching high energy densities in fast implosions of annular current sheaths (fast $Z$ pinches) opens new possibilities for a broad spectrum of experiments, from x-ray generation to controlled thermonuclear fusion and astrophysics. At present $Z$ pinches are the most intense laboratory x-ray sources (1.8 MJ in 5 ns from a volume 2 mm in diameter and 2 cm tall). Powers in excess of 200 TW have been obtained. This warrants summarizing the present knowledge of physics that governs the behavior of radiating, current-carrying plasma in fast $Z$ pinches. This survey covers essentially all aspects of the physics of fast $Z$ pinches: initiation, instabilities of the early stage, magnetic Rayleigh-Taylor instability in the implosion phase, formation of a transient quasiequilibrium near the stagnation point, and rebound. Considerable attention is paid to the analysis of hydrodynamic instabilities governing the implosion symmetry. Possible ways of mitigating these instabilities are discussed. Nonmagnetohydrodynamic effects (anomalous resistivity, generation of particle beams, etc.) are summarized. Various applications of fast $Z$ pinches are briefly described. Scaling laws governing development of more powerful $Z$ pinches are presented.

## CONTENTS

$\omega_{\text{LH}}$     lower-hybrid frequency
$\omega_{pe,i}$     electron (ion) plasma frequency

## I. INTRODUCTION

### A. A piece of history

Self-constricted plasma configurations are among the most fascinating objects in plasma physics, both because of their natural occurrence in a number of situations, including geophysics (lightning) and astrophysics (current channels at galactic scales), and because of their importance for a variety of applications. The first systematic attempts to analyze these configurations began in 1934, with the publication of a paper by W. H. Bennett (1934) on the equilibrium of streams of charged particles with a finite temperature. L. Tonks (1937) introduced the term "pinch" to describe these configurations.[1] Later, in the 1950s, the prefix "$Z$" was added to distinguish self-constriction by the axial ($z$) current from compression of a plasma column by an inductively driven azimuthal ($\theta$) current. Only the former configuration, the $Z$ pinch, will be considered in our paper. We note in passing that the other configuration is called a $\theta$ pinch.

A broad attack on the study of $Z$ pinches began in the early 1950s in conjunction with research on controlled thermonuclear fusion. The idea was to heat a deuterium-tritium (DT) mixture by an adiabatic and/or shock compression in a $Z$ pinch and then sustain this system in the equilibrium state until a sufficient amount of fusion energy was released. This early stage of pinch research is covered in a book by Bishop (1958). It was soon discovered, however, that the equilibrium pinch suffered from a large number of magnetohydrodynamic instabilities, including sausage and kink instabilities. Current disruptions caused by the development of these instabilities gave rise to voltage surges and the generation of accelerated deuterons that, in turn, produced bursts of neutron radiation. Realization that the neutrons were not of a "noble" thermal origin but were rather a side effect of a disastrous instability led to widespread pessimism regarding the chances for $Z$ pinches to produce fusion-relevant plasmas. As a result, $Z$ pinches virtually disappeared from the research programs of large fusion laboratories.

As a legacy of these years, there remain extensive theoretical analyses of the stability of pinch equilibria, summarized in particular in the survey by Kadomtsev (1966), and realization of the role of a so-called "Pease-Braginski current" (Pease, 1956; Braginski, 1958; see also a nice compact derivation in Pereira, 1990), a cur-

## BASIC NOTATIONS

Throughout this paper we use predominantly the SI system of units. The temperature is measured in energy units (for instance, we write the equation of state for the ideal gas as $p = nT$, with $T$ measured in Joules, and not $p = nkT$, with $k$ being the Boltzmann constant and $T$ measured in Kelvin). In the "practical" formulas we use a mixed system of units (for instance, the temperature is measured in electron volts).

| | |
|---|---|
| $\mathbf{B}$ | magnetic-field induction |
| $C$ | radial convergence |
| $\mathbf{E}$ | electric field |
| $D_m$ | magnetic diffusivity |
| $I$ | pinch current |
| $I_w$ | current in an individual wire |
| $I_Z$ | ionization energy of an ion in a charge state $Z$ |
| $L$ | anode-cathode distance |
| $T$ | temperature |
| $Z$ | the charge of a fully stripped ion |
| $Z_{\text{eff}}$ | average charge of the ions in a plasma |
| $a$ | Alfvén velocity |
| $c$ | speed of light |
| $\mathbf{g}$ | effective gravity acceleration |
| $h$ | characteristic thickness of the imploding shell |
| $\mathbf{k}$ | wave vector |
| $m$ | azimuthal mode number |
| $\hat{m}$ | mass per unit length of the pinch |
| $\hat{m}_w$ | mass per unit length of an individual wire |
| $n$ | particle number density |
| $p$ | pressure |
| $r_0$ | initial pinch radius |
| $r_{\text{min}}$ | pinch radius at a maximum compression |
| $s$ | sound speed |
| $t$ | time |
| $v_{Te}$ | electron thermal velocity |
| $v_{Ti}$ | ion thermal velocity |
| $\Gamma$ | growth rate |
| $\Lambda$ | the Coulomb logarithm |
| $\Pi$ | dimensionless pinch parameter |
| $\alpha$ | angle between the wave vector and the magnetic field |
| $\beta$ | ratio of the plasma pressure and the magnetic-field pressure |
| $\gamma$ | specific-heat ratio |
| $\varepsilon$ | electric permittivity of the vacuum |
| $\eta$ | electrical resistivity |
| $\lambda$ | wavelength of the perturbation, $\lambda = 2\pi/k$. |
| $\lambdabar$ | characteristic length scale of the perturbation, $\lambdabar = 1/k$. |
| $\mu$ | permeability of a vacuum |
| $\nu$ | kinematic viscosity |
| $\rho$ | mass density |
| $\chi$ | thermal diffusivity |
| $\omega$ | angular frequency |
| $\omega_{Ce,i}$ | electron (ion) gyrofrequency |

---

[1]Note the title of Sec. V of his more detailed paper (Tonks, 1939): "Constriction of Arc under its Own Magnetic Field—Pinch Effect." According to J. A. Phillips (1987), The term "pinch effect" was in fact first used in 1907 by C. Hering, to describe what would now be called "a sausage instabillity" of a liquid-metal conductor in induction furnaces.

TABLE I. Characteristic parameters of a fast $Z$ pinch.

| | |
|---|---|
| Height of the column, $L$ (cm) | 1–2 |
| Initial radius of imploding cylinder, $r_0$ (cm) | 2 |
| Convergence, $C \equiv r_0 / r_{min}$ | 10 |
| Mass per unit length, $\hat{m}$ (mg/cm) | 1–2 |
| Maximum pinch current, $I_{max}$ (MA) | 10 |
| Maximum voltage, $V_{max}$ (MV) | 1 |
| Maximum magnetic field on the pinch surface, $B_{max}$(T) | $10^3$ |
| Implosion time, $t_{imp}$ (ns) | 100 |
| Maximum kinetic energy of the implosion, $W_{max}$ (MJ) | 1 |

rent at which radiative losses can be fully compensated for by Ohmic heating (1.4 MA for hydrogen, independent of the density and the pinch radius). References to the early studies of $Z$ and $\theta$ pinches can be found in Kolb (1960).

## B. What are "fast" $Z$ pinches? (What is the scope of this review?)

Interest in $Z$ pinches revived in the mid 1970s and early 1980s, initiated by the rapid development of pulsed-power technology. Various versions of $Z$ pinches were tried, most notably fiber pinches and imploding gas puffs. For the fiber pinches (see, for example, Haines, 1982; Hammel, 1989), whose diameter ranged typically from tens of micrometers to a couple of hundred micrometers, the time for establishing radial equilibrium (a few nanoseconds) was short compared to the duration of the current pulse. In other words, they were evolving along a sequence of Bennett-type (Bennett, 1934) equilibria, in which the plasma pressure is approximately balanced against the magnetic forces.

By contrast, the annular gas puffs (see, for example, Stallings *et al.*, 1979; Spielman, Hanson, *et al.*, 1985; Smirnov, 1991) had an initial diameter of a few centimeters, and the driving current pulse width was comparable to the implosion time (which is the time between initial current flow through the gas puff and stagnation of the plasma on axis). In this case, a free acceleration of the gaseous shell towards the axis occupies the major part of the total current pulse width. After having reached a certain minimum radius, the plasma bounces back and ceases to exist; a Bennett-type equilibrium has never been reached. The word "fast" used in the title of this survey refers just to this class of pinch discharges and specifies the scope of the survey: our prime focus will be discussion of the properties of those pinches for which a run-in stage is definitive and duration of the whole process is too short to reach a Bennett-type state.

There is a significant difference in the important plasma instabilities for these two systems. Instabilities with an *e*-folding growth time much longer than the time of propagation of an acoustic signal over the pinch radius are important when considering quasiequilibrium systems and are, obviously, of much less importance in

the behavior of imploding systems. On the other hand, instabilities caused by the presence of large inertial forces (in particular, Rayleigh-Taylor instabilities, which will be discussed in detail in this paper) are insignificant for quasiequilibrium systems and become of paramount importance for fast $Z$ pinches. A nice discussion of various physics issues related to the implosion of thin shells can be found in Turchi and Baker (1973), perhaps the first paper specifically devoted to fast $Z$ pinches.

Despite a short lifetime (of order 10 ns in some cases), the plasma assembled by a fast-$Z$-pinch implosion provides unique possibilities for experimentation in a number of areas of physics. The growing interest in this area of research is reflected in particular by the fact that, at a recent conference on high-density $Z$ pinches (Pereira, Davis, and Pulsifer, 1997, Eds., AIP Conference Proceedings No. 409), more than half of the papers were directly related to fast (in the aforementioned sense) $Z$ pinches. The quasiequilibrium self-constricted plasma configurations, of the type of fiber pinches, have their own merits and probably deserve a separate survey. We feel that it would be difficult to cover both subjects in one paper, partly because of the differences in the dominant physical processes and partly just because of the space limitations.

As has already been mentioned, the recent progress in fast $Z$ pinches has been attained, to a great extent, because of major breakthroughs in pulsed-power technology. Pulsed-power technology will not be discussed in this survey in any detail. A very brief summary of the pertinent information will be presented in Sec. I.D. This review will concentrate on the physics issues of fast $Z$ pinches. We shall discuss in some detail simple models of various effects important for pinch performance, so that this survey could be used as a first introduction to the subject. On the other hand, we shall also consider more subtle and complicated issues, which could be skipped during a first reading of this paper.

The physics of fast $Z$ pinches is an active area of research. Many elements of this complex phenomenon are still not well understood and are the source of scientific disputes. Sometimes, the lack of experimental data and/or of a clear theoretical picture does not allow the discussion to rise above a qualitative, semispeculative level. Still, even on such occasions, the authors take the
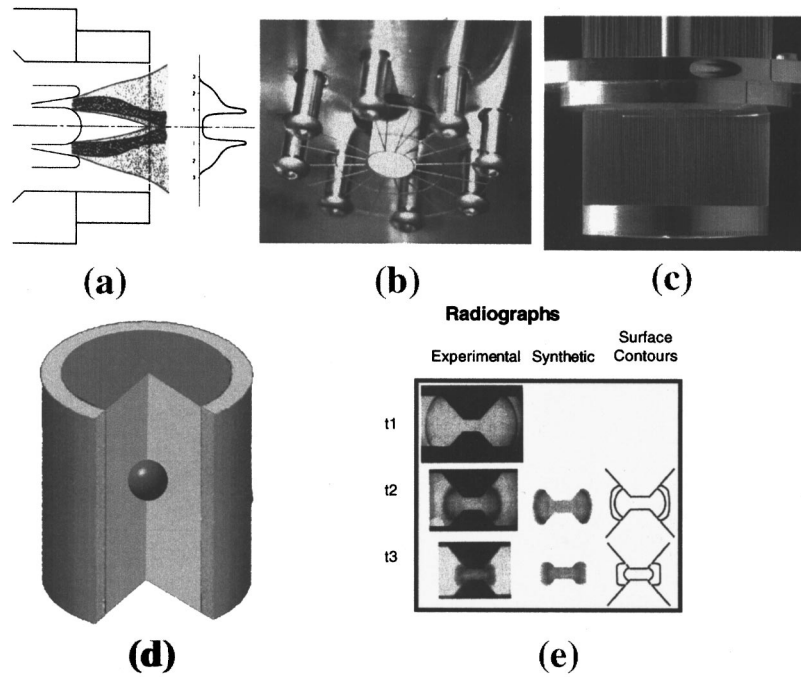
FIG. 1. Various types of fast $Z$ pinches: (a) An annular gaseous jet (reprinted with kind permission of C. Stallings); the axis of the diode is horizontal, the nozzle is a cathode, and the mesh is an anode; the plot at the right shows the radial density distribution. (b) A cylinder made of agar foam in a $Z$-pinch diode. The anode in this experiment was a transparent wire mesh; the cylinder (1-cm diameter) is surrounded by eight return-current posts. (c) a photograph of a 4-cm-diameter tungsten wire array used in the $Z$ facility. The array had 240 wires; the mass per unit length of the array was 2 mg/cm. (d) A high-$Z$ liner imploding on a low-density foam. An internal ICF capsule is situated in the center of the foam cylinder; (e) a quasispherical liner implosion. An aluminum liner slides along conical electrodes. The initial radius of the outer surface is 4 cm; the time sequence is $t_1=0$, $t_2=12.7\,\mu$s, $t_3=14\,\mu$s. The right column represents the results of 2D MHD computations (from Degnan *et al.*, 1995, reprinted with kind permission of J. Degnan).

risk of presenting their thoughts, with the humble hope that a reader will benefit from comparing her or his viewpoint with authors'.

To give some general impression of the parameter domain of present-day fast $Z$-pinch experiments, we provide in Table I some numbers (a much more detailed discussion will be presented later) that relate not to any specific experiment but rather to some "generic" fast $Z$ pinches. In every particular experiment, parameters may vary by a factor of 2–3.

By convergence (the third line in Table I) we mean the ratio of the initial pinch radius to the final pinch radius,

$$C = r_0/r_{\min}. \qquad (1.1)$$

Note that, because of the skin effect, the voltage $V_{\max}$ is not a well-defined quantity (for instance, inside a highly conducting shell there is no axial electric field at all); in Table I we are referring to the integral $V_{\max} = \int E dl$ between the anode and cathode at a distance from the axis equal to the initial pinch radius.

In addition to the most commonly studied parameter domain shown in Table I, there exists another group of experiments, involving implosions of much heavier liners (with $\hat{m} \sim$ a few g/cm), with a characteristic implosion time in the range of microseconds (see the end of Sec. I.C). These pinches fall under our definition of "fast" pinches but will be discussed only very briefly in our survey.

The imploding load is often called a "target," similar to the term used in inertial confinement fusion (ICF) research (see, for example, Lindl, 1995). The other traditionally used term is "the liner," which designates a thin imploding annular shell of whatever nature (gas puff, foil, foam, wire-array plasma, etc.).

We have tried to limit the references to books and papers in scientific journals that would be easily accessible to the reader. However, in some cases we had to cite conference proceedings.

## C. Specific types of fast $Z$ pinches

There exist a variety of initial configurations that are imploded in fast $Z$ pinches. Depending on the application (as will be discussed in more detail in later sections), the initial density profile is chosen to be uniform, annular, or peaked on axis. One initial configuration that we have already mentioned is a supersonic gas jet, with either an annular or a uniformly-filled gas density profile, originating from a nozzle situated at one of the electrodes. The gas jet flows through a fine mesh that serves as the opposite electrode, or there may be simply a hole that receives the jet [Fig. 1(a)]. More complex multishell gaseous jets are also possible.

To create an initial density profile that is more uniform axially between the electrodes, thin annular shells made of metal and plastic foils have also been used for

the initial load configuration. Another way of creating the initial configuration is by machining a cylinder from a low-density foam [Fig. 1(b), Derzon *et al.* (1997a)]. Development of aerogel technology allowed experimentalists to produce solid cylinders with average mass density as low as $\sim 1$ mg/cm$^3$ (3 mg/cm$^3$ have actually been used in experiments) and having very small deviations from cylindrical symmetry (Antolak *et al.*, 1997). Other foams, such as agar, have a coarser structure but have the advantage of being more easily machineable; this allows one to make both uniform and hollow annular cylinders of agar.

For the loads shown in Figs. 1(a) and (b), the substance is initially nonconducting. Before the current will flow through the pinch, breakdown of the material should occur. Because a breakdown is a statistical process, it may cause considerable initial nonuniformities of the pinch. To try to have a more predictable initiation of the discharge in a foam, one sometimes uses thin conducting coatings on the surface of the foam. In the case of gaseous jets, one or another method of preionization can be used.

More recently (see, for example, Matzen, 1997), considerable progress in the technology of fabricating very fine wire arrays has allowed assembly of highly symmetrical cylindrical shells consisting of hundreds of very fine (several micrometers in diameter) metal wires [Fig. 1(c)]. The initial state of the imploding shell is in this case, obviously, conducting. One may therefore expect a more symmetric initiation of the discharge. For specific applications, a foam cylinder, uniform or annular, or a more complex structure may be inserted into the wire array [Fig. 1(d)].

Thus far we have been discussing *Z* pinches with an implosion time in the range of tens of nanoseconds. There exist devices in which the imploding objects are relatively heavy metal shells and the implosion time is as long as hundreds of nanoseconds to microseconds. This kind of *Z* pinch also falls under the aforementioned definition of "fast" *Z* pinches and will be covered by our survey. As an example, we mention implosions of metal shells (Baker *et al.* 1978; Degnan *et al.*, 1995). A schematic of the latter experiment, in which quasispherical implosions were successfully realized, is shown in Fig. 1(e) Quasispherical targets may also be pursued in lower-mass configurations.

## D. Pulsed power

The remarkable progress made during the last few years in fast-*Z*-pinch parameters became possible owing to progress in pulsed-power technology and in the development of sophisticated diagnostics instrumentation. As has already been emphasized, this review is directed to the discussion of the physics of *Z* pinches and will not address the equally important issues of pulsed-power technology and pinch diagnostics. However, to give the reader some idea of the pertinent work, we briefly summarize the status of both areas.
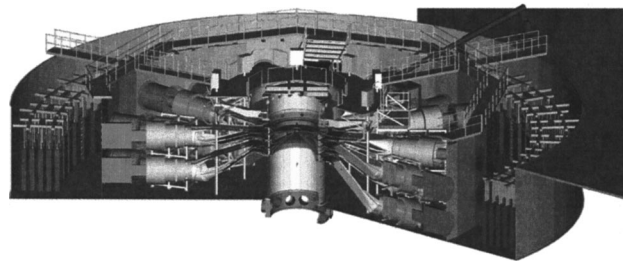


FIG. 2. Schematic of the *Z* facility. The diameter of the facility is 30 m. The outermost part is formed by Marx generators. They are connected to 36 water-insulated transmission lines which, in turn, feed magnetically insulated vacuum transmission lines converging at the diode. The diode is situated inside the central tank.

The power and current available for *Z*-pinch implosions reached new heights during the last decade: the pulsed-power generator Saturn (Spielman *et al.*, 1989) reached an electrical power of 20 TW and a maximum current of $\sim 10$ MA, and the 50-TW Particle Beam Fusion Accelerator (PBFA II, now called "*Z*") was modified to drive fast-*Z*-pinch implosions, at currents of $\sim 20$ MA (Spielman *et al.*, 1996). Both generators are situated at Sandia National Laboratories (Albuquerque, New Mexico). The kinetic energy in imploding liners that were 2 cm long at an initial radius of 2 cm reached $\sim 0.35$ MJ at Saturn and $\sim 1.2$ MJ at *Z*. A schematic of the *Z* facility is shown in Fig. 2. There are other high-power generators used in *Z*-pinch research. In Russia, the best known is the Angara-5 generator (Al'bikov *et al.*, 1990), with a maximum current of $\sim 4$ MA and a maximum power to the load of $\sim 10$ TW. Generators of a similar size include Double Eagle at Physics International, Blackjack 5 at Maxwell Laboratories, and Proto II at Sandia National Laboratories. Worldwide, about 15 generators operating at the current level of 1–3 MA and power to the load of $\sim 1$–5 TW are used in *Z*-pinch research (some of them are described in Camarcat *et al.*, 1985). There are also numerous smaller generators. Most of the larger generators use so-called magnetically insulated transmission lines (MITL) to deliver power to the axisymmetric diode assembly. These magnetically insulated lines are, in turn, fed by transmission lines insulated with water. The power to the water transmission lines is supplied by high-voltage Marx generators. A wealth of information on these issues can be found in the proceedings of pulsed-power conferences. A typical geometry of the diode assembly, where the *Z*-pinch target is situated, is shown in Fig. 3.

To drive the slower and heavier loads of the type shown in Fig. 1(e) with an implosion time of the order of 1 $\mu$s, slower generators are required. Examples of such generators are Shiva Star situated at Phillips Laboratory, Albuquerque, New Mexico (Degnan *et al.*, 1995), and Pegasus, situated at Los Alamos National Laboratory.

## E. Diagnostic instrumentation

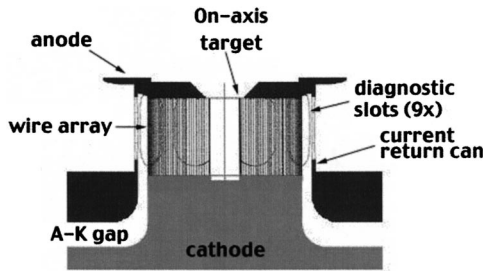Electric parameters of the discharge and the current through the pinch are inferred by measuring the electric

FIG. 3. Cross-section view of the *Z* diode with on-axis annular target. There are nine cutaway slots in the current-return can for diagnostic access. The *Z* machine is configured with the anode physically on the top of the target; other machines, such as Saturn, are configured with the anode down. The power from the magnetically insulating transmission lines flows to the diode through the gap in the lower part of the figure.

and magnetic fields at specific points of the device in the generator with millimeter-size magnetic loops and capacitive probes. To measure the current through the pinch column, it would be necessary to measure the magnetic field inside the return-current conductor (Fig. 3). This is difficult to do because of the very large magnetic fields in a region of strong radiation and heat fluxes. Therefore the magnetic field (and the current) are usually measured in the MITL, at distances larger than ~3 cm from the axis of the *Z* pinch. The voltage is measured at the insulator stack. A description of the probes, and further references, can be found in Stygar *et al.* (1997). A possible way of measuring the magnetic field in the plasma column is to use a Faraday rotation technique (Branitskii *et al.*, 1992a; 1992b; Sarkisov *et al.*, 1995b).

Optical measurements are useful for the characterization of the early stage of the *Z*-pinch implosion, when the x-ray radiation does not yet overwhelm the optical detection system. Optical interferometry and holography allow one to detect low-density blow-off plasma at an early stage, as well as to observe instabilities of individual wires in the wire arrays. These measurements have a spatial resolution of a few tens of micrometers to millimeters and a temporal resolution of ~1 ns. Further details and references can be found, for example, in Haines (1997); Muron, Hurst, and Derzon (1997); and Deeney, McGurn, *et al.* (1997). Emission tomography is described by Veretennikov *et al.* (1992).

For later stages of the *Z*-pinch implosion, the x-ray radiation becomes significant and is successfully used for characterization of the pinch. Total radiation intensity is typically measured with bolometers, with a temporal resolution of ~0.5 ns. Calorimeters can be used to measure the total radiation energy. X-ray diodes and photoconducting detectors are used to make broadband time-resolved measurements of x-ray spectra (Spielman *et al.*, 1997). Multichannel scintillation detectors have also been developed for this purpose (Averkiev *et al.*, 1992). To characterize the radiation in x-ray lines, plasma temperatures, and ionization states, x-ray spectroscopy is used (Leeper *et al.*, 1997; Pikuz *et al.*, 1997). X-ray pinhole framing cameras provide a spatial resolution as

small as 100 micrometers, with time duration of the exposure as small as 100 picoseconds.

The high-energy electron beams sometimes generated in *Z* pinches can be detected by the gamma radiation from electrodes, and high-energy ion production can be observed by gamma spectroscopy of activated materials. The presence of fast deuterons is inferred from neutron radiation.

A complete description of the status of diagnostic instrumentation would require the inclusion of many tens if not hundreds of additional references and would lead us well beyond the intended scope of this paper. We point out that many diagnostics papers can be found in the January 1997 and January 1999 issues of the *Review of Scientific Instruments* and in the proceedings of the 1997 Conference on Dense *Z* Pinches edited by Pereira, Davis, and Pulsifer (1997).

## II. IMPLOSION IN THE IDEAL CASE OF THE ABSENCE OF INSTABILITIES

In this section we discuss the case of an ''ideal'' implosion that might occur in the absence of instabilities. This will give us a kind of a reference point to allow us to see more clearly effects of possible complications caused by instabilities. Stable, purely cylindrical implosions can be numerically simulated with a great deal of detail; a great deal of information obtained in such simulations is available in the published literature (e.g., Hammer *et al.* 1996; Peterson *et al.*, 1996). However, we prefer to concentrate on simple analytical models that allow the reader to follow more easily the chain of causes and effects. Working in this spirit, we start from an analysis of the simplest possible system, a structureless perfectly conducting thin shell. After that, we gradually add complicating factors, like finite conductivity, radiation, etc.

### A. Implosion of a thin shell

In the simplest case of a thin annular shell (like the one formed by the wire array), the equation of radial motion can be written as

$$\frac{\hat{m}}{2\pi r}\ddot{r} = -\frac{B^2}{2\mu} = -\frac{\mu I^2}{8\pi^2 r^2},\tag{2.1}$$

where $B = B(t)$ is the magnetic field at the surface of the pinch and $I = I(t)$ is the pinch current. Let us measure the current in units of the maximum current $I_{\max}$, the time in units of the time $\tau$ within which the current reaches its maximum, and the radius in units of the initial radius $r_0$. In other words, we introduce dimensionless variables

$$\tilde{r} = r/r_0, \quad \tilde{t} = t/\tau, \quad \tilde{I} = I/I_{\max}.\tag{2.2}$$

Rewritten in these variables, Eq. (2.1) is converted to

$$\tilde{r}\ddot{\tilde{r}} = -\Pi\tilde{I}^2,\tag{2.3}$$

where

$$\Pi = \frac{\mu I_{max}^2 \tau^2}{4\pi\hat{m}r_0^2} \qquad (2.4)$$

is a dimensionless scaling parameter of the problem. Two implosions with the same functional dependence of current on time [i.e., with the same dependence $\tilde{I} = \tilde{I}(\tilde{t})$] occur in a similar fashion if the parameter $\Pi$ for them is the same. In particular, the instant in time when the pinch collapses on the axis, measured in units of $\tau$, is the same for both implosions.

To provide good efficiency for converting the energy stored in the pulsed-power generator into kinetic energy of the imploding pinch, one should choose an optimum mass of the pinch material. This mass should be such that the implosion time is approximately equal to the time within which the current reaches its maximum value: if the mass is too large, the current pulse ends before the pinching occurs, and if the mass is too small, the pinching occurs before the current reaches its maximum, also implying poor efficiency. In other words, for every current pulse shape there exists an optimum value of the parameter $\Pi$.

Let us consider in closer detail the initial stage of the implosion of a thin shell [Eq. (2.1)]. When the pinch radius has not yet decreased considerably with respect to its initial value $r_0$, one can represent $r$ as $r = r_0 - \Delta r$, with $\Delta r$ small. In all our semiquantitative estimates we shall use a simple model of the current through the pinch:

$$I = I_{max}\sin^2\left(\frac{\pi t}{2\tau}\right). \qquad (2.5)$$

At an early stage of the implosion, the pinch current can be approximated, with reasonable accuracy, by a parabolic dependence on time,

$$I = I_{max}\left(\frac{\pi t}{2\tau}\right)^2, \qquad (2.6)$$

For the dependence (2.6) one easily obtains for $\Delta r$

$$\frac{\Delta r}{r_0} = \frac{\pi^4\Pi}{480}\left(\frac{t}{\tau}\right)^6. \qquad (2.7)$$

Note that the pinch radius departs from its initial value very slowly, $\sim t^6$. For a load with a mass corresponding to collapse at $t = \tau$, even at $t = (\frac{2}{3})\tau$ the pinch radius is decreased by a mere 10% of its initial value. This discussion shows that a pinch has a long "latent" phase followed by a very fast collapse that occurs within a small fraction ($\sim 0.1$–0.2) of the total implosion time $\tau$. Calculated time histories of the wire-array radius and the pinch current in one of the shots at the Saturn accelerator are shown in Fig. 4.

An important characteristic of the system is the kinetic energy $W_{kin}$ of the shell at the point at which it reaches some desired minimum radius $r_{min}$. This can be a radius determined by a finite thickness $h$ of the shell (i.e., $r_{min} \sim h$), or a radius of an inner cylinder as in the scheme shown in Fig. 3. To find $W_{kin}$ one can use the energy relationship that is obtained by multiplying Eq.
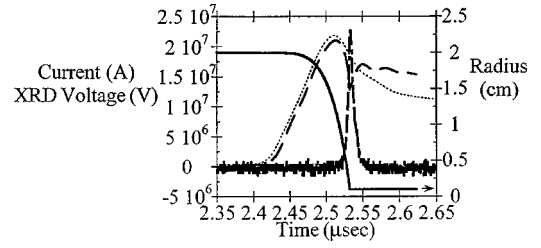


FIG. 4. Shot 104 at the Z accelerator: dotted line, measured current; dashed line and solid line, current and wire-array radius, both calculated with Screamer code; and a Kimfol-filtered (200–280 eV) x-ray diode signal, $\times 10^6$. From Struve et al., 1997, reprinted with kind permission of K. Struve. The initial wire array had 290 wires at a radius of 2 cm, the W wires were 7.5 $\mu$m in diameter. A long "latent period" during which the shell radius decreases very slowly is clearly visible.

(2.1) by $\dot{r}$ and integrating by parts from $t = 0$ to $t = t^*$, where $t^*$ corresponds to the point where $r = r_{min}$. One finds

$$W_{kin} = \frac{\mu}{4\pi}\int_0^{t^*}\frac{dI^2}{dt}\ln\left(\frac{r}{r_{min}}\right)dt; \qquad (2.8)$$

here $W_{kin}$ is a kinetic energy per unit length of the pinch at $t = t^*$. The mass of the liner enters Eq. (2.8) only implicitly through the implosion time $t^* = t^*(\hat{m})$ and through the dependence of the radius on time, $r = r(t,\hat{m})$.

At large convergence, one can obtain a simple approximate expression for $W_{kin}$. To do that, one should note that the logarithm in the integrand of Eq. (2.8) is almost constant and equal to $\ln C$ for most of the implosion. The contribution of the part where the logarithm begins to change (roughly speaking, after the pinch radius reaches $r_0/2$) is small because the time within which the pinch implodes from $r_0/2$ to $r_{min}$ is very short compared to the total current pulse width [see Fig. 4 and comments after Eq. (2.7)]. So, replacing the logarithm in the integrand of Eq. (2.8) by a constant value $\ln C$ (corresponding to the final convergence $C = r_0/r_{min}$, i.e., typically, to $C \sim 10$–20), one finds

$$W_{kin} \approx \frac{\mu I^2(t^*)\ln C}{4\pi}. \qquad (2.9)$$

One sees that the maximum of the transferred energy corresponds to a mass such that the time $t^*$ roughly corresponds to the maximum of the current. This statement has a so-called "logarithmic accuracy," i.e., it is valid up to terms of the order of $1/\ln C$. To make a more accurate estimate of the optimum implosion time, one should take a derivative of $W_{kin}$ over $\hat{m}$. From Eq. (2.8) one finds

$$\frac{\partial W_{kin}}{\partial\hat{m}} = \frac{\mu}{4\pi}\int_0^{t^*}\frac{dI^2}{dt}\frac{1}{r}\frac{\partial r}{\partial\hat{m}}dt. \qquad (2.10)$$

Obviously, the derivative $\partial r/\partial\hat{m}$ is positive: a heavier liner implodes more slowly and, at a given time, has a larger radius. Therefore, if $t^*$ corresponds to the current maximum, the derivative $\partial W_{kin}/\partial\hat{m}$ is positive. It

reaches zero (i.e., the kinetic energy reaches a maximum) at some point beyond the maximum of the current. This point usually corresponds to a current that is 20–30% less than the current maximum. For a current wave form like that in Eq. (2.5), the optimum value of the parameter $\Pi$ is equal to approximately 4.

In real life, for a given pulse-power generator, the current wave form cannot be considered as independent of the parameters of the load (because of the contribution of the load impedance to the overall impedance of the circuit). This circumstance can be taken into account by solving equations for the pinch together with the circuit equations (see, for example, Katzenstein, 1981; Struve *et al.*, 1997). One should also emphasize that the kinetic energy is not necessarily an appropriate figure of merit. For example, in experiments on generation of radiation the figure of merit could be the radiated energy. The contribution to the radiated energy comes not only from the kinetic energy of the pinch but also from Joule heating (see Sec. VIII.A) and $p\,dV$ work on the plasma during the stagnation phase (Peterson *et al.*, 1997, 1998). Still, the kinetic energy is an important and clearly defined characteristic of the implosion and we shall concentrate our discussion on it.

Using Eq. (2.9), one can derive an expression for the volume density of the kinetic energy $w_{\mathrm{kin}}$ at the stagnation point in the case of an empty liner:

$$w_{\mathrm{kin}} = \frac{W_{\mathrm{kin}}}{\pi r_{\mathrm{min}}^2} \approx 2 p_m^* \ln C, \tag{2.11}$$

where $p_m^*$ is the magnetic pressure at the surface of the pinch at $r = r_{\mathrm{min}}$. If this energy is converted to the thermal energy of the monatomic ideal gas, then the gas pressure will be $p = (2/3) w_{\mathrm{kin}}$, or

$$p = \frac{4}{3} p_m^* \ln C. \tag{2.12}$$

One sees that, in such a scenario, the gas pressure is indeed considerably higher than the magnetic pressure, and the pinch will rapidly expand after stagnation. The pinch rebound was detected in experiments with aluminum wire arrays on the Saturn facility (Sanford *et al.*, 1997a).

If one deals with a liner made of heavy elements, then, in fact, a considerable amount of energy will be spent on ionization, reducing $p$ compared to the estimate (2.12). In implosions of wire arrays, temperatures in the range of hundreds of electron volts and electron densities in the range of $10^{22}$ are typical (Maxon *et al.*, 1996; Deeney, Nash, *et al.*, 1997; Matzen, 1997; Sanford *et al.*, 1997b). Radiative losses also lead to pressures smaller than Eq. (2.12).

If the radiation-loss time is considerably shorter than the acoustic time $r_{\mathrm{min}}/c_s$ (where $c_s$ is the sound speed), then, in the absence of instabilities, the pinch might experience a collapse to ever smaller radii (a radiative collapse, see, for example, Meierovich, 1986). The Joule heating, especially with the anomalous resistance included, works in the opposite direction (Robson, 1991), as do the radiation imprisonment and effects of electron degeneracy (Haines, 1989; Chittenden and Haines, 1990). Radiative collapse in a real situation may also be prevented from happening by the constraints imposed by circuit equations (a rapid increase of the pinch inductance may decrease the current; Haines, 1989; Choi and Dumitrescu-Zoita, 1997).

## B. Targets with initially uniform density distribution

In this section we consider implosions of targets with initially uniform density distribution, like foam cylinders, or smooth radial density distributions, e.g., gas puffs. In this case, a shock wave propagates ahead of the current-carrying sheath and reaches the axis considerably earlier than the sheath. We assume that the skin depth is small compared to the radius of the column, as is the case in real situations.

The converging cylindrical shock, if it possesses a good symmetry produces a strong increase in density and temperature which formally diverges on the axis (Guderley, 1942; see also Whitham, 1974). After the shock is reflected from the axis and again reaches the surface of the cylinder, a kind of adiabatic compression begins, in which the plasma pressure is approximately equal to the magnetic pressure, and the sound speed in the plasma is comparable to the Alfvén velocity. This means that a kind of transient Bennett-type equilibrium is formed for a few acoustic transit times.

In this discussion so far, we have ignored the role of radiation. This is negligible with imploding deuterium-tritium (DT) gas puffs. If, however, one deals with implosions of heavier elements, then the radiation of the plasma behind the shock can become important. In the extreme case of very strong radiation losses, the plasma behind the shock radiates its energy much faster than the time within which the shock could propagate across the radius of the pinch. In this extreme case the shock will not be formed at all, and all the material impacted by the magnetic piston will just stick to the piston. This corresponds to the so-called snow-plow model studied in great detail in the early years of pinch research (1950s). We shall use the term "snow-plow" in just this sense, to designate a simple model in which all the material swept by the magnetic piston merely sticks to it. This case is similar to that discussed in the previous section and we shall start from it, leaving discussion of the second possibility (weak radiation) until the Sec. II.B.2.

When mixtures of gases are used, and the densities are low enough, the picture may be complicated by a radial separation of the ion species under the action of the ambipolar radial electric field (Bailey *et al.*, 1982; Barak and Rostoker, 1982; Rahman, Amendt, and Rostoker, 1985). Gordeev (1987) contends that in a low-density gas-puff implosion of a multispecies plasma, the mutual friction between the ion components may cause an enhanced penetration of the magnetic field.

### 1. Snow-plow model (strongly radiating plasma)

The equations of motion for a magnetic piston sweeping the plasma like a snow plow read as

$$\frac{\hat{m}^*}{2\pi r}\ddot{r} - \rho(r)\dot{r}^2 = -\frac{\mu I^2}{8\pi^2 r^2}, \tag{2.13}$$

$$\dot{\hat{m}}^* = -2\pi r\dot{r}\rho(r), \tag{2.14}$$

where $\rho(r)$ is the initial density distribution and $\hat{m}^* = \hat{m}^*(t)$ is the instantaneous mass accreted at the piston. The second term on the left-hand side of Eq. (2.13) describes the momentum imparted to the piston by the accreting material. We assume that the density at a certain radius remains unchanged until the very moment of the magnetic piston's arrival. For two implosions with initial density distributions having the same functional dependence on $r/r_0$, the same similarity law applies as for Eq. (2.14), i.e., the two implosions are similar if the parameter $\Pi$ for them is the same.

Consider an early stage of the implosion of a uniform cylinder in the framework of the snow-plow model. In this case, at the same mass per unit length as in a thin shell, the current sheath moves towards the axis faster than in the case of a thin shell. The reason is merely the smaller mass involved in the implosion at an early stage. To illustrate this point more quantitatively, consider an analog of Eq. (2.7) assuming that the initial density distribution is uniform, i.e., $\rho = \hat{m}/\pi r_0^2$. One now has

$$\frac{\Delta r}{r_0} = \frac{\pi^2}{4}\sqrt{\frac{\Pi}{30}}\left(\frac{t}{\tau}\right)^3. \tag{2.15}$$

This solution is valid until $\Delta r$ is less than, roughly speaking, $r_0/3$. We see that the implosion begins faster than for a thin shell. The collapse on axis also occurs earlier than for a thin shell of the same mass per unit length. Still, the latent period is present in this case, too.

For the snow-plow model [Eq. (2.13)], the analog of Eq. (2.1) reads

$$W_{\text{kin}} = \frac{\mu}{4\pi\hat{m}}\int_0^{t^*}\frac{d(\hat{m}^* I^2)}{dt}\ln\frac{r}{r_{\min}}dt, \tag{2.16}$$

where $\hat{m}$ is the total mass per unit length, and $\hat{m}^*$ is the mass swept by the current sheath by time $t$:

$$\hat{m}^* = 2\pi\int_r^{r_0} r'\rho(r')dr'. \tag{2.17}$$

We assume here that one is dealing with the implosion of a simple gas puff or a foam cylinder, without an external shell [otherwise, one would have to add the mass of this shell to both $\hat{m}$ and $\hat{m}^*$ in Eq. (2.13)]. Using the same arguments as in the case of a thin shell, one can show that, at high convergences and smooth density distributions, $W_{\text{kin}}$ is still approximately determined by Eq. (2.9). From elementary mechanical considerations one can find that the power released in the inelastic interaction of the initially resting substance with a moving piston is (per unit length) $\dot{\hat{m}}^*\dot{r}^2/2$. Integrating this expres-
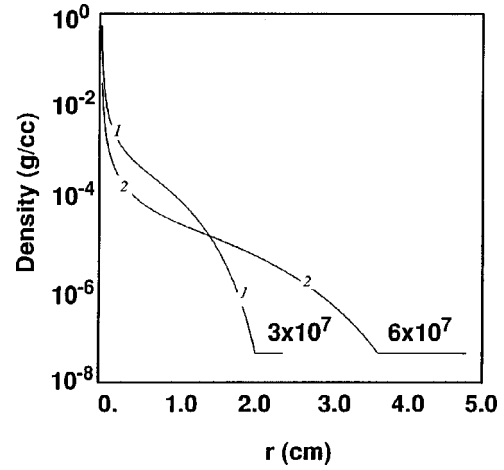


FIG. 5. Density distributions for constant-velocity implosions for velocities $3\times10^7$ cm/s and $6\times10^7$ cm/s. The current wave form was determined self-consistently for the Saturn circuit equations. From Hammer et al., 1996, reprinted with kind permission of J. Hammer.

sion over time, one finds that, at $C\gg1$, the part of the energy that was radiated from the accreted mass is, within an order of magnitude, $1/\ln C$ of the final kinetic energy (i.e., relatively small). This is so because most of the mass is accreted before the liner reaches a radius of, say, $r_0/3$, when the liner velocity is still small compared to its final velocity at $r=r_{\min}$.

An interesting feature of Eq. (2.13) is that, at the properly chosen radial density distribution, there are conditions for which the surface of the pinch does not experience radial acceleration. Such a regime may be desirable, since it may be stable with respect to the Rayleigh-Taylor instability. This idea has been explored by Hammer et al. (1996). To approach a state of constant velocity, the outermost part of the pinch should experience a sudden kick that would impart to it the desired velocity $v$. As soon as this state has been reached, further evolution of the system is described by Eq. (2.13), with the first term on the left-hand side of this equation omitted. One obtains the following equation for the desired density profile (Hammer et al., 1996):

$$\rho(r) = \frac{\mu I^2[(r_0-r)/v]}{16\pi^2 v^2 r^2}. \tag{2.18}$$

The density should rapidly increase near the axis ($\propto 1/r^2$), and essentially all the mass should be concentrated within the radius $\sim 2r_{\min}$. Figure 5 depicts the required density distributions. For such sharply varying density distributions one cannot use Eq. (2.9) to estimate the kinetic energy. The final kinetic energy in this case is

$$W_{\text{kin}} = \frac{\hat{m}v^2}{2}, \tag{2.19}$$

with the mass $\hat{m}$ related to the implosion velocity by Eqs. (2.17) and (2.18), with $r=r_{\min}$ in the former equa-

tion. The optimum velocity (at which $W_{kin}$ is at a maximum) is the velocity at which $r=r_{min}$ is reached at the current maximum. It is also important to note that the radiative losses $W_{rad}$ in this case are considerable. Using the same arguments that followed Eq. (2.17) one can show that the total radiated energy is $W_{rad}=W_{kin}$ (see Hammer *et al.*, 1996).

## 2. Weakly radiating plasma

In this case, the shock wave splits from the piston and propagates in front of it, heating and compressing the plasma. As the initial temperature of the preshocked plasma is small, the shock has a very large Mach number and can be considered a strong shock (Landau and Lifshitz, 1987). For a gas with adiabatic index $\gamma$, the plasma density ($\rho_1$) and plasma pressure ($p_1$) behind the shock are

$$\rho_1=\frac{\gamma+1}{\gamma-1}\rho, \ \ p_1=\frac{2}{\gamma+1}\rho u^2, \tag{2.20}$$

where $u$ is the shock velocity. If the magnetic piston is moving with some constant velocity $v$, there is a simple relationship between $u$ and $v$; this is a direct consequence of the mass conservation equation, $\rho u=\rho_1(u-v)$: $u=(\gamma+1)v/2$. For the ideal monatomic gas ($\gamma=\frac{5}{3}$), $u=(\frac{4}{3})v$, i.e., the shock velocity is approximately 30% higher than the velocity of the piston. This means that the shock converges on axis when the pinch radius is equal, roughly speaking, to $r_0/3$. This is a crude estimate, as it does not take into account variations in $v$ and effects of cylindrical geometry. Still, it does not differ strongly from more elaborate analyses, in particular from the "slug" model of Potter (1978) and the energy analysis of Miyamoto (1984).

Potter's model assumes that the plasma behind the shock is uniform, with parameters related to the parameters in front of the shock by Eqs. (2.20). The pressure $p_1$ is, on the other hand, equal to the magnetic pressure. This allows one to close the set of equations and to find the position of the shock and the piston as a function of time. The prediction is that the shock will reach the axis at $r\approx0.3r_0$. After the shock is reflected from the axis and reaches the piston, a quasiequilibrium state is formed in which the plasma pressure is approximately equal to the magnetic pressure. One sees that this is quite a different situation from an implosion of a thin shell, in which case the particle pressure in the final state is much higher than the magnetic pressure.

Such solutions are of interest in implosions of low-*Z* targets, in particular, DT gas puffs and deuterated carbon foams. Targets of heavier materials may remain not fully ionized behind the shock. In this case the use of the power-law adiabats may break down. As a considerable amount of energy is spent on ionization, the temperature behind the shock is lower than in the fully ionized case, and the density higher (Zeldovich and Raizer, 1967). In such a situation, the separation between the piston and the shock front is reduced compared to what was discussed above, and the snow-plow model of Sec. II.B.1 becomes relevant.

In a plasma with incompletely stripped ions, the tail of the electron distribution function experiences losses caused by excitation and ionization events; therefore, the tail may become depleted, affecting the rate of excitation and the radiation intensity (see, for example, Clark, Davis, and Cochran, 1986; DeGroot *et al.*, 1997a). An example of an analysis of experimental data on x-ray spectra from implosions of the foam loads on the Saturn device, with nonequilibrium effects included, can be found in MacFarlane *et al.* (1997). In quasistatic pinches, an important channel of heat loss is an enthalpy flow to the electrodes related to the pinch current (Haines, 1960). In fast pinches this channel is usually subdominant.

We have discussed three limiting cases of implosions: that of a thin shell, that of a nonradiating uniform (not annular) column, and that of a strongly radiating uniform column (snow-plow model). Of course, a whole range of intermediate cases is also possible. In particular, in gas-puff implosions with annular gas puffs, the initial density on axis is never zero, because of a finite angular divergence of the jet. A converging shock would then propagate in a relatively low-density gas in front of the main shell and would cause a significant density and temperature increase on axis prior to arrival of the main shell. This is a possible explanation for the early formation of a dense on-axis column in experiments by Shiloh, Fisher, and Bar-Avraham (1979).

## C. Three-dimensional implosions

As has already been mentioned in Sec. I.C, one may deliberately implode shells with a geometry other than cylindrical. Figure 1(e) depicts an implosion of an approximately spherical shell whose polar areas are sliding along the conical electrodes. This scheme was successfully realized in experiments by Degnan *et al.* (1995). The magnetic pressure at the surface of the shell is larger in the polar areas (because of the smaller distance from the axis). To compensate for this effect (which would lead to deviations from the spherical implosion), the shell thickness was made larger in the polar parts. To avoid jetting at the point of the sliding contacts of the shell with the electrodes, the angle at their apex was made greater than 45°.

Another technique for producing quasispherical implosions is tailoring of the thickness of the initially cylindrical liner, so that the thickness decreases from the equatorial plane to the ends (Fig. 6). The liner implosion then occurs as shown in Fig. 6, with the volume inside the liner experiencing a three-dimensional (3D) compression after $t=t_2$. Such a scheme has been successfully tested in experiments with relatively massive aluminum liners by Alikhanov *et al.*, (1977). Numerical simulations of 3D implosions have been recently performed by Lisitsyn, Katsuki, and Akiyama (1999).
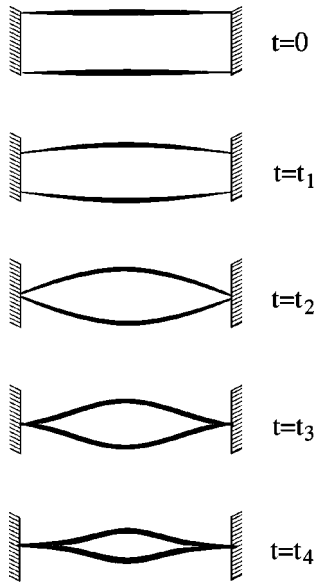
FIG. 6. Producing a quasispherical implosion with an initially cylindrical liner of varying thickness. The liner is thicker near the equatorial plane (see Drake *et al.*, 1996).

## D. Electrode phenomena

So far, we have been considering problems with a pure cylindrical symmetry, i.e., problems in which all parameters depend only on *r*. Perfect cylindrical symmetry cannot be reproduced in real life, even if the system is magnetohydrodynamically stable. Indeed, the pinch always has a finite length, and there is contact between the pinch plasma and the electrodes. This creates some axial nonuniformity and thereby violates pure cylindrical symmetry. The presence of electrodes may affect the pinch performance in a number of ways.

First, there is some friction between the liner and the surface of the electrode. This effect may be significant for high-temperature and low-density pinch plasmas. The presence of tangential shear flow in the transition region between the electrode and the liner may excite the Kelvin-Helmholtz instability (see Chandrasekhar, 1961) and shear-flow turbulence. This would be turbulence of supersonic flow (the plasma velocity far from the wall is much higher than the speed of sound in the plasma shell), with strong radiative losses. Very little is known about turbulent momentum transfer under such circumstances. The first observation of Kelvin-Helmholtz instability in an ICF-relevant environment was reported by Hammel *et al.* (1994).

Second, there is a heat flux to cold, massive electrodes. Its significance is again determined by the density and temperature of the liner. This heat flux causes an axial variation of the plasma temperature near the electrodes, thereby violating the cylindrical symmetry of the implosion.

Third, there may occur some mass influx from the surface of the electrode that makes the end part of the pinch heavier and causes it to lag with respect to the equatorial part of the pinch.
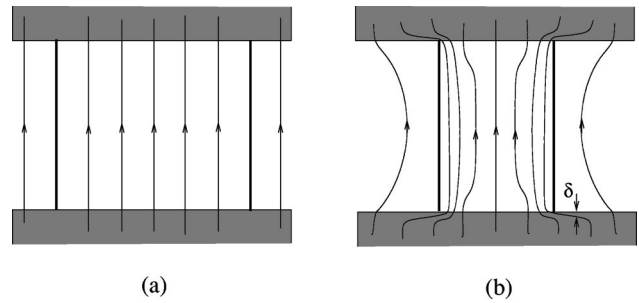


FIG. 7. Distortion of the axial magnetic field in the course of a liner implosion ($\delta$ is the skin depth). Strong enhancement of the initial magnetic field occurs within a skin layer. As the perfectly conducting liner moves towards the axis, the magnetic flux initially enclosed by the liner has to be transferred through a thin skin layer. Thick lines depict a cylindrical liner, thin lines with arrows are magnetic-field lines.

Fourth, conducting electrodes impose a "frozen-in" condition on the normal component of the magnetic field. To illustrate the possible role of this effect, consider a liner implosion in the presence of a weak initial axial magnetic field $B_{z0}$ (such geometries are supposed to be used in experiments on the generation of strong magnetic fields; see, for example, Alikhanov *et al.*, 1967). If (as it usually is) the bias magnetic field is small compared to the azimuthal magnetic field of the pinch, it does not considerably affect the pinch dynamics during the run-in phase. Consider, however, what happens to the magnetic field itself. The axial magnetic flux through every element of the electrode and liner is conserved because of their high conductivity. This creates the situation shown in Fig. 7: a thin near-electrode layer appears where the embedded magnetic field becomes almost radial in direction; the thickness of this layer is of the order of the skin depth $\delta$, which is very small compared to the pinch radius. From the conservation of the magnetic flux, it follows that the radial magnetic field inside the skin layer should be $B_r \sim B_{z0} r/\delta$. This estimate corresponds to the intermediate stage of the run-in, where the pinch radius is equal to, say, half of the initial radius. For a typical implosion at a time of ~30 ns, the skin depth in the electrode material is of the order of $10^{-3}$ cm, and, for $r \sim 1$ cm, one obtains $B_r \sim 10^3 B_{z0}$. Even if the bias magnetic field is small, say, $10^4$ G, the magnetic field in the skin is very large and may become comparable with the self-magnetic field of the pinch. This, in turn, will cause a thermal explosion of the electrode skin layer, because of the very high current density, and also a change in the dynamics of the liner implosion near the surface of the electrodes.

In some experimental settings, in order to provide better diagnostic access, one of the electrodes is made with a hollow center (Fig. 8). This may lead to a different phenomenon, similar in some sense to the plasma focus effect (for a description of the latter see Sec. 4 in Vikhrev and Braginski, 1986). When, in the course of the implosion, the liner slides past the edge of the hole, a current-carrying "bridge" may be formed from the materials of both the liner and the electrode (panel 2).
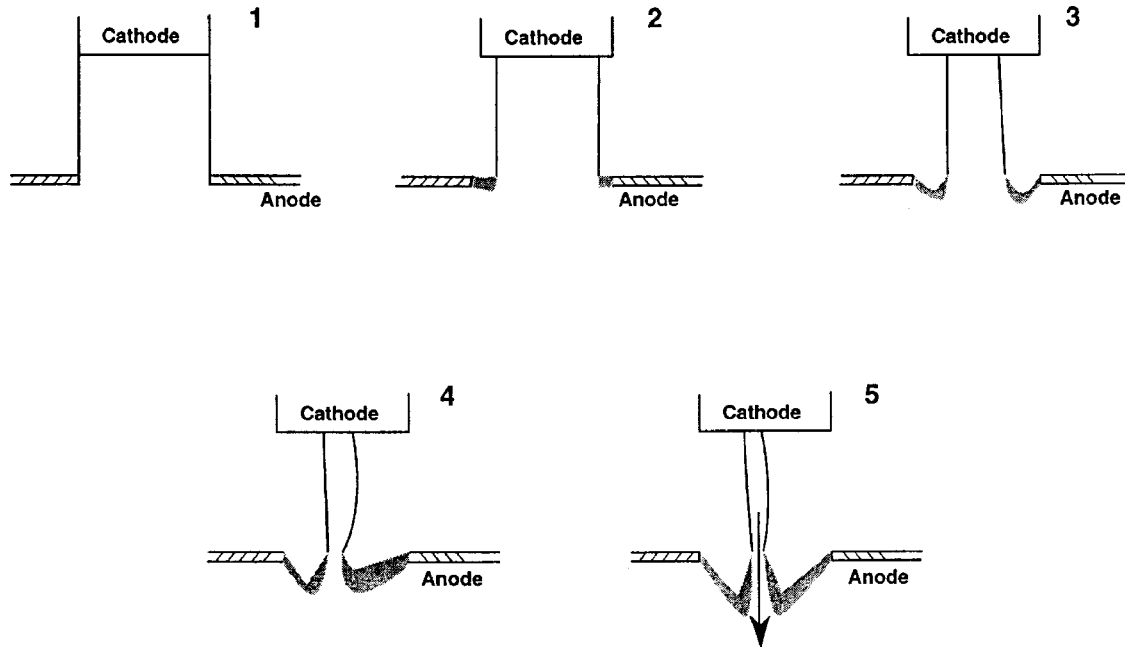
FIG. 8. Possible scenario of the implosion of a wire array in the case of a hollow anode. The picture is made deliberately asymmetric to emphasize the statistical character of the bridge formation.

The density of this bridge would presumably be less than the density of the liner itself. Anomalous resistivity may turn on, causing considerable heating and radiation from this region. The bridge experiences a magnetic pressure directed downward and begins to evolve as shown in panels 3 and 4. The further evolution of the bridge should lead to its early self-implosion at some axial point, formation of the "neck" (panel 5), and, possibly, the breakup of the current channel, with generation of high-energy particle beams. The collapse should be accompanied by injection of material in both directions from the collapse point. Bright features appearing near the anode hole relatively early in the pulse were observed by Derzon *et al.* (1997a), which persisted until relatively late (Fig. 9).

### E. Structure of an imploding shell

Knowledge of the structure of an imploding shell is required for the stability analysis that will be made in later sections of this review. Consider the implosion of a thin shell whose thickness $h$ is such that the time of propagation of the compression wave through the distance $h$ is small compared to the characteristic time of the implosion process. This assumption is certainly valid for thin enough shells. Then the shell can be considered as being in a quasi-steady-state mechanical equilibrium governed by the following equation:

$$\rho g = -\frac{\partial}{\partial x}\left(p + \frac{B^2}{2\mu}\right), \tag{2.21}$$
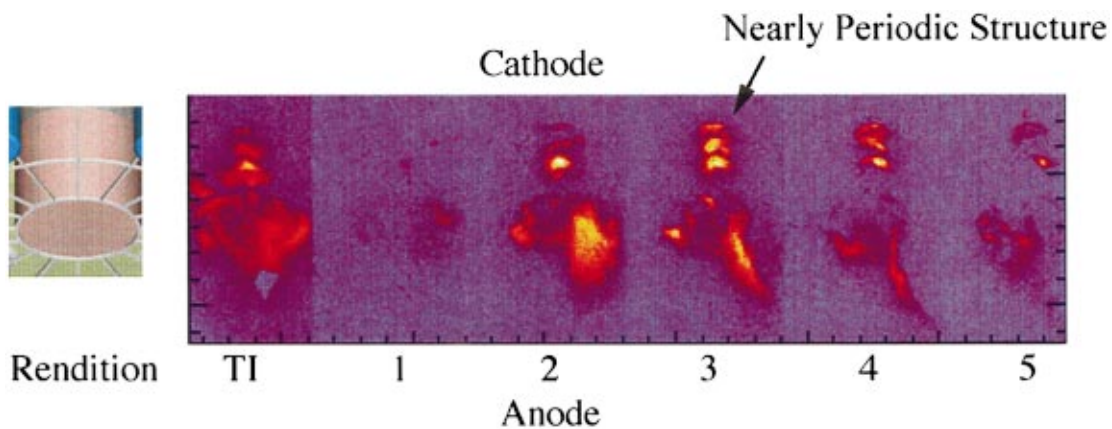


FIG. 9. Scale-size rendition of target compared to time-integrated (TI) and gated x-ray images of the foam target. The image consists of a time-integrated frame and five 100-ps frames 3 ns apart. The third frame is near the peak in emission. Plasma jetting along the axis outside of the pinch and near the single mode structure between the electrodes is observed. The diameter of the anode ring was 1 cm, and the mass of the foam was 78 mg+.08 mg. The peak current in this shot was 7 MA, and the current had, roughly, a 60-ns rise time [Color].
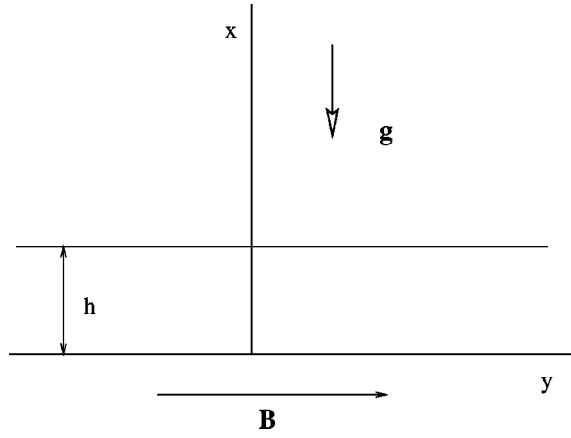
FIG. 10. The slab geometry used in the stability analysis; $\mathbf{g} \equiv -\mathbf{e}_x g (g > 0)$.

where $g$ is the effective gravity acceleration (in the co-moving frame) and $x$ is a coordinate directed towards the axis. We are using here a planar model because of the small thickness of the shell. The geometry of the problem is illustrated in Fig. 10.

There is no magnetic field at the inner surface of the shell (no current inside the shell) and therefore the acceleration is related to the magnetic field $B_0$ at the outer surface of the shell via the equation

$$\rho g h \sim B_0^2 / 2\mu, \tag{2.22}$$

where $h$ is the shell thickness.

First let us assume that the temperature of the shell is determined by Ohmic heating. A rough estimate of the thermal energy delivered to the unit area of the shell can be made by multiplying the Poynting vector by the characteristic time $\tau$ of the implosion process:

$$E_0 B_0 \tau / \mu. \tag{2.23}$$

The electric field on the surface of the shell depends on the relationship between the skin depth $h_{\text{skin}}$ and the total thickness $h$ of the shell:

$$E_0 \sim \frac{B_0 h_{\text{skin}}}{\tau} \max\left(1, \frac{h_{\text{skin}}}{h}\right). \tag{2.24}$$

We assume first that heat losses via radiation are negligible. Then, the thermal energy per unit area of the shell is

$$\frac{B_0^2}{2\mu} h_{\text{skin}} \max\left(1, \frac{h_{\text{skin}}}{h}\right). \tag{2.25}$$

This thermal energy determines the plasma pressure inside the shell. For the thickness of the skin layer we take its value at some characteristic point halfway through the implosion. Note that the estimate (2.25) provides only a general scaling law; the specific numerical factor depends on the current wave form.

If the ionization energy is small, so that the thermal energy per unit volume is of the order of the plasma pressure (later in this section, we discuss the situation in which ionization energy is significant), Eqs. (2.22) and (2.25) show that, in a quasiequilibrium state, the shell
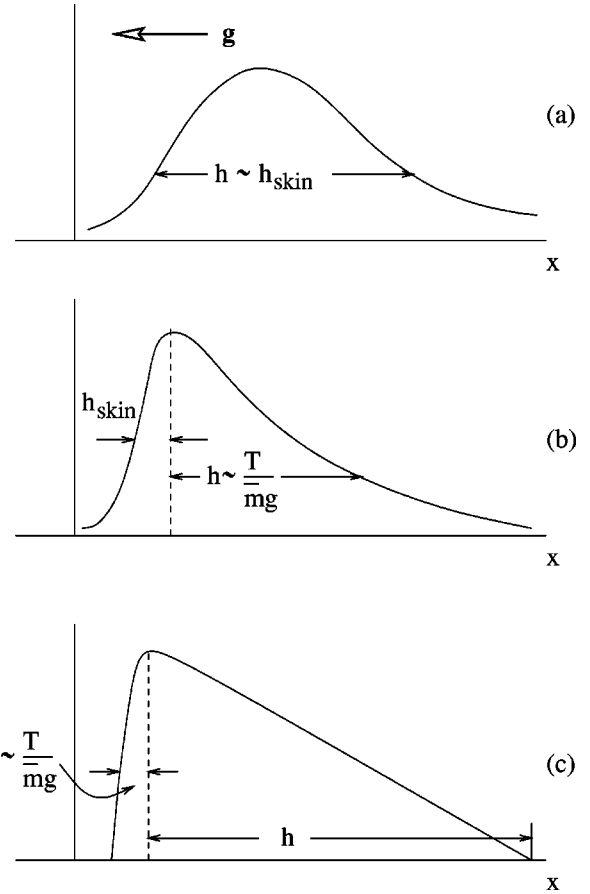


FIG. 11. Density distribution in the shell: (a) the case in which the density distribution can be characterized by a single length scale $h$; (b) thin skin layer, $h_{\text{skin}} \ll h$; (c) skin layer much thicker than the shell thickness.

thickness is necessarily of the order of the skin depth $h_{\text{skin}}$ [Fig. 11(a)].

Consider now the other possibilities. If the shell experiences some turbulent motion produced by hydrodynamic instabilities, then a new source of heating becomes available and may deliver much more thermal energy to the shell than follows from Eq. (2.25). One situation in which thermal energy may be large is an implosion of a sufficiently thick gas puff or foam annulus, when the shock wave propagates ahead of the piston and heats the plasma. When the thermal energy of the shell is considerably greater than the energy delivered by Ohmic heating, an equilibrium with the shell thickness much greater than the skin depth $h_{\text{skin}}$ becomes possible [Fig. 11(b)]. In the region beyond the skin layer, the magnetic pressure in Eq. (2.21) is negligible. At a uniform temperature and a uniform plasma composition, one then obtains the familiar exponential density distribution,

$$\rho \propto \exp(-x/h), \tag{2.26}$$

with the scale length $h$ defined as

$$h = T/\bar{m}g, \tag{2.27}$$

where $\bar{m}$ is an average atomic weight (half a proton mass for a hydrogen plasma).

The opposite limiting case is that of very fast radiative losses and/or a large ionization energy, as may be the case in a plasma of high-*Z* elements. This case is of particular interest for the shells formed from wire arrays, and we discuss it in some detail, following the general ideas of the papers by Hussey, Roderick, and Kloc (1980), Hussey and Roderick (1981), Grigor'ev and Zakharov (1987), Chukbar (1993a), and Hammer *et al.* (1996).

The thermal energy of the plasma in this case is much smaller than that determined by Eq. (2.25), leading to a corresponding decrease in the plasma temperature. At low temperatures, the skin depth becomes greater than the shell thickness, $h_{\mathrm{skin}} > h$. The axial electric field is then uniform over the shell thickness. We assume that the temperature is also uniform, providing a uniform conductivity and a uniform axial current. The latter, in turn, means that the magnetic field varies linearly over *x*. As it must vanish at the inner side of the shell (we assume that there is no axial current inside the imploding shell), we find that

$$B = B_0 \left( 1 - \frac{x}{h} \right), \tag{2.28}$$

where *h* is the shell thickness. For further analysis, it is convenient to introduce the relationship $p = s_{\mathrm{iso}}^2 \rho$, with $s_{\mathrm{iso}} = \sqrt{T/\overline{m}}$ being the speed of the isothermal sound waves. As follows from Eq. (2.27), the assumption that the skin depth is greater than the shell thickness implies that almost all the energy delivered to the shell by Ohmic heating is radiated to make the plasma pressure less than the magnetic pressure: $\rho s_{\mathrm{iso}}^2 \ll B_0^2/2\mu$. In this case, as follows from Eqs. (2.21), one automatically has $gh \gg s_{\mathrm{iso}}^2$. With this observation made, one can find the solution of Eq. (2.21) [with *B* as in Eq. (2.28)]:

$$\rho = \rho_0 \left\{ \left( 1 + \frac{s_{\mathrm{iso}}^2}{gh} \right) \left[ 1 - \exp\left( -\frac{gx}{s_{\mathrm{iso}}^2} \right) \right] - \frac{x}{h} \right\}; \quad \rho_0 = \frac{B_0^2}{\mu g h}. \tag{2.29}$$

We have taken into account that the density should become zero at $x=0$; then, at $x=h$, it is small (in the parameter $s_{\mathrm{iso}}^2/gh \ll 1$), as it should be. Our simple model does not resolve the structure of the further transition to zero density near the inner side of the shell. The density distribution (2.29) is shown in Fig. 11(c). Note that *h* now is *not* determined by Eq. (2.27), because the magnetic force is now dominant in the pressure balance.

For the solution (2.29) the mass per unit area of the shell is approximately equal to $\rho_0 h/2$; it is determined by the initial conditions of the experiment. However, Eq. (2.29) does not allow one to determine $\rho_0$ and *h* separately. The additional equation needed is provided by a condition of thermal balance, which equates Joule heating and radiative losses. This condition, generally speaking, contains a different combination of the parameters $\rho_0$ and *h* and can, therefore, serve as a second equation, provided the temperature is determined experimentally.

## III. EARLY STAGE OF THE DISCHARGE

### A. Breakdown of gas puffs

Although at present fast-*Z*-pinch research is concentrated on wire-array implosions, other fast *Z* pinches, in particular, gas puffs (see, for example, Stallings *et al.* 1979; Branitskii *et al.*, 1991, 1992a, 1992b, Deeney *et al.* 1993; Baksht, Datsko, Kim, *et al.*, 1995) and pinches with foam targets (Derzon *et al.*, 1997a) are also of a considerable interest. Therefore we start this section with the issue of initializing these types of pinches. What we present here is not a quantitative theory, but rather a broad qualitative discussion aimed at identifying the critical physics issues.

In our discussion of gas puffs, we shall present most of the numerical estimates for the density range $\sim 3 \times 10^{17}$–$3 \times 10^{18} \, \mathrm{cm}^{-3}$. We mean here peak densities, in the middle of the gas stream. Taking a representative value of $\sigma_a \sim 10^{-15} \, \mathrm{cm}^2$ for the cross section of electron scattering on atoms, one finds that the mean free path for electron scattering, $\lambda_{ea} = 1/n_a \sigma_a$, where $n_a$ is a neutral atom density, is much shorter than the typical height of the pinch. If the applied voltage were such that the energy acquired by the electron between two collisions was small compared to the ionization potential, the electron avalanches would develop quite slowly. The seed electron would experience a random walk with a superimposed average drift in the direction of the anode; its energy would gradually increase and reach the excitation threshold; at this point, with a high probability, it would lose energy through excitation and only with a small probability would reach the ionization threshold $I_{\mathrm{ion}}$ (this, incidentally, is a standard picture of gas breakdown at densities above the Paschen pressure minimum; see Meek and Craggs, 1978; Raizer, 1991). In the situation of fast *Z* pinches, where the voltage is rapidly growing, before the aforementioned process produces sufficient electron multiplication, the voltage reaches a level at which electrons acquire ionization energy between two successive collisions:

$$eE\lambda_{ea} > I_{\mathrm{ion}}, \tag{3.1}$$

where *E* is the electric-field strength. Then, a typical *e*-folding time for avalanching will be only $1/v_e n_a \sigma_i$, where $\sigma_i$ is the ionization cross section).

Before going further, we note that in gas-puff experiments the radial density distribution is relatively smooth, with a gradual transition from the nominal density inside the jet to a much lower density at the jet periphery [Fig. 1(a)]. Therefore, with the voltage growing, condition (3.1) will be first satisfied at low densities. But the density cannot be too low; in order to produce a considerable charge multiplication on its way to the anode, the electron would have to experience at least several ionizing collisions, i.e., the product $L n_a \sigma_i$ (where *L* is the anode-cathode distance) should be greater than, say, 10:

$$L n_a \sigma_i > 10. \tag{3.2}$$

Equation (3.2) imposes a lower limit on the density. At $\sigma_i \sim 3 \times 10^{-16} \, \text{cm}^2$ and $L \sim 1.5 \, \text{cm}$ the required densities are $\sim 2 \times 10^{16} \, \text{cm}^{-3}$, and this is where breakdown will occur first. The time for developing significant ionization is $\sim 10 / v_e n_a \sigma_i$ ($\sim 5$ ns at $n_a = 2 \times 10^{16} \, \text{cm}^{-3}$).

With applied voltage rapidly growing, the inequality in Eq. (3.1) will be met in the deeper layers of the jet and the ionization front will move towards higher densities. Eventually, the conductivity of the outer current-carrying shell becomes so high that the skin effect becomes important. After this time further increase of the current occurs in the outer layers of the gas puff (this skin-dominated stage of ionization has been analyzed by Vikhrev and Braginski, 1986). At this stage, further ionization of the inner layers is produced by radiation from the current-carrying shell, and, at the later stages of the implosion, by shock heating.

In gas puffs, the isodensity surfaces are usually not cylindrical but rather conical, because of the divergence of the jet (see Hussey, Matzen and Roderick, 1986). Deeney et al. (1994) and Barnier et al. (1998) developed special nozzles producing almost cylindrical jets. Superimposed on the regular flow, smaller-scale density fluctuations produced by hydrodynamic turbulence may be present. This brings additional complications to the picture of the breakdown.

In very-low-density pinches, where even the maximum density of the jet is less than roughly $10^{16} \, \text{cm}^{-3}$, the electron multiplication factor becomes insufficient [see Eq. (3.2)] and a different breakdown mechanism should come into play. It should strongly depend on the generation of electrons at the cathode (Baksht, Russkikh, and Chagin, 1997), via, probably, photoemission.

Note that, at low gas densities, even a very weak current may cause magnetization of electrons, thereby affecting the avalanching process. At a density of $10^{16} \, \text{cm}^{-3}$ the electron-neutral elastic collision frequency of, say 30-eV electrons is $3 \times 10^9 \, \text{s}^{-1}$ and becomes lower than the electron gyrofrequency at a magnetic field of only 0.015 T. In a 4-cm-diameter column such a magnetic field would be created by a current of only $\sim 1.5$ kA (!). Therefore even a relatively weak axial magnetic field (weak compared to the pinch azimuthal field at the maximum current) may affect the breakdown process and thereby the overall pinch performance. The favorable effect of an axial magnetic field $\sim 0.3$ T has been recorded in experiments by Gasque et al. (1996) and Baksht, Russkikh, and Chagin (1997). Of course, we do not claim that the bias magnetic field has no other effects on pinch physics (in particular, on the pinch stability at the later stages of the implosion, when it increases because of the radial compression). We merely emphasize that even a very weak field can influence the breakdown of gas puffs and make it more "regular."

The gas breakdown itself is a statistical process and may lead to formation of azimuthally asymmetric current-carrying channels, especially at lower densities where electrode effects become important (and bring about a new source of nonuniformities). Therefore the pre-ionization of the gas by some external source might be beneficial. This is shown in the papers of Stallings et al. (1979), Ruden et al. (1987), Baksht, Russkikh, and Fedyunin (1995), Baksht, Russkikh, and Chagin (1997), and Rousskikh et al. (1999).

The presence of a long enough prepulse may also be beneficial for creating a uniformly ionized column. The effect of the prepulse is determined by its time duration and its voltage. In particular, in Baksht, Russkikh, and Fedyunin (1995) the prepulse (1.5 $\mu$s, 1 kV) did not cause a breakdown because the axial line density $n_0 L < 3.6 \times 10^{15} \, \text{cm}^{-2}$ was well below the Paschen optimum for Ar. Such a prepulse would have caused a breakdown of Ar with a density an order of magnitude higher. Whether this would be beneficial for a further fast implosion is not clear, because during the long prepulse numerous ionization-radiation instabilities (see Sec. III.C) could develop and lead to strong perturbation of the initial state. Prepulse breakdown was reported by Smith and Dogget (1985), who also studied the current distribution of argon gas puffs with a density below $10^{16} \, \text{cm}^{-3}$ during the first 20 ns of the discharge.

## B. Breakdown of foams

As the commonly used foams of $CH_x$, $SiO_2$, and agar ($\approx CH_2O$) are insulators, the question of the time and quality of the breakdown exists for these loads, too. In particular, it is important to know whether breakdown occurs at the outer surface, or whether some discharge channels are formed in the bulk of the foam. Very little is known at the moment about these issues, so our discussion must necessarily be limited.

To be more specific, we shall discuss the breakdown of $SiO_2$ foam. The breakdown voltage for $SiO_2$ foam could be quite large. This can be understood from the following qualitative considerations. If we replaced the foam with a gas of the same average particle density, i.e., with $6 \times 10^{20} \rho_0 \, (\text{mg/cm}^3) / A$ particles per $\text{cm}^3$, the gas density would be quite high. For example, for $\rho_0 = 5 \, \text{mg/cm}^3$ and $A = 20$, the particle density would be $1.5 \times 10^{20} \, \text{cm}^{-3}$. At room temperature, this density would correspond to a pressure of approximately 5.5 atm; the Paschen product (pressure times length) would then be, roughly speaking, 1000 times higher than its optimum value for the majority of gases. This would correspond to breakdown voltages in the range of a hundred kilovolts. The high voltages needed for initiation of discharge in foam loads and the corresponding delay of the onset of current flow may cause strong leaks and even a closure of the gap in the magnetically insulating transmission line (see Fig. 3).

As soon as the voltage reaches $\sim 100$ kV, breakdown occurs. At high densities, it has a tendency to develop in the form of a narrow channel which, generally speaking, is not straight (Raizer, 1991). The energy required to ionize a breakdown channel to a singly charged state is very small. An estimate from below for this quantity is

$$W_{\text{ion}} > \pi L a_0^2 I_{\text{ion}} \rho / A m_p, \tag{3.3}$$

where $L$ is the column length, $a_0$ is its radius, $I_{ion}$ is the ionization energy, $\rho_0$ is the foam density, $m_P$ is the proton mass, and $A$ is an average atomic weight. In "practical" units,

$$W_{ion}(\text{J}) \approx 3 \times 10^3 L(\text{cm})[a_0(\text{cm})]^2 \rho_0(\text{mg/cm}^3)/A. \qquad (3.4)$$

Taking $L = 1$ cm, $a_0 = 0.05$ cm, $\rho_0 = 5$ mg/cm$^3$, and $A = 20$, one obtains $W_{ion} \approx 0.2$ J. After the first breakdown channel is formed, new breakdowns may still occur, because the inductive voltage induced in the bulk of the dielectric can be quite high until 3–5 channels are formed. So, one can expect that, after this first phase of the current pulse, the column will carry several discharge channels. Though the energy released in the breakdown is very small compared to the total energy delivered to the pinch during the whole implosion process, the consequences of the formation of nonaxisymmetric breakdown channels can be quite severe because a channel will have a density different from that of the external medium and will serve as a strong perturbation during the magnetohydrodynamic phase of the implosion. The appearance of thin breakdown channels in fiber pinches with dielectric (frozen deuterium) fibers was discussed by Meierovich and Sukhorukov (1991).

In a state of single ionization, the plasma should have a temperature of 2 to 3 eV. This would correspond to a relatively low magnetic diffusivity (Huba, 1994), $D_M \sim 5 \times 10^5$ cm$^2$/s. With this diffusivity, the resistive broadening of the current channel should be slow (for $t = 10$ ns the broadening would be $\sim 1$ mm). In other words, as soon as several highly conducting channels are formed, the initial current will be trapped in them. With continuing ionization of the column, further current buildup will occur in a thin skin layer at the surface of the column. But, as we have already emphasized, the initial current will remain trapped within several narrow channels inside the column. The presence of this current will cause some distortions of the equilibrium; the trapped magnetic field will grow proportionally with convergence. Formation of several channels was observed in experiments with gaseous liners at the Angara-5-1 facility (Volkov, Utyugov, and Frolov, 1993). The reason for their formation and persistence during the whole implosion event could be just the one suggested above.

An ideal situation would be, of course, production of breakdown uniformly over the surface of the cylinder and interception of so much current that the voltage drop inside the cylinder becomes insufficient to produce any internal breakdowns. In this sense, an interesting option is the use of a thin conducting coating. The coating should not necessarily be thicker than the skin depth. What is sufficient (and relatively easily achievable even for metal coatings with a thickness of the order of a fraction of a micron) is that the $L/R$ time of the circuit be considerably greater than 10–20 ns. There is experimental evidence that conductive coatings and a prepulse have a favorable effect on the quality of the discharge (Nash et al., 1997a).

The presence of a prepulse can have a considerable effect on the breakdown of the coated foam. Even if the voltage during the prepulse is in the range of only a few kilovolts, it is sufficient, in the time frame of $\sim 1$ $\mu$s, to fully evaporate the conducting coating. Depending on the voltage and the prepulse length, the evaporated material can expand by up to a few millimeters. The conductivity of this relatively cold vapor will be low and, probably, insufficient to shield the liner inductively. On the other hand, the presence of a gaseous corona around the foam load may turn on the same breakdown mechanism as in the case of gas puffs (Sec. III A). A small axial magnetic field ($\sim 0.3$ T) may be beneficial in producing a more symmetric current-carrying shell.

The aforementioned scenario in which the coating is evaporated without ionization corresponds to just one possible shape of the prepulse, with a long "pedestal" of a low voltage. If the prepulse is shorter, with a higher voltage, then a fast transition from vapor to a highly ionized plasma may occur.

The effect of a current prepulse on the explosion of a single carbon fiber was studied by Lebedev et al. (1998a) and Aliaga-Rossel et al. (1998). During the first 80 ns after arrival of the main pulse, the fiber exposed to a prepulse showed a less-developed coronal plasma; later on, the differences between the wires exposed and not exposed to a prepulse became insignificant. Mosher et al. (1998) reported a better uniformity of discharges in preheated white-hot wires.

### C. Thermal instabilities; filamentation and striations

It has been known since the mid 1980s that, early in the pulse, surface layers of the gas-puff pinch experience fast instabilities that cause formation of bright stripes perpendicular to the axis and (usually later) parallel to the axis. We call the first of these "striations" and the second "filaments." Such patterns have been clearly observed, for instance, in a study by Branitskii et al. (1991) at the Angara-5-1 facility (Fig. 12). In this particular experiment the maximum current was 3 MA, the voltage was 0.4–0.6 MV, and the current rise time was $\sim 100$ ns. The loads were usually Xe gas puffs with a height of 1 cm, an initial diameter of 3 cm, and a mass per unit length of $\sim 0.1$ mg/cm. Ripples with a wavelength $\sim 1$ mm were formed immediately after arrival of the current pulse and were gradually replaced by filamentary structure with the same wavelength; these filaments persisted halfway to the current maximum. Azimuthal instabilities were not affected by replacing Xe with Ne.

These modes develop very rapidly compared to Rayleigh-Taylor instability and should have a different nature. They are usually identified with thermal instabilities in which, once the temperature in some fluid element increases or decreases, it continues to increase or decrease. Possible causes of such behavior are an increase in radiation losses at decreasing temperatures and positive feedback in the Joule heating. In its "pure" form this instability does not require mass redistribution
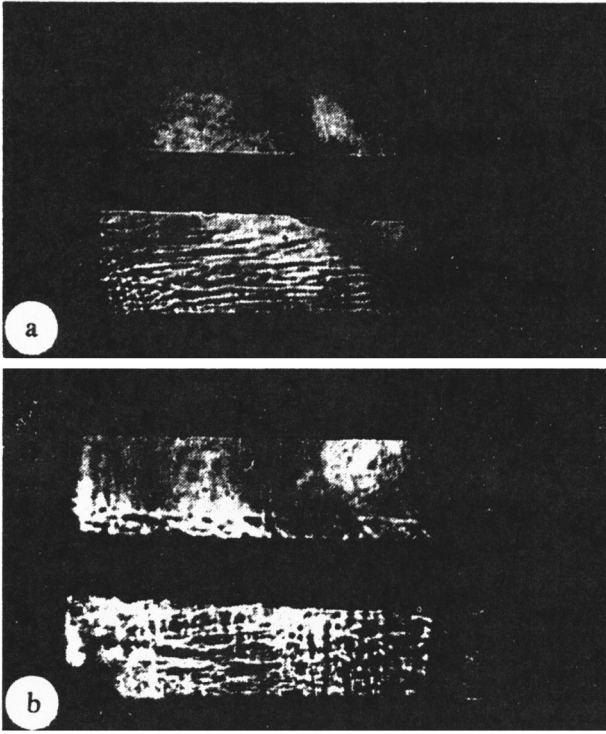
FIG. 12. Laser shadowgraphs of a Xe liner implosion at the Angara-5 facility (Branitskii *et al.*, 1991, reprinted with kind permission of V. Smirnov). The frames are separated by 30 ns; the current was 1.6 MA. The axis of the discharge is vertical. The cathode is at the bottom. The anode (a thick dark strip in the middle of the figure) was made of a mesh, so that the plasma penetrates beyond the anode and produces some perturbations there.

and may occur at times that are short compared to the acoustic time for the spatial scale of the instability (Afonin, 1995).

If the parameters of the system are such that the growth rate of thermal instability becomes comparable to the growth rate of Rayleigh-Taylor instability, the two instabilities become strongly coupled. Such a situation was discussed by Imshennik and Neudachin (1987, 1988). In the absence of gravity (and hence the Rayleigh-Taylor instability), the slow thermal instability gets coupled with acoustic motions. This instability can be called "radiative-condensation instability" because of the formation of clumps of colder matter at its nonlinear stage (Aranson, Meerson, and Sasorov, 1993). Various aspects of these instabilities have been considered by Velikhov *et al.* (1972), and Haines (1974).

We discuss these instabilities here for the case in which the thickness of the cylindrical conducting shell is much less than the skin depth and in which the mechanical motions of the shell can be neglected ("fast" thermal instability). First, by solving Maxwell's equations we relate the current perturbation to the perturbation of the resistivity, and then we plug this perturbation into the thermal balance equation.

The properties of a thin shell can be characterized by the "surface conductivity" $\sigma_s$, which is the product of the shell thickness and the conductivity proper, or by a "surface resistivity" $\eta_s \equiv 1/\sigma_s$. The surface current can be presented as

$$\mathbf{J}_t = \mathbf{E}_t / \eta_s, \tag{3.5}$$

where $\mathbf{E}_t$ is the tangential component of the electric field. For perturbations, one has

$$\delta\mathbf{J}_t = \delta\mathbf{E}_t / \eta_s - (\delta\eta_s / \eta_s^2)\mathbf{E}_t, \tag{3.6}$$

where the sign "$\delta$" designates the perturbations, and the unperturbed quantities do not bear this sign. As we are going to consider perturbations with scale lengths shorter than the shell radius, we replace the cylindrical geometry by a planar one, with the $x$ axis corresponding to the radial coordinate, and the $y$ axis corresponding to the azimuthal coordinate. In the unperturbed state, the current and the electric field have only $z$ components, while the magnetic field has only a $y$ component. The unperturbed magnetic field is zero inside the shell (in our geometry, at $x<0$).

As there are no currents outside the shell, the magnetic field there is curl free and can be represented as a gradient of some scalar function $\psi$, $\delta\mathbf{B} = -\nabla\psi$. This function satisfies the Laplace equation $\nabla^2\psi = 0$. We consider perturbations of the form $\exp(\Gamma t + ik_y y + ik_z z)$, where Re$\Gamma$ is a growth rate. In addition to the Laplace equation for $\psi$, we shall need the $x$ component of Faraday's law,

$$ik_y \delta E_z - ik_z \delta E_y = -\Gamma \delta B_x. \tag{3.7}$$

The solution of the Laplace equation for the $x>0$ ($x<0$) half space reads as

$$\psi_\pm = A_\pm \exp(\mp kx), \tag{3.8}$$

where $k = \sqrt{k_y^2 + k_z^2}$. We need to supplement these equations with the boundary conditions at the $x=0$ surface: the continuity of the normal component of the magnetic field [this yields $A_+ = -A_-$ in Eq. (3.8)], and the jump condition for the tangential components of the magnetic field in terms of the surface current (3.6). Using these conditions, after some elementary algebra one finds the following expression for the perturbation of the current:

$$\delta J_z = -J_z \frac{k_y^2}{k^2} \frac{1}{1 + (\Gamma/\Gamma_0)} \frac{\delta\eta_s}{\eta_s}, \tag{3.9}$$

where $1/\Gamma_0$ is a characteristic decay time for the current perturbations,

$$\Gamma_0 = \frac{2k\eta_s}{\mu} \equiv \frac{2k\eta}{\mu h}, \tag{3.10}$$

where $h$ is the shell thickness. The $y$ component of the current perturbation is $\delta J_y = -(k_z/k_y)\delta J_z$, and $k_y$ is related to the azimuthal mode number $m$: $k_y = m/r$. It is also convenient to introduce the angle $\alpha$ between the unperturbed magnetic field and the wave vector: $\sin\alpha = k_z/k$. Note that, according to Eq. (3.9), for highly conductive shells, where the resistive decay time is very long compared to the time of the process, the relative current perturbation $\delta J_z/J_z$ can be small even for considerable perturbation of the resistivity, $(\delta\eta_s/\eta_s)\sim 1$.

Now we turn to the equation for thermal balance. It can be presented in the form

$$\dot{Q}(T) = \eta_s(T)J^2 - q(T), \tag{3.11}$$

where $Q$ is the plasma-energy content per unit area of the shell and $q$ is the power loss (radiation) per unit area. The equilibrium state corresponds to a balance of the two terms on the right-hand side:

$$\eta_s(T_0)J^2 - q(T_0) = 0. \tag{3.12}$$

The equation for the temperature perturbation, with the equilibrium condition (3.12) taken into account is

$$C_V \frac{\partial \delta T}{\partial t} = 2q \frac{\delta J_z}{J_z} + q \frac{\eta_s'}{\eta_s} \delta T - q' \, \delta T, \tag{3.13}$$

where the prime designates the derivative of the corresponding quantity with respect to the temperature, and $C_V$ is the heat capacity per unit area of the shell. Using Eq. (3.11), one then obtains the dispersion relation

$$\Gamma = \frac{q \, \eta_s'}{C_V \eta_s} \left[ 1 - \frac{2 \cos^2 \alpha}{1 + (\Gamma/\Gamma_0)} \right] - \frac{q'}{C_V}. \tag{3.14}$$

Instead of exactly solving this (quadratic) equation, we present a qualitative discussion of possible instabilities in some limiting cases. One extreme case is that of a strong temperature dependence of the heat losses and a weak temperature dependence of the resistivity. In this case, one can neglect the first term on the right-hand side of Eq. (3.14). The remaining term predicts an instability of $q' < 0$, in other words, if the radiative losses decrease with a temperature increase. This may happen in an optically thin plasma dominated by free-bound radiation or by line radiation in which some strong transitions disappear with increasing temperature because of a change in the ionization state.

In the opposite limiting case, in which the temperature dependence of the resistivity is dominant, one can neglect the last term on the right-hand side. Instabilities present in this case are driven by the temperature dependence of the resistivity. Somewhat paradoxically, these instabilities are present for either sign of $\eta_s'$; the sign determines their spatial structure. At $\eta_s' > 0$, to make the right-hand side as large as possible (at $\Gamma$ positive), one has to choose $\alpha = \pi/2$ ($m = 0$). In other words, the fastest growing modes at a positive temperature dependence of the resistivity are the axisymmetric modes ("striations"). At $\eta_s' < 0$, the most unstable modes correspond to $\alpha = 0$, in other words, to the purely azimuthal perturbations. For them one has (with $q' = 0$)

$$\Gamma = \frac{q|\eta_s'|}{C_V \eta_s} \frac{1 - (\Gamma/\Gamma_0)}{1 + (\Gamma/\Gamma_0)}. \tag{3.15}$$

The largest growth rate corresponds to $\Gamma_0 \to \infty$, or, according to Eq. (3.10), to large $m$ number (thin filaments stretched along the axis). Our simple model does not include the thermal conductivity along the surface of a layer. If included, it would limit from below the size of both striations and filaments.

The positive dependence of resistivity on temperature is typical for low temperature, where the degree of ionization grows and electron-neutral collisions are replaced by Coulomb collisions with much higher cross sections. Accordingly, striations should form predominantly at the early stage of the pulse. This instability, as well as the other thermal instabilities, can reach a strongly nonlinear stage. They will eventually cause redistribution of matter (the process that we have not included into the analysis presented above). Such nonlinear structures may exist much longer than $\eta_s'$ is positive and may seed the Rayleigh-Taylor instability.

The negative dependence of resistivity on temperature takes over later, when the plasma becomes singly ionized. Therefore filamentation should develop later than striations, in agreement with the aforementioned experimental data by Branitskii *et al.* (1991) (Fig. 12). The presence of azimuthally asymmetric structures in the foam loads was recorded on the Saturn device (Lazier *et al.*, 1997), although in this case their appearance might also have been caused by a discrete azimuthal structure of the return-current conductor.

## D. Early stage of a wire-array discharge; merging of wires

The driving of pulsed currents through single metal wires and dielectric fibers has been the subject of numerous experimental studies[2] and theoretical analyses.[3]

An important feature of the discharge in a single wire is that the wire core, at least for thick wires, may remain cold and expand very slowly. The core is surrounded by a plasma "corona" that contains only a small fraction of mass but carries almost all the current. This conclusion was made in the paper by Aranchuk *et al.* (1986) specifically devoted to experimental studies of single-wire explosions [see also an earlier paper by Aranchuk, Bogolyubskii, and Tel'kovskaya (1985)]. They found that, in explosions of 20-$\mu$m-diameter copper wires, only 2–7% of the total mass was carrying the current and radiating. The rest of the mass remained cold. This corona was subject to violent unstable motions, while the core remained more or less cylindrical. The maximum current through the wire was 0.5 MA, and the current rise time was approximately 100 ns. The halo plasma can be formed because of desorption during a prepulse (a point made by Bartnik *et al.* 1990) or just because of the evaporation of the whole wire. This relatively low-density halo provides better conditions for the breakdown (cf. Sec. III.A). A strong effect of wire cleanliness on formation of the corona was reported by Bartnik

---

[2]See, for example, Skowronek and Romeas (1985), Aranchuk *et al.* (1986), Sethian *et al.* (1987), Bartnik *et al.* (1990), Mosher and Colombant (1992), Sarkisov and Etlicher (1995), Sarkisov *et al.* (1995), Sarkisov, Shikanov, *et al.*, 1995a, Beg *et al.* (1997), Aliaga-Rossel *et al.* (1998).

[3]See, for example, Coppins *et al.* (1988), Rosenau *et al.* (1988), Bud'ko, Liberman, and Kamenets (1990), Neudatchin and Sasorov (1991), Sasorov (1991) and Bobrova *et al.* (1992).

et al. (1994). A long-lasting core of the exploded wire was observed by Kalantar and Hammer (1993). Sarkisov, Etlicher et al. (1995) and Sarkisov, Shikanov et al. (1995a) detected a thick core in explosions of 20-$\mu$m copper wires; they used absorption of the 532-nm laser light to detect the evolution of the exploding wire. Beg et al. (1997) performed a very detailed study of explosions of carbon (7- and 33-$\mu$m diameter) and aluminum wires (25-$\mu$m diameter) at the maximum current of ~100 kA and a current rise time of 55 ns. For the thicker wires, the core existed at least until the current maximum, whereas for the 7-$\mu$m carbon wire it disappeared within ~10 ns [we note in passing that the paper by Beg et al. (1997) contains a wealth of information on wire pinches, including detailed characterization of the instabilities in coronal plasma, and detection of electron beams]. Detailed numerical simulations of the development of the $m=0$ instability have been recently published by Chittenden et al. (1997). One theory attributes formation of the corona to Ohmic heating of the low-density plasma due to anomalous resistivity (Sasorov, 1991; Haines et al. 1996). We shall return to this issue in Sec. VII.A. Afonin (1999) has studied a 1D model of a wire explosion accounting for the changes of the resistivity during transition from metal to liquid, and to a weakly ionized gas, and corresponding changes of the skin thickness. His model also predicts the halo formation.

The behavior of the plasma corona of the wires assembled in a cylindrical array is very different from that of separate wires, because of the presence of a strong common magnetic field. A curious feature of such arrays is that the common magnetic field near the surface of the wire array is $\mu I/2\pi r$, where $r$ is the array's radius. The magnetic field produced by a certain wire at the location of its closest neighbor (i.e., at a distance $2\pi r/N$, where $N$ is the number of wires in the array) is $\mu I/(2\pi)^2 r$, i.e., universally smaller by a factor of $2\pi$ than the common field.

This common field accelerates the light coronal plasma towards the center of the array and therefore there is reason to believe that the current will be forced to flow in the wire cores. This assumption is supported by the fact that the dynamics of a wire-array implosion correspond, to good accuracy, to a model in which the whole mass of the wire array is involved in the implosion, at least for a sufficiently large number of wires in the array (see Sanford et al., 1999a, 1999b). The systematic study carried out in these papers on the effect of number of wires on the pulse width of the radiation emission also points to a significant decrease in precursor plasma for a large number of wires. There is good agreement of the radiation pulse with simulations based on the assumption that all of the wire mass is involved in the implosion (see, for example, Fig. 11 in Spielman et al., 1998). It should be noted that, for a smaller number of thicker wires, the effect of current interception by the coronal plasma may be significant, with a large amount of blow-off plasma accelerated to the center of the array (Aivazov et al., 1988; Lebedev et al. 1998b, 1999; see also numerical simulations by Chittenden et al., 1999).

Limiting ourselves to the case of a large number of wires, we assume that essentially all of the mass of the wire is involved in hydrodynamic motions. As is well known (see Kadomtsev, 1966; Bateman, 1980), a wire is unstable with respect to magnetohydrodynamic (MHD) sausage and kink modes. For perturbations with wavelengths exceeding the wire radius, $k_z < r_W^{-1}$, growth rates are

$$\Gamma \sim \sqrt{\frac{B_w^2 k_z^2}{\mu(\hat{m}/N\pi r_w^2)}}, \tag{3.16}$$

where $B_w$ is the magnetic-field intensity at the surface of the wire (we ignore the factor of 2–3 difference between the growth rates of the kink and sausage modes). Numerical results pertaining to specific radial profiles of the current and the density can be found, for example, in Felber (1982) and Pereira, Rostoker, and Pearlman (1984).

As stated above, we assume that all of the wire mass is involved in the hydrodynamic motion. The modes with $k_z \sim 1/r_w$, where $r_w$ is the instantaneous radius of an individual wire, create perturbations randomly distributed over the wire length and cause a gradual broadening of the wire (an increase in the effective $r_w$). Assuming that the growth rate of short-wave perturbations is large compared to the characteristic times involved in the problem (so that the perturbations reach a nonlinear state), the expansion velocity is independent of initial perturbations. In this regime the expansion velocity can be evaluated (in particular from dimensional considerations) as $v \sim \Gamma r_w$. Using expression (3.16) and noting that $B_w = \mu I/2\pi N r_w$, one finds

$$v \sim I\sqrt{\frac{\mu}{4\pi\hat{m}N}}. \tag{3.17}$$

In "practical" units,

$$v(\text{cm/s}) \sim \frac{3\times10^6 I(\text{MA})}{\sqrt{N\cdot\hat{m}(\text{mg/cm})}}. \tag{3.18}$$

Solving the equation $\dot{r}=v$ with $I$ as in Eq. (2.6), one finds that $r_w$ reaches half of the interwire gap, $\pi r/N$, at

$$\frac{1}{\tau} \sim 15\left[\frac{\hat{m}(\text{mg/cm})}{N}\right]^{1/6}\left[\frac{r(\text{cm})}{\tau(\text{ns})I_0(\text{MA})}\right]^{1/3}. \tag{3.19}$$

For a wire array with the "standard" Z parameters, $t/\tau$ is ~0.5. Therefore development of MHD instabilities in the wires can, in principle, cause an early merging of the wires. Note that at $t/\tau \sim 0.5$ the current in the wires attains only a quarter of its maximum value, and the array's diameter experiences only a very small change. This is why we neglected the change of $r$ in the preceding discussion. In a more sophisticated version of this analysis, one should take convergence into account.

If the MHD mechanism of wire merging is indeed the dominant one, one can make some predictions with re-

gard to the initial state of the liner thus formed; it will be grossly nonuniform, with the spatial scale of the nonuniformities of the order of half the interwire distance. These nonuniformities will be both axial and azimuthal. This observation may be of some value for numerical simulations of Rayleigh-Taylor instability of the type carried out by Peterson *et al.* (1996, 1997, 1999). In a model suggested by Haines (1998), the perturbations developing in the wires are assumed to be uncorrelated. Based on this assumption, Haines comes to the conclusion that the amplitude of macroscopic axisymmetric perturbations (which has to be obtained by averaging over the azimuth), should scale as $N^{-1/2}$, with $N$ being the number of wires in the array. Experimentally, an increase in the number of wires had a favorable effect on the implosion symmetry (Sanford *et al.*, 1996, Deeney, Nash, *et al.*, 1997, 1998). The authors of these papers relate improved performance to early formation of a continuous shell in the case of a large number of wires (see also a more recent study by Sanford *et al.*, 1999a, 1999b).

In summary, the merging of wires most probably occurs in a turbulent fashion, with development of perturbations on a scale of the order of the instantaneous wire radius. When merging occurs, the shell thus formed has a thickness of the order of the interwire distance and nonuniformities of the same scale. The amplitude of nonuniformities is of the order of 1. This sets the stage for the further evolution of the liner, in which two competing processes occur: smoothing out of the inhomogeneities by virtue of hydrodynamic motions and thermal conductivity, and enhancement of those modes that are Rayleigh-Taylor unstable.

## IV. HYDRODYNAMIC STABILITY OF AN IMPLODING LINER

The Rayleigh-Taylor instability plays an important role in essentially all high-energy-density experiments, including experiments with fast $Z$ pinches and ICF capsules. This instability is universal and very difficult to stabilize. It is a key factor in limiting the performance of fast $Z$ pinches and other pulsed-power devices. As one might expect, there are hundreds of publications devoted to the study of this instability in general and its occurrence in pulsed-plasma systems in particular. We shall certainly not be able to cover all the relevant results in this relatively compact paper. The interested reader can find further references in the surveys by Sharp (1984), Kull (1991), and Lindl (1995), the latter survey considering specifically the physics of ICF capsules. A summary of experimental results for ICF capsules was given by Kilkenny *et al.* (1994). As a good general introduction, we recommend Chandrasekhar's book (1961), which, however, deals only with incompressible systems.

In this section we discuss the instability of an ideal fluid, without accounting for dissipative processes like viscosity, thermal conductivity, and electrical resistivity in the body of the fluid (although we allow for the pres-

ence of shock waves, which are, of course, dissipative structures). Dissipative effects are discussed in Sec. V.

Generally, theoretical analysis of the magnetic Rayleigh-Taylor instability involves very lengthy calculations that are beyond the scope of this survey. Still, to give the reader the background to follow some important arguments more closely, we present a complete derivation of the growth rates for one relatively simple system: a slab of a uniform, incompressible, perfectly conducting fluid supported from below by a horizontal magnetic field (Harris, 1962). After that, mostly on the qualitative level, we shall add new elements to the picture of stability.

One should remember that, in implosions of thick metal shells of the type used by Degnan *et al.* (1995), the structural strength of the material can have a considerable stabilizing effect early in the implosion process. This effect has not yet been studied in great detail and we shall not discuss it below. Some further information and pertinent references can be found in Ruden and Bell (1997); experimental data were presented by Atchinson *et al.* (1997).

### A. Stability of a slab of an incompressible fluid

The geometry of the problem is illustrated by Fig. 10: the slab thickness is $h$, the force of gravity is directed downward in the $x$ direction, with $\mathbf{g_x} = -\mathbf{e_x}g$ and $g>0$; the unperturbed magnetic field $B$ occupies the lower half of the space, $x<0$, and is parallel to the axis $y$. In the geometry of a cylindrical implosion of a thin shell, $x$ corresponds to the radial coordinate (directed in this case to the axis), $y$ corresponds to the azimuthal ($\theta$) coordinate, and $z$ to the axial coordinate. The unperturbed magnetic field that supports the slab is related to the gravity and fluid density as

$$\rho g h = \frac{B^2}{2\mu} \equiv p_m,  \qquad (4.1)$$

where we use the notation $p_m$ to designate the magnetic pressure.

As the unperturbed state does not depend on time or the coordinates $y$ and $z$, one can seek solution of the problem in the form of harmonic perturbations in these variables, i.e., in the form $f(x)\exp(-i\omega t+ik_y y+ik_z z)$. The instability corresponds to Im $\omega>0$. Sometimes, instead of $\omega$, one uses the growth rate,

$$\Gamma = -i\omega. \qquad (4.2)$$

The linearized hydrodynamics equations are

$$-\omega^2\rho\boldsymbol{\xi} = -\nabla\delta p \quad \text{and} \qquad (4.3)$$

$$\nabla\cdot\boldsymbol{\xi} = 0, \qquad (4.4)$$

where $\boldsymbol{\xi}$ is the displacement of the fluid element with respect to its unperturbed position, and $\delta p$ is the pressure perturbation. These equations yield $\nabla^2\delta p=0$, with the solution

$$\delta p = A\exp(kx) + B\exp(-kx), \qquad (4.5)$$

where

$$k=\sqrt{k_x^2+k_y^2} \tag{4.6}$$

and where $A$ and $B$ are arbitrary constants. One finds then from Eq. (4.3) that

$$\xi_x=\frac{k}{\rho\omega^2}[A\exp(kx)-B\exp(-kx)]. \tag{4.7}$$

At the upper and lower boundaries of the slab, one should impose boundary conditions of the pressure balance at the perturbed boundary. These conditions are

$$\delta p-\rho g\xi_x=0, \text{ for the upper boundary and} \tag{4.8}$$

$$\delta p-\rho g\xi_x=\delta p_m, \text{ for the lower boundary,} \tag{4.9}$$

with $\delta p_m=B\,\delta B_y/\mu$. To find the magnetic-field perturbation at a perfectly conducting surface, one should use the condition that the magnetic field has a zero normal component at the surface, or, in other words, that

$$\mathbf{n}\cdot\delta\mathbf{B}+\mathbf{B}\cdot\delta\mathbf{n}\equiv-\delta B_x+B\,\delta n_y=0, \tag{4.10}$$

where $\mathbf{n}$ is the unperturbed outer normal to the lower surface, $\mathbf{n}=(-1,0,0)$, and $\delta n_y=\partial\xi_x/\partial y=ik_y\xi_x$. Perturbation of the vacuum magnetic field is curl free, whence

$$\delta\mathbf{B}=-\nabla\psi. \tag{4.11}$$

where $\psi$ is a scalar potential. It satisfies the Laplace equation,

$$\nabla^2\psi\equiv\frac{\partial^2\psi}{\partial x^2}-k^2\psi=0. \tag{4.12}$$

Its solution, evanescent at $x\to-\infty$, is

$$\psi=C\exp(kx), \tag{4.13}$$

where $C$ is another arbitrary constant. Substituting this solution into Eq. (4.11) to find $\delta B_x$, substituting the resulting expression for $\delta B_x$ into Eq. (4.10) to express $C$ in terms of the value of $\xi_x$ at the lower boundary, and returning to Eq. (4.11) to express $\delta B_y$ in terms of $\xi_x$, one finds that the magnetic pressure perturbation $\delta p_m=B\,\delta B_y/\mu$ at the lower boundary is

$$\delta p_m=-2\frac{k_y^2}{k}p_m\xi_x. \tag{4.14}$$

This equation shows that magnetic pressure increases or decreases at the bumps ($\xi_x<0$) or dips ($\xi_x>0$) of the sinusoidally perturbed surface. This can also be rephrased as a statement that the magnetic-energy perturbation is positive, thereby providing a stabilizing effect (the perturbation of the gravitational energy, for unstable perturbations, is negative).

Using Eq. (4.14) and substituting solutions (4.5) and (4.7) into the boundary conditions (4.8) and (4.9), one finds two linear homogeneous equations for the constants $A$ and $B$. From the condition that the determinant of this set of equations is zero, one obtains the following dispersion relation for the eigenfrequencies of the problem:

$$\left(\frac{\omega^2}{kg}\right)^2-\frac{2k_y^2h}{k}\frac{1+\exp(-2kh)}{1-\exp(-2kh)}\frac{\omega^2}{kg}-1+\frac{2k_y^2h}{k}=0. \tag{4.15}$$

Introducing an angle $\alpha$ between the magnetic field and the wave vector,

$$\cos\alpha=k_y/k, \tag{4.16}$$

one can present the roots of this dispersion relation as

$$\begin{aligned}\frac{\omega^2}{kg}&=kh\cos^2\alpha\,\frac{1+\exp(-2kh)}{1-\exp(-2kh)}\\&\pm\left\{\left[kh\cos^2\alpha\,\frac{1+\exp(-2kh)}{1-\exp(-2kh)}\right]^2\right.\\&\left.+1-2kh\cos^2\alpha\right\}^{1/2}.\end{aligned} \tag{4.17}$$

The plus sign corresponds to a stable root. The nature of a stable mode becomes particularly clear in the limit $k\to\infty$, where the eigenmode corresponding to this root is strongly localized near the upper surface, with $A/B$ in Eq. (4.5) becoming of the order of 1 [this means that, near the upper surface, the second term in Eq. (4.5) is exponentially small compared to the first one]. The stable mode is an analog of the gravity wave on the surface of a fluid (see, for example, Landau and Lifshitz, 1987). At smaller $k$, the eigenfunction of this mode encompasses the whole layer but is still somewhat more concentrated near the upper surface, where the gravity force is directed towards the fluid, so that the stabilizing contribution dominates.

The second root corresponds to a mode that can be stable or unstable, depending on the wave number $k$. The mode is unstable at small $k$'s and stable at large $k$'s. The critical wave number $k_0$ at which the mode becomes stable, is

$$k_0=\frac{1}{2h\cos^2\alpha}. \tag{4.18}$$

For $\alpha\sim45°$ the critical wave number is of the order of $h^{-1}$. At large $k$'s, the magnetic-energy perturbation (positive) overbalances the gravitational-energy perturbation (negative, for a mode localized near the lower surface), whence the stability at large $k$'s.

For perturbations with $\alpha=\pi/2$, however, the system is unstable at all $k$'s. A perturbation with $\alpha=\pi/2$ is sometimes called a flute mode. Its remarkable feature is that it does not perturb the vacuum magnetic field and therefore the positive (stabilizing) contribution of the magnetic-energy perturbation vanishes. In cylindrical geometry this mode corresponds to axisymmetric perturbations, with no dependence on the azimuthal angle $\theta$.

At small $k$'s the growth rate reduces to

$$\Gamma=\sqrt{kg[\sqrt{1+\cos^4\alpha}-\cos^2\alpha]} \tag{4.19}$$

and becomes independent of the thickness of the layer. For these large-scale perturbations the layer can be considered as a structureless, infinitesimally thin gravitating sheet. The overall dependence of the growth rate [Eq. (4.17)] on the wave vector for several values of $\alpha$ is shown in Fig. 13. At $\alpha=0$ (a purely azimuthal mode in
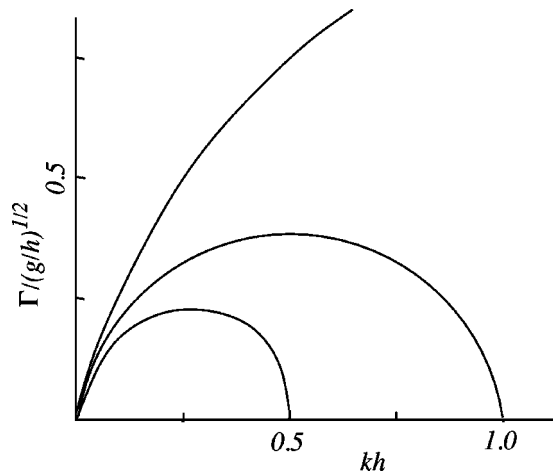
FIG. 13. Growth rates for several values of the propagation angle $\alpha$; the values of $\alpha$ are $\pi/2$, $\pi/4$, and 0 (from the top to the bottom curve).

the cylindrical geometry) the growth rate is equal to $\sqrt{kg(\sqrt{2}-1)}$ (see, Harris, 1962; Kleev and Velikovich, 1990).

These results pertain to stepwise density distributions. A broader class of density distributions of incompressible fluids has been studied by Munro (1988). If the lower surface of the fluid is free, then there exist modes with the growth rate $(kg)^{1/2}$. At large $k$ they are strongly localized near the interface and have a large growth rate. If, however, the transition is smooth enough, the growth rate is limited from above. Some further discussion of these modes can be found in Inogamov (1985), Bychkov, Liberman, and Velikovich (1990), and Bud'ko et al. (1989).

### B. Effects of compressibility

The most important new element that emerges from finite compressibility is the presence of propagating acoustic waves. Various aspects of the Rayleigh-Taylor instability in compressible fluids have been widely discussed.[4] We discuss here a slab of plasma whose temperature in the unperturbed state is constant, supported from below by a uniform magnetic field in a geometry identical to that shown in Fig. 10, under the assumption of perfect plasma conductivity and a vanishingly thin transition layer between the plasma and the magnetic field. Later, in Sec. IV.C, we address issues related to a finite thickness of the transition layer.

If the composition of the plasma does not change in the vertical direction, then plasma density and pressure follow an exponential dependence [Eq. (2.26)], $p$, $\rho$ $\propto \exp(-x/h)$ with a scale length $h$ determined by Eq.

_____

[4]See, for example, Catto (1978), Bernstein and Book (1983), Parks (1983), Landau and Lifshitz (1987), Gratton, Gratton, and Gonzales (1988), Lezzi and Prosperitti (1989), Gonzales and Gratton (1990), Budko and Liberman (1992), Ryutov and Toor (1998).

(2.27). It turns out that the problem in the case of a sharp plasma-vacuum transition has an exact solution (Bernstein and Book, 1983, Parks, 1983, Gratton, Gratton, and Gonzales, 1988). When acoustic waves (that are present now in a fluid) propagate in a plasma with exponentially decreasing density (as is the case in a constant-temperature slab supported from below), their amplitude grows exponentially. Therefore in the perturbation analysis one must allow for the presence of solutions growing exponentially in the vertical direction; it would be incorrect to constrain the solution to an exponential decrease. Further details related to this issue can be found in a comprehensive analysis by Gratton, Gratton, and Gonzales (1988).

A dispersion relation for unstable modes can be conveniently presented in the form derived by Ryutov and Toor (1998). Using the same notation as in Sec. IV.A, one can write this relation as

$$\omega^4 - k^2g^2 + 2\cos^2\alpha\,kg\left[\omega^2\left(2\cos^2\alpha\,\frac{kgh^2}{s^2}-1\right)\right.$$
$$\left. + 2k^2gh(1-kh\cos^2\alpha)\right] = 0, \qquad (4.20)$$

where

$$s^2 = \frac{\gamma p}{\rho} = \frac{\gamma T}{\bar{m}} = \gamma gh \qquad (4.21)$$

is the speed of sound. Its unstable solution behaves in much the same manner as the solution of Eq. (4.15): at small $k$'s ($kh \ll 1$) the growth rate is determined by the same expression as for the incompressible fluid, i.e., by Eq. (4.19). At larger $k$'s it decreases and becomes zero at some critical $k = k_0$, which is exactly the same as Eq. (4.18).

Formally, Eq. (4.20) has unstable solutions even at $k > k_0$. However, these solutions correspond to modes whose amplitude grows in the vertical direction faster than $\exp(x/2h)$, so that the energy density diverges at large $x$. One this basis, Gratton, Gratton, and Gonzales (1988) correctly consider these solutions to be unphysical. What happens with perturbations at $k > k_0$ can be more clearly demonstrated by an analysis of the initial-value problem based on the use of the Laplace transform: if one stirs the plasma near the lower boundary and creates there perturbations with spatial scales much smaller than $1/h$, then a part of the perturbation is radiated as acoustic waves in the upward direction, and a part stays near the boundary as a stable surface wave.

Let us discuss in further detail the reason why, at small $k$'s, the scale height $h$ drops out from the dispersion relation so that all information on the structure of the plasma slab disappears from the dispersion relation; the speed of sound also disappears. First one notes that the sound speed $s$ is related to the other parameters of the problem through Eq. (4.21). The sound propagation time over the distance $\sim 1/k$ is $1/ks$. Using Eq. (4.21), one can easily show that for long enough perturbations with $k < k_0 \sim 1/h$, the instability $e$-folding time ($\sim 1/\sqrt{kg}$) becomes shorter than the sound-propagation

time $(1/ks)$. Basically, this means that the parts of the slab that are separated by a distance exceeding $1/k_0$ cannot communicate with each other by acoustic signals propagating inside the slab; therefore they evolve independently of each other.

From these considerations we see that, for modes with a parallel scale length exceeding the thickness of the layer, $k < 1/h$, one can neglect the interaction between different points along the surface of the imploding shell. The shell itself, for such modes, can be considered as a thin structureless surface possessing some inertia (determined by the mass per unit area). This is a very important observation that helps one to make some clear predictions regarding the evolution of the modes with $k < 1/h$ (see Sec. IV.D).

These arguments also allow one to arrive at some conclusions with regard to the stability of the wire array before the wires merge: if one considers the $m=0$ perturbation with wavelengths much greater than the interwire distance, the fact that the array consists of separate wires does not manifest itself in any way, and expression (4.19) correctly describes the growth rate.

The stability of some modes with wavelengths comparable to the interwire distance has been studied by Felber and Rostoker (1981) and Samokhin (1988). Felber and Rostoker have shown that there exist two types of modes: those in which the wires remain within the meridianal planes (medial modes, according to terminology introduced by Hammer and Ryutov, 1999), and those in which the wires bend along the surface of the cylinder (called lateral modes by Hammer and Ryutov). A complete linear stability analysis for arrays consisting of a large number of wires (Hammer and Ryutov, 1999) has shown that a $\sqrt{kg}$ scaling holds for surprisingly short wavelengths, approaching the interwire spacing. The growth rate for the lateral modes is as high as the growth rate for the medial Rayleigh-Taylor modes. For wavelengths shorter than the interwire spacings, an approximately linear dependence on $k$ takes over. For the $m=0$ medial mode, Desjarlais and Marder (1999) have considered both linear and nonlinear stages of the instability. The amplitude of the initial perturbation for the $m=0$ mode was determined on the basis of Haines' theory (Haines, 1998), mentioned at the end of Sec. III.D of this survey.

## C. Smooth transition between the plasma and the magnetic field; local modes

The finite character of the plasma resistivity smoothes the transition between the vacuum magnetic field and the plasma. Rapid development of short-wavelength flute perturbations (for which the critical wave number is infinite) also smears out the transition. We shall use the notation $h_1$ to denote the thickness of the transition; $h_1$ can be smaller than or comparable to the total thickness of the shell $h$ (Sec. II.E). For perturbations with wave numbers below $1/h_1$, one can use the results of the previous section. In this section, we consider perturbations with wave numbers much greater than $1/h_1$, the

so-called local modes. The growth rate of these modes depends on the local value of the density gradient $\rho'$. Since within the transition layer the characteristic value of the magnetic-field strength is of the order of the vacuum magnetic field, these short-wavelength perturbations can be unstable only if they are of a flute type (otherwise, perturbation of the magnetic energy becomes prohibitively high). The growth rate for flute perturbations has been derived by Chen and Lykoudis (1972):

$$\Gamma^2 = \left( \frac{g^2}{a^2+s^2} + \frac{g\rho'}{\rho} \right), \qquad (4.22)$$

where $a^2 = 2p_m/\rho$ is the local value of the Alfvén speed. For $\rho' > 0$ the local modes are universally unstable. Taking into account the rough estimates $\rho'/\rho \sim 1/h_1$ and $gh \sim a^2+s^2$ that follow from the equilibrium condition, one can estimate the growth rate of the localized modes as

$$\Gamma^2 \sim g/h_1 . \qquad (4.23)$$

Note that the presence of the magnetic field within the shell does not change the conclusion made in Sec. VI.B regarding the properties of the long-wavelength perturbations: at $k \ll 1/h$, the instability $e$-folding time is shorter than the time needed for the Alfvén wave to propagate over the distance $1/k$. Therefore, even if the magnetic field penetrates into the shell, the long-wave perturbations behave as perturbations of a massive, structureless, infinitesimally thin sheet.

Another comment should be made regarding perturbations localized near the interface between the plasma and the magnetic field. The growth rate of modes localized near this interface, at large $k$'s, does not reach saturation, because the parameter $\rho'/\rho$ near the interface becomes infinite. On the other hand, if the interface is smeared and the density decreases, say, exponentially, the growth rate of localized perturbations ($k \gg 1/h$) does reach saturation (see also the comment at the end of Sec. IV.A).

## D. More on the stability of a thin shell; effects of accretion

As has been shown in Secs. IV.A and IV.B, the analysis of perturbations with wavelengths exceeding the shell thickness can be carried out without taking account of the internal structure of the shell. This allows one to obtain a relatively simple description of the instability, including effects of the cylindrical implosion geometry (Harris, 1962) and of mass accretion (Gol'berg and Velikovich, 1993; DeGroot et al., 1997b); one can even gain some insights into the nonlinear phase of the problem (Ott, 1972; Bashilov, Pokrovskii, 1976; Manheimer, Colombant, and Ott, 1984; Basko, 1994; Book, 1996). We derive the equations in the planar case. Later, in Sec. IV.F, we discuss the effects of a cylindrical geometry.

Consider a thin shell accelerated by a magnetic pressure $p$ in the $x$ direction (Fig. 14). The horizontal line at $x=0$ depicts the initial position of the shell. We shall
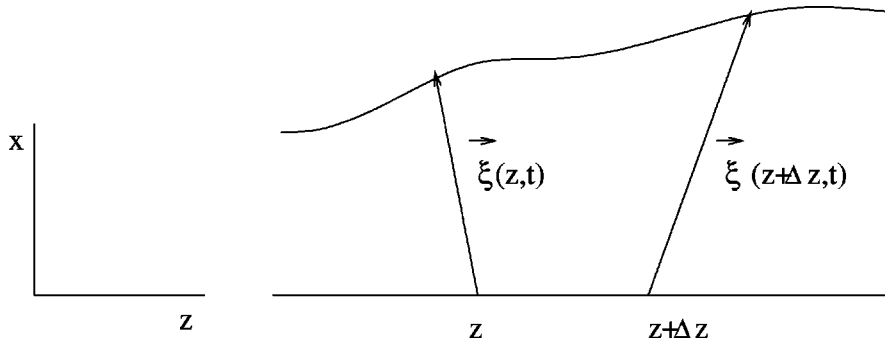
FIG. 14. The Lagrange coordinates $\xi(z,t) \equiv (\xi_x(z,t); \xi_z(z,t))$ describing implosion of a thin shell.

analyze only the most dangerous flute perturbations, which are aligned with the magnetic-field lines, directed along the $y$ axis. In other words, we consider perturbations that do not depend on the coordinate $y$. The motion occurs in the $(x,z)$ plane. The magnetic pressure then is uniform even on the perturbed surface of the shell.

Following Ott, we denote by $\xi_x(z,t)$ and $\xi_z(z,t)$ the $x$ and $z$ displacements of a certain element of the shell (whose initial location on the shell surface was $z$). In other words, at this point we are using a Lagrangian description of the perturbations. These displacements are not assumed to be small; we are going to obtain a nonlinear set of equations. We shall also take into account the possibility of mass accretion on the shell from the gas initially situated at the $x>0$ half space, assuming that the gas just sticks to the shell (strongly radiating plasma; see Secs. II.B and II.C). In the unperturbed motion one obviously has $\xi_z=0$ and

$$\frac{\partial}{\partial t}\left( \sigma_0 \frac{\partial \xi_x^0}{\partial t} \right) = p, \quad \frac{\partial \sigma_0}{\partial t} = \rho \frac{\partial \xi_x^0}{\partial t}, \tag{4.24}$$

where $\rho$ is the density of the cold, resting gas swept by the shell and $\sigma_0$ is the mass per unit area of the shell (varying with time because of accretion).

Let us denote by $\Delta z$ an initial distance between the two neighboring points at the surface (Fig. 14). One of them gets displaced to the point $(\xi_x(z,t), \xi_z(z,t))$, the other to the point $(\xi_x(z,t)+\Delta z\,\partial \xi_x(z,t)/\partial z, \xi_z(z,t) + \Delta z\,\partial \xi_z(z,t)/\partial z)$. Let the mass of this element of the surface be $\Delta m$. The change in mass occurs because of accretion. Using simple geometrical considerations identical to those used by Ott (1972), one finds

$$\Delta \dot{m} = \rho \left( \frac{\partial \xi_z}{\partial z} \dot{\xi}_x - \frac{\partial \xi_x}{\partial z} \dot{\xi}_z \right) \Delta z, \tag{4.25}$$

or

$$\dot{\sigma} = \rho \left( \frac{\partial \xi_z}{\partial z} \dot{\xi}_x - \frac{\partial \xi_x}{\partial z} \dot{\xi}_z \right), \quad \sigma \equiv \frac{\Delta m}{\Delta z}, \tag{4.26}$$

where the dot designates a partial derivative with respect to time. Equations of motion can be obtained in the same way as in the paper by Ott (1972). They read as

$$\frac{\partial}{\partial t}\left( \sigma \frac{\partial \xi_x}{\partial t} \right) = p\frac{\partial \xi_z}{\partial z}; \quad \frac{\partial}{\partial t}\left( \sigma \frac{\partial \xi_z}{\partial t} \right) = -p\frac{\partial \xi_x}{\partial z}. \tag{4.27}$$

If the shell is being accelerated into the vacuum, then

$\sigma$ does not depend on time, and one does not need Eq. (4.26) for $\sigma$. In this case Eqs. (4.27) become linear equations. This observation was made by Ott; the Lagrangian formulation of the problem in this case leads to linear equations describing even finite-amplitude perturbations. Note that Bashilov and Pokrovskii (1976) generalized Ott's nonlinear solution to the cylindrical case. We shall comment on the properties of the nonlinear solution later. For now, let us consider small perturbations of the shell. To distinguish the perturbations, we shall mark them by a symbol "$\delta$." We get

$$\frac{\partial}{\partial t}\left( \sigma_0 \frac{\partial \delta \xi_x}{\partial t} \right) = (p - \rho v^2)\frac{\partial \delta \xi_z}{\partial z} - \dot{v}\,\delta\sigma;$$

$$\frac{\partial}{\partial t}\left( \sigma_0 \frac{\partial \delta \xi_z}{\partial t} \right) = -p\frac{\partial \delta \xi_x}{\partial z}; \tag{4.28}$$

$$\frac{\partial \delta\sigma}{\partial t} = \rho v \frac{\partial \delta \xi_z}{\partial z},$$

where $v = \partial \xi_x^0/\partial t$.

If there is no material in front of the accelerated shell ($\rho=0$), then the set of Eq. (4.28) becomes particularly simple:

$$\frac{\partial^2 \delta \xi_x}{\partial t^2} = g\frac{\partial \delta \xi_z}{\partial z}; \quad \frac{\partial^2 \delta \xi_z}{\partial t^2} = -g\frac{\partial \delta \xi_x}{\partial z}. \tag{4.29}$$

Here $g \equiv p/\sigma_0$ is the effective gravity force. For perturbations with $\exp(-ikz)$ dependence on the coordinates this equation yields the familiar expression for the growth rate [cf. Eq. (4.19) with $\alpha=\pi/2$]: $\Gamma=(kg)^{1/2}$.

An interesting point here is the surface density perturbation of the shell. The quantity $\sigma$ that we have been using so far is the Lagrangian density: a mass that corresponds to a segment of the shell whose end points originated at the ends of the initial segment $\Delta z$, divided by this $\Delta z$ [see Eq. (4.26)]. If there is no accretion, then the density thus defined is constant. But the real density of the shell defined as a mass $\Delta m$ occupying some segment $\Delta l$ on the surface of the shell, divided by this $\Delta l$, is changing (because $\Delta l$ is changing). One can show that the surface density is redistributed over the shell in such a way that the density decreases on the bulges of the surface and increases in the troughs (Fig. 15). This feature suggests that, in the process of self-acceleration of an instability at the nonlinear stage, the areas of lower (higher) density tend to move ahead (lag behind) faster than in a linear approximation. We shall return to this issue in Sec. IV.G.
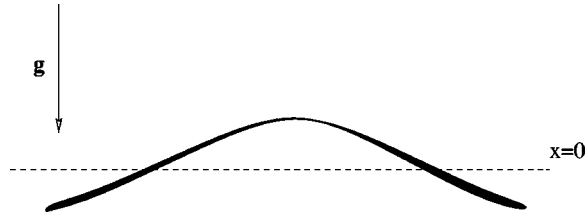
FIG. 15. Surface-density redistribution in the flute mode. The thickness of the solid line roughly corresponds to the density. The dashed line depicts the initial position of the shell.

Consider now a linear instability in a more general case where accretion of the material is substantial and one has to use the general set of Eqs. (4.28). A characteristic time over which the system's parameters change, in particular, the mass per unit area and the acceleration, is

$$\tau \equiv \sigma/\dot{\sigma} = \sigma/(\rho v). \qquad (4.30)$$

As the $e$-folding time for short-wavelength perturbations decreases with increasing $k$, at large enough $k$'s it becomes much shorter than $\tau$. This happens at $k \gg \rho^2 v^2/g\sigma$. The magnetic pressure is related to the ram pressure of the accreted material via $\rho v^2 \sim p$. Using this relationship, one finds that the limit of large growth rates corresponds to

$$k \gg \rho/\sigma, \qquad (4.31)$$

in agreement with DeGroot *et al.* (1997b). At some medium point in the acceleration process the right-hand side of Eq. (4.31) is of the order of the inverse path traveled by the shell, in other words, the inverse pinch radius. In this case one can consider all the unperturbed parameters entering the set (4.28) as constant. This yields the following equation for the instantaneous growth rate:

$$\Gamma^4 = \left(\frac{k}{\sigma}\right)^2 [p(p - \rho v^2)]. \qquad (4.32)$$

This expression differs from the corresponding expression of DeGroot *et al.* (1997b); in particular, Eq. (4.32) predicts that the growth rate approaches zero at $p$ close to $\rho v^2$ when the shell is moving without acceleration. Note that the instability in an overstable mode, $\mathrm{Im}\,\Gamma \neq 0$, is present even at $p < \rho v^2$ (Vishniac, 1983).

For wavelengths that do not satisfy condition (4.31), the perturbation growth cannot be adequately defined in terms of the instantaneous growth rate; in this domain one has to solve the full set of differential Eqs. (4.28). Qualitatively, in this domain the accretion still should lead to a decrease of the perturbation growth (see Gol'berg and Velikovich, 1993). Cochran, Davis, and Velikovich (1995) have shown by solving numerically a 2D set of radiative hydrodynamics equations that uniform gas puffs are more stable with respect to axisymmetric Rayleigh-Taylor instability than annular gas puffs—in agreement with the general trend predicted by Eq. (4.32).
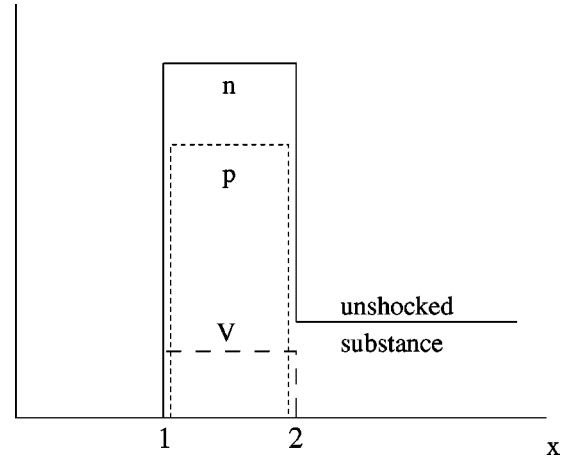


FIG. 16. Density, pressure, and velocity distribution in a plasma column when strong shock is excited. The magnetic piston is situated at surface 1, the shock wave at surface 2.

### E. The case of a detached shock wave

In the previous section we discussed the stability of a system in which the gas sticks to the surface of the piston. As we mentioned in Sections II.B and II.C, such a model correctly reflects a situation in which the gas collected by the piston is strongly radiating, so that the distance between the shock and the piston is negligible (the ultimate case of the snow-plow model). For the short current pulses typical of experiments on fast $Z$ pinches and for low initial temperature of the matter, a strong shock will form that will propagate ahead of the piston. In this section, we discuss the situation of a weakly radiating plasma, in which the plasma behind the shock remains hot, with the pressure at the surface of the magnetic piston equal to the magnetic pressure (Fig. 16). There exists a broad class of exact (self-similar) solutions describing plasma flow between the shock and the piston in the planar case, i.e., at the early stage of the implosion (see, for example, Gol'berg and Velikovich, 1993). The stability of this solution with respect to Rayleigh-Taylor modes was discussed by Gol'berg and Velikovich (1993), who, in particular, formulated boundary conditions at the surface of the shock wave, and later by DeGroot *et al.* (1997b). We present here only our own qualitative discussion of the problem.

We denote by $h$ the thickness of the layer between the shock and the piston. The modes with $k \gg 1/h$ localized near the piston do not differ significantly from the modes considered in Sec. IV.B. Among those, only perturbations close to flute modes are unstable. However, for these unstable modes the growth rate is large $\sim(kg)^{1/2}$. These perturbations will cause a gradual broadening of the transition between the plasma and the magnetic field.

Consider now long-wavelength modes ($k \ll 1/h$). For these modes, the transition layer is "thin" and, according to the results of Secs. IV.A–IV.C, can be considered essentially as a structureless surface. A growth rate could be estimated again as $\sim(kg)^{1/2}$. In the $k \ll 1/h$ case, unlike the opposite case, the modes with an arbi-

trary orientation of the wave vector are unstable. The mass of the layer gradually increases as additional material is swept up by the shock wave. At small $k$'s (small growth rates) the change of mass within one $e$-folding time may be considerable, and the concept of an instantaneous growth rate may break down (Gol'berg and Velikovich, 1993).

The thickness of the layer $h$ is relatively small even for a nonradiating plasma; since the shock is strong, the density behind the shock is determined by Eq. (2.20). For a fully ionized gas with $\gamma = \frac{5}{3}$ the density is four times higher than the density before the shock, and the thickness of the shocked material is, roughly speaking, four times less than the distance travelled by the shock. If one is dealing with a weakly ionized gas in which a considerable fraction of the energy is spent on ionization of the shocked gas, "the effective $\gamma$" becomes smaller than $\frac{5}{3}$ and the layer of shocked material becomes even thinner.

At a convergence of ~3–4 (for a gas with $\gamma = \frac{5}{3}$), the shock reaches the axis and upon rebounding returns to the piston, leaving behind a hot plasma with a pressure approximately equal to the magnetic pressure. Further compression of the hot material occurs in a quasistatic manner, almost adiabatically, with the plasma pressure equal to the magnetic pressure (Potter, 1978). This adiabatic compression in the absence of radiative losses may occur only if the current continues to grow. The plasma boundary at this phase decelerates and stops at the current maximum. The pinch at this point is very similar to an equilibrium Bennett pinch (Bennett, 1934). Of course, the Rayleigh-Taylor instability ceases to exist. Of the hydrodynamic instabilities, only those driven by the curvature of the magnetic-field lines remain. Their $e$-folding time is of the order of $r/s$, where $s$ is the speed of sound. A stability analysis of these modes goes beyond the scope of our survey. A discussion of this problem in a purely MHD approximation can be found in Kadomtsev (1996) and Bateman (1980); among possible equilibria there are diffuse equilibria that are stable with respect to the $m = 0$ mode (so-called "Kadomtsev equilibria"). Asymptotically, at large radii, the pressure in these equilibria decreases as $r^{-10/3}$. Nonlinear evolution of a sausage instability for an incompressible fluid was studied by Book, Ott, and Lampe (1976). It should be remembered that the plasma column after stagnation can be so hot that the MHD approximation breaks down, and non-MHD effects, in particular, those caused by large ion orbits, become important. A general characterization of the parameter space for stability in a Bennett-type pinch, identifying the subdomains where various anomalies may surface, is offered by Haines and Coppins (1991).

## F. Effects of cylindrical convergence

As we have seen, the most dangerous modes are flute modes with wave numbers $k$ of the order of the inverse shell thickness $1/h$. Until a very late stage in the implosion, when the liner is about to collapse on axis, the wavelengths of these modes are small compared to the linear radius ($kr \gg 1$). Therefore their instantaneous growth rate should be adequately described by the planar model discussed in the previous three sections. Still, cylindrical convergence effects may become important earlier in the implosion; two reasons are discussed below.

The first is the effect of convergence on the mass $\sigma$ per unit area: one obviously has $\sigma = \sigma_0 (r_0/r)$. This may alter the sheath thickness from what it was in the case of a planar system with the same time-history of acceleration. Accordingly, the maximum growth rate is different from the planar case. In addition, there is a direct enhancement of the amplitude of even stable perturbations due to cylindrical convergence effects (like the growth of an amplitude of a cylindrically converging light wave).

The second effect is an increase in the azimuthal component of the wave vector, $k_\theta = m/r$; as the mode number $m$ does not change with time, $k_\theta$ scales as $1/r$ (recall that, in our notations, $k_y \equiv k_\theta$). This causes a gradual decrease in the angle $\alpha$ between the wave vector and the direction of the magnetic field and may eventually lead to stabilization of the mode by making the product

$$k \cos^2 \alpha \equiv \frac{k_y^2}{\sqrt{k_z^2 + k_y^2}} \qquad (4.33)$$

less than $1/2h$, thereby causing stabilization of the mode [see Eq. (4.18)]. Remember that, in a purely cylindrical system, $k_z$ does not change with time.

The growth of perturbations at the linear stage of instability is determined by the exponentiation factor (see, for example, Lindl, 1995),

$$\xi(t) = \xi_0 \exp G(t), \qquad (4.34)$$

where

$$G(t) \equiv \int_0^t \Gamma(t')dt', \qquad (4.35)$$

and $\Gamma$ is the instantaneous growth rate (4.2).

The linear approach breaks down as soon as the amplitude reaches a certain level $\xi = \xi_{NL}$. A rough estimate for $\xi_{NL}$ is $\xi_{NL} \sim 1/h$ for the most dangerous perturbations (with $k \sim 1/h$) and $\xi_{NL} \sim 1/k$ for long-wavelength perturbations (with $k \ll 1/h$). The transition to the nonlinear stage occurs at the instant of time determined from the equation

$$G(t) = \ln(\xi_{NL}/\xi_0). \qquad (4.36)$$

Since the initial perturbations are small, say, a couple of orders of magnitude less than $\xi_{NL}$, the logarithm is equal to 4–5 and weakly depends on both $\xi_0$ and $\xi_{NL}$.

For long-wavelength perturbations, the growth rate does not depend on the structure of the shell, and the function $G$ has a universal dependence on time determined by the solution of Eq. (2.1). In this solution, the radius is a unique function of time and, therefore $G$ can also be expressed in terms of the instantaneous value of the radius. A plot of $G/(kr_0)^{1/2}$ vs the convergence is presented in Fig. 17 for the current given by Eq. (2.5)
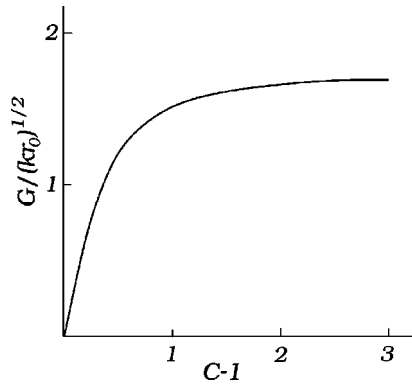
FIG. 17. Plot of the amplification factor vs convergence for a load imploding on axis at the time of the maximum of the pinch current for purely axisymmetric perturbations.
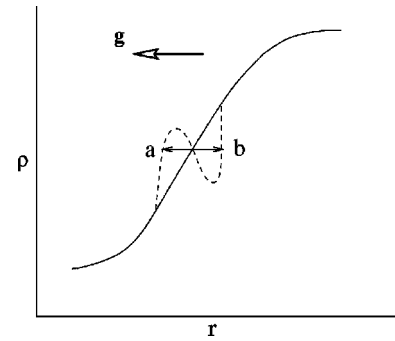


FIG. 18. Variation of the density distribution caused by local displacement of the fluid element. The average gradient within the segment $ab$ becomes zero.

and the parameter $\Pi$ (Eq. 2.4) corresponding to stagnation at the point of the maximum current (i.e., $\Pi \approx 4$).

However, for the most dangerous perturbations with $k \sim 1/h$, the function $G$ also depends on the thickness $h$ of the shell, which in general varies with time. A factor that acts towards reducing $h$ is growing acceleration [the scale height is inversely proportional to $g$; see Eq. (2.27)], while factors acting in the opposite direction are radial convergence (which increases mass per unit area), possible onset of anomalous resistivity, and increase in temperature. So, the issue of the transition to the nonlinear regime for the fastest growing modes is more complicated. If one assumes that the thickness $h$ remains constant during the implosion, one can use the plot of Fig. 17 to roughly find the transition point by assuming that $k \sim 1/h$ and imposing the condition that $G$ be approximately equal to, say, 4. For a shell thickness equal to 0.1 of the initial liner radius [and, accordingly, $(kr_0)^{1/2}=3$], nonlinear effects become important (i.e., $G$ becomes equal to approximately 4) at a convergence equal to 4.

As in to our previous discussion, we have considered here only modes with small azimuthal numbers $m$; the modes with large $m$ are stabilized at a moderate convergence because of the aforementioned effect of growing $k_y (k_y \sim 1/r)$.

## G. Nonlinear effects; turbulence and turbulent broadening of the shell

We begin this discussion by considering the local modes with $k > 1/h$. When the displacement $\xi_x$ becomes greater than $1/k$, it changes the density gradient, which drives the instability and determines the growth rate, by a factor of the order of unity (Fig. 18). This signifies that further development of the perturbations depends on their amplitude. In the case of short-wavelength perturbations, where the growth rate does not substantially depend on $k$, one can expect development of random motions with a broad spectrum of length scales and the amplitude of a particular scale of the order of $1/k$. The characteristic turnaround time of the vortices should be of the order of the inverse growth rate $1/\Gamma \sim (h/g)^{1/2}$.

These random motions cause a kind of diffusion evolution of the density profile with the diffusion coefficient $\Gamma/k^2 \propto 1/k^2$. One can see that the greatest contribution comes from the largest length scale compatible with the local approximation ($1/k \sim h$). But this means that the diffusive approximation does not correctly describe the situation, that is, the characteristic step size is of the order of the gradient length scale. This is a fundamental difficulty of nonlinear theories of the Rayleigh-Taylor instability. A diffusive description may become relevant if the mode with the largest scale is, for one reason or another, suppressed. We shall not discuss here this rather artificial possibility.

Dimensional arguments similar to those used in the theory of mixing at the interface of two semi-infinite fluids (Youngs, 1991) show that broadening should occur according to the law

$$h = \varepsilon g t^2, \tag{4.37}$$

where $\varepsilon$ is some numerical factor. In Youngs' case $\varepsilon$ is approximately equal to 0.07.

Let us now turn our attention to large-scale perturbations, with $k$ much less than the inverse shell thickness. We consider only the most dangerous flutelike (axisymmetric) perturbations. This type of motion can be properly described by Ott's equations [Eq. (4.29)]. One can expect that, as there are no other scales in this problem, the nonlinearity turns on when the amplitude of the perturbations becomes of the order of $1/k$. This hypothesis can be easily checked on the basis of the exact solution obtained by Ott (1972). For a single-mode initial perturbation the time evolution of the shell is illustrated by Fig. 19 (Basko, 1994). Strong deformations from a sinusoid indeed appear at $\xi_x \sim 1/k$.

For a long-wavelength perturbation, entering the nonlinear phase does not mean stabilization or slowing down. Quite the contrary, the effects of the mass redistribution (Fig. 15) cause an acceleration of the mode development. This, in particular, manifests itself in the formation of singular spikes within a finite time (Fig. 19). The time of the spike formation is equal to $2(kg)^{-1/2}\ln(2/k\xi_{x0})$. Although the Lagrangian description breaks down after the formation of singularities, there is no reason why the lighter parts of the shell should not continue their accelerated motion to the axis,
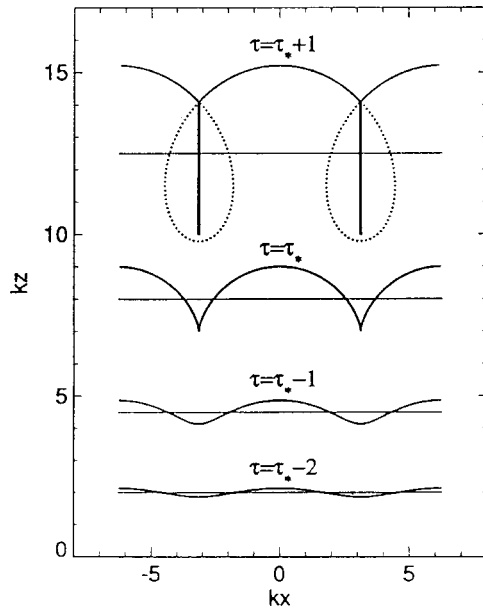
FIG. 19. Development of a nonlinear mode of a thin shell (from Basko, 1994, reprinted with kind permission of M. Basko). The time is measured in units of the inverse growth rate. The time $\tau_*$ of the first appearance of the cusps is, in these units, equal to $-\ln(k\xi_{\xi 0})$ where $k\xi_{\xi 0}$ is the initial amplitude of the perturbation. The vertical axis corresponds to a radial coordinate, and the horizontal axis to an axial coordinate.

so there are no signs of a self-stabilization here. The picture grows more complex if one takes into account development of multiple modes growing from initially random perturbations. The shorter wavelengths grow faster and reach their strongly nonlinear stage earlier than the longer ones. The mode that has the strongest effect on the distortion of the shell is the mode with a scale length comparable to the shell thickness. This mode may reach an amplitude several times greater than the instantaneous shell thickness because of the presence of some numerical factors in the scaling problem.

We conclude this discussion by noting that, for shells that are not very thin (with a thickness of the order of 0.1 of the initial radius), reaching a convergence of ~10–20 seems feasible (Fig. 20). The thinner the shell, the faster the instabilities reach their nonlinear phase. Whether an instability at this nonlinear stage will cause a gradual broadening of the sheath and mixing with the magnetic field or cause more coherent structures of the type shown in Fig. 21(a) to develop (causing disruptions of the current and violent destruction of a well-defined shell) is an open question. Numerical simulations and theoretical analyses (e.g., Peterson et al. 1996, 1997; Thornhill et al., 1997) seem to point in the direction of more violent scenarios (Fig. 22).

## H. More on the relationship between flute and nonflute modes

Let us examine the case in which the thickness of a current-carrying transition region is comparable to the

overall thickness of the shell, $h_1 \sim h$. As we know, one should distinguish between flute modes, for which the wave number is perpendicular to the magnetic field (an axisymmetric mode in the cylindrical geometry), and nonflute modes. As a representative example of the latter, we consider a mode propagating at an angle of 45° with respect to the magnetic field. A qualitative plot of the growth rates vs the wave number $k$ for these two modes is shown in Fig. 23. The curve for the flute mode lies above the curve for the nonflute mode. At small $k$'s, one can make an exact prediction of the growth rate [Eq. (4.19)], which in this limit is independent of the specifics of the density and magnetic-field distribution inside the shell. The reason for this was discussed in Secs. IV. A. and IV. B.

At larger $k$'s, the nonflute mode becomes stable. A specific value of the critical wave number $k_0$ is determined by the details of the density and magnetic-field distribution within the shell thickness. Within an order of magnitude, $k_0 \sim 1/h$. For a flute mode the growth rate at large $k$'s reaches saturation as determined, to within an order of magnitude, by Eq. (4.22). In fact, the growth rate of the local modes ($k \gg 1/h$) is determined by the layer in which the mode is localized. Note that the maximum growth rate of the local modes is a well-defined quantity; it corresponds to the maximum value of the right-hand side of Eq. (4.22) over the thickness of the sheath (roughly speaking, the maximum value of $\rho'/\rho$, assuming that this maximum does exist).

Figure 23 underlines the exceptional role played by the flute (axisymmetric) mode in the dynamics of imploding liners. The prevalence of the flute mode becomes even more visible at the nonlinear stage of the instability. When the shell becomes strongly distorted with respect to its unperturbed state [Fig. 21(a)], the magnetic field at the tips of the fingers remains the same as in the unperturbed state (or even increases, if one takes into account effects of the cylindrical geometry), while the mass density in the fingers decreases. This causes a catastrophic self-acceleration of the breakup process and may cause total disruption of the pinch.

This scenario of developing axisymmetric modes at their nonlinear stage, which can be traced back to Hussey, Roderick, and Kloc (1980), Baker and Freeman (1981), Kloc, Roderick, and Hussey (1982), and Roderick and Hussey (1986), has found confirmation in modern simulations of randomly distributed axisymmetric perturbations (Peterson et al. 1996, 1997, 1999; Matuska et al. 1996, Benattar et al., 1999). Figure 22 depicts isodensity contours with a clearly visible fingerlike structure. The breakup of the shell was also found in the case where the initial perturbation was a single mode or a mixture of up to three single modes (Douglas, Deeney, and Roderick, 1998).

Nothing like this can happen for nonflute modes, at least for a thin-shell liner, with $h \ll r$. This is because of a very different reaction of the magnetic field to strongly nonlinear, nonaxisymmetric perturbations of the type shown in Fig. 21(b); the magnetic field does not penetrate to the "fingertips" in this case and is, on the con-

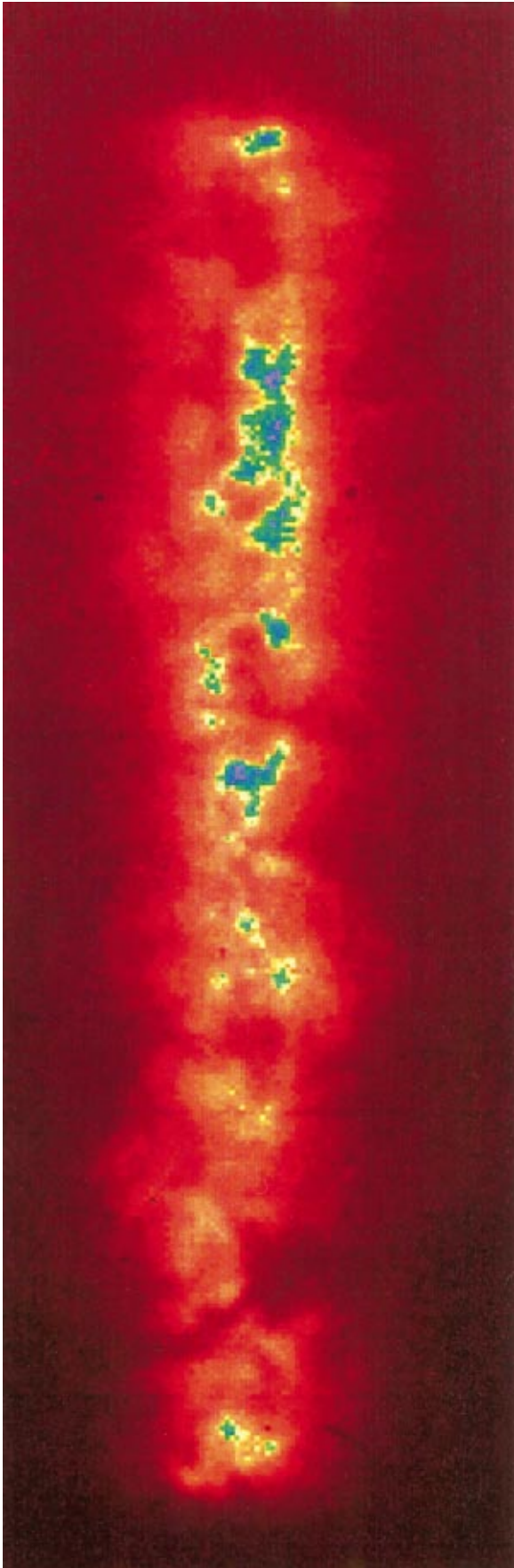FIG. 20. View of 200–280-eV pinch radiation taken from 88° at *Z* (from Deeney, Douglas, *et al.*, 1998, reprinted with kind permission of C. Deeney). The radiation is created by the stagnation of a nested wire array on-axis. The diameter of the radiating zone is approximately 2 mm. The initial diameter of the outer (inner) wire array was 40 mm (20 mm). The current waveform was similar to that shown in Fig. 4 [Color].
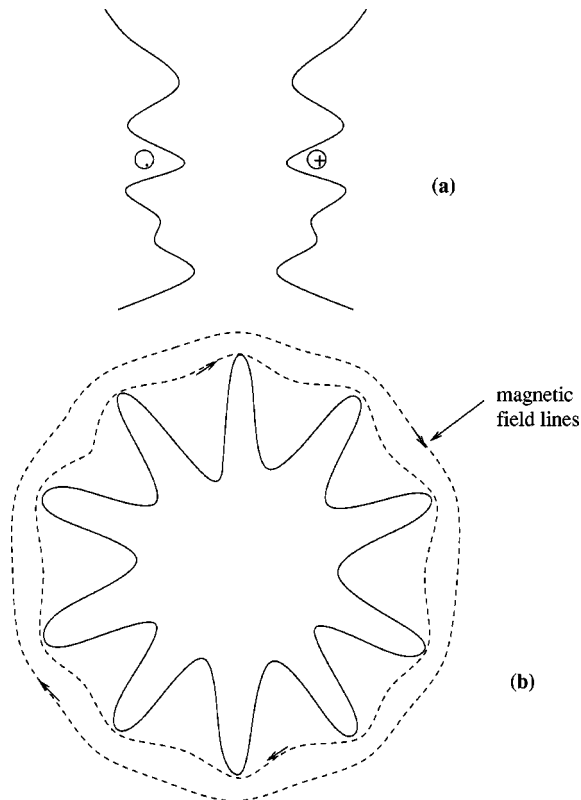
FIG. 21. Nonlinear stage of the development of the Rayleigh-Taylor instability: (a) flute (axisymmetric) mode, a vertical cross section; (b) nonaxisymmetric mode, a horizontal cross section.

trary, increasing at the lagging parts of the liner surface. Therefore one can expect an early nonlinear saturation of the nonaxisymmetric modes and a correspondingly weaker effect on the liner implosion. As we shall see (Sec. VI.F), this suggests that one might even introduce nonaxisymmetric perturbations, deliberately to damp too rapid growth of axisymmetric fingers.

The dominance of axisymmetric modes seems to be in agreement with experimental data. Figure 20 shows an x-ray pinhole image of the pinch near the point of maximum compression in the $Z$ accelerator. The features perpendicular to the pinch axis are most pronounced—as one should expect in the case of axisymmetric perturbations. Note that in cylindrical implosions driven by an ablative force (Hsing *et al.* 1997; Hsing and Hoffman, 1997) the high-$m$ modes could be dominant players in the dynamics of the implosion, reaching a nonlinear stage and affecting the maximum convergence. This underlines once again the exceptional role of the magnetic drive in selecting the $m=0$ mode as the most dangerous one.

On the other hand, experiments on both gas-puff implosions (e.g., Shiloh, Fisher, and Bar-Avraham, 1978; Burkhalter *et al.* 1979; Wong *et al.* 1998) and wire-array implosions (e.g., Deeney, Nash, 1998, Spielman *et al.* 1998) show that the "final" imploded state always manifests significant deviations from perfect axial symmetry, which can be attributed to low-$m$ ($m=1,2$) modes with $k_z$ of the same order as for $m=0$ perturbations. Accord-
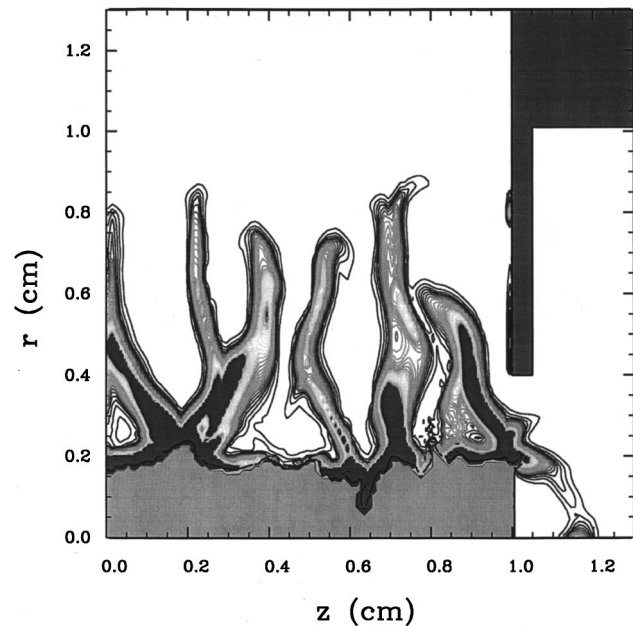


FIG. 22. Numerical results showing the possibility of current disruption by the $m=0$ mode (a 40-mm-diameter tungsten wire array on PBFA-$Z$ after impacting a 2.5-mm-radius foam). From Peterson *et al.*, 1999, reprinted with kind permission of D. Peterson.

ing to the discussion at the end of Sec. IV.F, development of low-$m$ modes is not prohibited. The aforementioned experimental results show that they may reach a level comparable to the $m=0$ mode. A quantitative analysis of the degree of nonaxisymmetry late in the implosion may help in understanding and control of hydrodynamic stability.

## V. EFFECTS OF DISSIPATIVE PROCESSES

### A. Viscosity

The effects of plasma viscosity are among those whose influence on the Rayleigh-Taylor instability have been studied in the greatest detail, starting with Chandrasekhar's monograph (1961), which considered the stability of a boundary between two semi-infinite viscous fluids. A careful analysis of viscous effects in the case of a slab was performed by Mikaelian (1996); see also references therein.

Viscous terms in the hydrodynamic equations are most important for small-scale motions. Therefore it is reasonable to consider their effect on perturbations with a length scale that is small compared to the characteristic scale of the density gradient $h$ [Fig. 11(a)]. If an element of the fluid is displaced by a small distance $\xi$ in the vertical direction, it experiences the action of the buoyancy force produced by the difference between the densities inside this element and in the surrounding substance, $\delta\rho \equiv \rho_i - \rho_e = -(\partial\rho/\partial x)\xi$. The force is equal to $\delta F = -Vg\delta\rho$, where $V$ is the volume of the liquid element ($\sim 1/k^3$). The viscous force acting on an element of size $\sim 1/k$ moving in the resting fluid is (Landau and
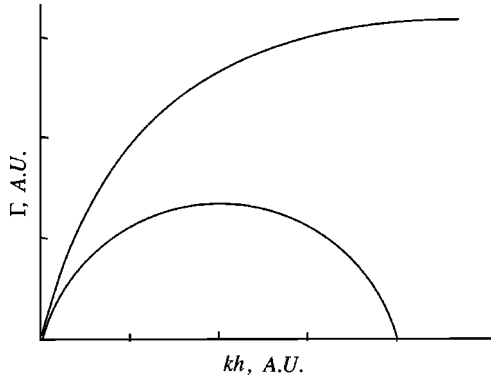
FIG. 23. Overall sketch of the growth rate for a flute mode (upper curve) and a mode propagating at 45° to the magnetic field (lower curve) for a shell with a smooth density distribution that can be characterized by a single spatial scale $h$; $k$ is a tangential wave number. Shown in the figure is a *maximum* growth rate over all modes with a given **k**. This comment becomes significant at large **k**, for which localized (in $x$) modes form essentially a continuous spectrum, occupying the whole range of $\Gamma$, from the maximum (shown in the figure) to zero.

Lifshitz, 1987) $\delta F_{\mathrm{visc}} \approx -\rho \nu k^2 \dot{\xi} V$ where $\nu$ is the kinematic viscosity. In this way one arrives at the following equation of motion:

$$\ddot{\xi} = \frac{g}{\rho}\frac{\partial \rho}{\partial x}\,\xi - \nu k^2 \dot{\xi}. \qquad (5.1)$$

From Eq. (5.1), one gets the following expression for the growth rate:

$$\Gamma = \sqrt{\frac{g}{h}}\left(\sqrt{1 + \varepsilon_{\mathrm{visc}}\frac{(kh)^4}{4}} - \sqrt{\varepsilon_{\mathrm{visc}}}\frac{(kh)^2}{2}\right), \qquad (5.2)$$

with $h^{-1} \equiv (1/\rho)\partial \rho/\partial x$, and

$$\varepsilon_{\mathrm{visc}} \equiv \frac{\nu^2}{gh^3}. \qquad (5.3)$$

The dimensionless parameter $\varepsilon_{\mathrm{visc}}$ characterizes the role of viscosity. For implosions of wire arrays, the parameter $\varepsilon_{\mathrm{visc}}$ is typically very small. Kinematic viscosity is related to the mean free path $l_{ii}$ of the plasma ions as $\nu \sim l_{ii} v_{Ti}$. Using estimate (2.27), relating the thickness of the shell and the gravity acceleration, one finds that

$$\varepsilon_{\mathrm{visc}} \sim \frac{A}{Z_{\mathrm{eff}}+1}\left(\frac{l_{ii}}{h}\right)^2. \qquad (5.4)$$

Here we have taken into account the relationship $\bar{m}/m_i = A/(Z_{\mathrm{eff}}+1)$. In implosions of metal liners, the ion-ion mean free path is orders of magnitude smaller than the liner thickness. Therefore, in this situation, $\varepsilon_{\mathrm{visc}}$ is universally small. Only modes with very short wavelengths are affected by the viscosity: $kh > \varepsilon_{\mathrm{visc}}^{-1/4}$. Note that for these small-scale perturbations viscosity still does not provide complete stabilization. It just reduces the growth rate, which now becomes $\Gamma \approx \varepsilon_{\mathrm{visc}}^{-1/2}(kh)^{-2}\sqrt{g/h}$.

In gas-puff systems, with lower densities and higher temperatures in the imploding plasma, one may reach

conditions under which $\varepsilon_{\mathrm{visc}}$ becomes $\sim 1$. A transition to the case $\varepsilon_{\mathrm{visc}} \sim 1$ may, in particular, occur in the implosion of two coaxial gaseous shells, where the outer shell hits the inner shell, causing a sudden increase in temperature and, accordingly, in the viscosity (recall that the Coulomb collision cross section decreases with the temperature). At even higher temperatures one may find that the ion gyroradius becomes less than the ion mean free path (see also Sec. VI. I). This causes a reduction in the shear viscosity (Braginski, 1965) but the bulk viscosity remains high. The bulk viscosity appears in a manner similar to that of the thermal conductivity, which we shall describe shortly.

## B. Thermal conductivity and internal relaxation

Now we turn to a discussion of the effects of thermal conductivity. The characteristic time for smoothing of temperature perturbations of a scale $1/k$ is $\tau \sim 1/k^2\chi$, where $\chi$ is the thermal diffusivity. Usually, in unmagnetized plasma, the thermal diffusivity is large compared to the kinematic viscosity (see Braginski, 1965; Huba, 1994).

In models of an incompressible fluid, the temperature of the medium does not explicitly enter the governing equations. This shows that the effects of thermal conductivity may enter the problem of the Rayleigh-Taylor instability only via the finite compressibility of matter. Therefore we shall base our discussion on Eq. (4.20), which takes compressibility effects into account. The thermal conductivity affects the dissipation of mechanical motion by creating a phase shift between the density perturbation of a certain liquid element and the pressure perturbation introduced by this change in density. Then an irreversible part appears in the $pdV$ work.

If the thermal conductivity is very large, it maintains a uniform temperature in the perturbations (isothermal perturbations). In particular, the sound speed that enters Eq. (4.20) for the growth rate becomes an isothermal sound speed. However, Eq. (4.20) still has unstable roots, with growth rates not much different from the adiabatic case. For short-wavelength perturbations, $k > 1/h$, as described by Eq. (4.22), the thermal diffusivity has a stabilizing effect (Catto, 1978). The characteristic time for the heat to diffuse over the scale length $1/k$ of the perturbation is $\tau \sim 1/k^2\chi$. The growth rate significantly decreases if this time is less than the characteristic growth rate for adiabatic perturbations, $(g/h)^{1/2}$. There may exist other relaxation processes in the system, for example, establishing the ionization equilibrium (see, for example, DeGroot et al., 1997a). Such processes also affect the growth rate of perturbations by causing a phase shift between $\delta p$ and $\delta \rho$.

## C. Resistivity

As has been pointed out by Hussey et al. (1995), Hammer et al. (1996), and Benattar et al. (1999), magnetic-field penetration through the imploding shell may influence the Rayleigh-Taylor instability of flute

(axisymmetric) modes. One might expect that it would add some dissipation and thereby decrease the growth rate. However, as was shown by Hammer *et al.* (1996), there may exist modes that do not perturb the currents and therefore do not induce any additional dissipation. For a profile of the type of Eq. (2.28), such a mode is localized near the surface $x=0$ and has a growth rate unaffected by the resistivity. The presence of this mode is related to the singularity of $\rho'/\rho$ as $x$ goes to zero.

As soon as the density profile near $x=0$ gets smoothed by the development of the instability, the short-wavelength perturbations are affected by the finite resistivity. The expression for the growth rate of these mode reads (Hammer *et al.*, 1996).

$$\Gamma = \sqrt{g\frac{\rho'}{\rho} + \left(\frac{D_M k^2}{2}\frac{s^2}{a^2}\right)^2} - \frac{D_M k^2}{2}\frac{s^2}{a^2}, \qquad (5.5)$$

where $D_M$ is a magnetic diffusivity, $D_M = \eta/\mu$, and $s$ and $a$ are the sound velocity and Alfvén velocity, respectively. Note that in a strongly radiating plasma, in which the magnetic pressure is much greater than the plasma pressure [see discussion related to Eqs. (2.28) and (2.29) in Sec. II. E] and for which, accordingly, $s \ll a$, the stabilizing effect of resistive losses contains a small parameter $s^2/a^2$ and is relatively insignificant.

So far, we have been discussing the instability of the purely flute mode, i.e., the only mode that remains unstable at large wave numbers in the case of a perfectly conducting plasma (see Secs. IV. A–IV. C). The short-wavelength modes that have a cross-field (azimuthal) component of the wave vector are stabilized in such a plasma by virtue of the restoring force produced by a curved magnetic field that is frozen into the plasma and follows its displacements. It is clear that the high plasma resistivity decouples the plasma displacement and the magnetic field. A complete analysis of this problem goes beyond the scope of our survey. Here we restrict ourselves to the notion that in the case of plasma pressure comparable to the magnetic pressure and skin depth comparable to the whole thickness of the layer (Alfvén velocity comparable to the sound velocity), the resistive uncoupling becomes significant at $D_M > sh$, where $s$ is the sound velocity. In other words, the finite resistivity may lead not only to stabilizing but also to destabilizing effects.

# VI. POSSIBLE WAYS OF MITIGATING THE RAYLEIGH-TAYLOR INSTABILITY

## A. General comments

In the previous two sections we discussed in some depth the physics of the Rayleigh-Taylor instability. One important (and already mentioned) difference between the stability of an imploding liner and the stability of a steady-state object, like a plasma in a device with magnetic confinement, is that implosion takes a finite time, while a steady-state plasma configuration is supposed to last essentially forever. Therefore, if some instability is present in the steady-state system, the perturbations cer-

tainly reach a nonlinear stage independent of the initial perturbations. A saturated turbulence then exists for as long as the plasma does, sustained by external particles and energy sources. In imploding systems, on the other hand, the exponentiation factor $G$ introduced by Eq. (4.35) is finite and sometimes not very large (on the order of 5). Under such circumstances, one can hope to reduce the deleterious role of instability by making more perfect initial states, with relative root-mean-square perturbations of less than $10^{-2}$. Conversely, if the growth rate can be reduced by, say, 20% ($\Delta G/G \sim 0.2$), the requirements for the symmetry of the initial state could be reduced by a factor of 2.

Therefore one possible line of defense is to create more perfect initial states (smaller initial perturbations) and look for ways to reduce the linear growth rate. If this approach fails and the instability reaches a nonlinear stage, one can try to prevent the most disastrous scenarios associated with self-accelerating growth of the "bubbles" and gross violations of the cylindrical symmetry of the liner [Fig. 21(a)]. In the following discussion, we mention various effects that may influence the linear and nonlinear stages of the problem. We emphasize that the original stability analyses that we are referring to were often not directly related to fast pinches.

The mitigation methods discussed below do not provide an ultimate solution for instability effects. Moreover, many of them introduce complications into the experimental setting. Still, we present a more or less complete set of existing suggestions with the hope that they may help in finding an efficient solution. One more general conclusion that can be drawn with respect to mitigation is that very little can be done to affect the linear stability of long-wavelength perturbations of an "empty" thin shell ($\lambda \gg h$, where $h$ is the shell thickness); the linear behavior of these perturbations is described by Eq. (4.19), which does not contain any free external parameters.

## B. Magnetic shear

As was mentioned in Secs. IV.A and IV.B, the most dangerous modes are axisymmetric modes that do not create any ripple in the magnetic-field lines, maintaining their circular (straight in the planar geometry) shape. These modes remain unstable at high wave numbers, $k \sim 1/h$, and have a large growth rate, $\sim (g/h)^{1/2}$. Conversely, modes with a finite azimuthal component of the wave number become stable if the wave number is high enough. It is well known from the theory of magnetically confined plasmas (see the original paper by Suydam, 1958, and general surveys by Bateman, 1980, and Freidberg, 1982) that one may achieve reduction of the growth rate or even stabilization of flute modes by creating a magnetic shear, i.e., by creating a situation in which the magnetic-field vector, remaining normal to the gravity force, would change direction over the depth of the transition layer. In the $Z$-pinch geometry this would require introducing the axial magnetic field $B_z$, possibly, varying over the thickness of the shell.

For the reasons discussed in Sec. IV.B, one can assume that magnetic shear will have no effect on the stability of long-wavelength modes, $\lambda \gg h$. One can, however, hope that the growth rate of modes with $\lambda \sim h$ (and these are the most dangerous modes) will be reduced. Indeed, applying a general approach based on the energy principle (Suydam, 1958), Gratton, Gratton, and Gonzalez (1988) have shown that, for the local modes ($\lambda \ll h$), the presence of the shear leads to the appearance of a stabilizing contribution to Eq. (4.22) for the growth rate:

$$\Gamma^2 = \frac{g^2}{a^2 + s^2} + \frac{g\rho'}{\rho} - \frac{a^2 \zeta^2}{4}. \tag{6.1}$$

The parameter $\zeta$ is the $z$ derivative of the angle formed by the magnetic field with the direction of the wave vector at the point where the magnetic field is normal to the wave vector. If the $z$ component of the magnetic field is zero, then the shear is also zero. If the $z$ component of the magnetic field is comparable to the azimuthal component, then $\zeta \sim 1/h$. In this case the magnetic shear can considerably reduce the growth rate of the local modes and can even completely stabilize them. In other words, the magnetic-shear stabilization has some promise for local modes.

As we have already mentioned, the shear does not stabilize the large-scale modes, with $\lambda \gg h$. Still, the presence of an axial magnetic field enclosed by the liner may have some effect on the stability. Using an approach similar to that developed by Harris (1962), one can show that, if the magnetic field has components $B_{ye}$ and $B_{ze}$ on the outer side of the shell, and a component $B_{zi}$ on the inner side of the shell (there is no $y$ component of the magnetic field inside the shell if there is no axial current inside the shell), the dispersion relation for the $\lambda \gg h$ modes, an analog of Eq. (4.19), becomes (see Bud'ko, Liberman, Velikovich, and Felber, 1990)

$$\omega^4 - 2kg\omega^2 \frac{B_{ye}^2 \cos^2 \alpha + (B_{ze}^2 + B_{zi}^2)\sin^2 \alpha}{B_{ye}^2 + B_{ze}^2 - B_{zi}^2} - k^2 g^2 = 0, \tag{6.2}$$

where $\alpha$ is defined according to Eq. (4.16) and the acceleration is $g = (B_{ye}^2 + B_{ze}^2 - B_{zi}^2)/2\mu\sigma$. The dispersion relation (6.2) universally has an unstable root that scales as $\sqrt{kg}$ (we assume that the acceleration is directed inward, i.e., $B_{ye}^2 + B_{ze}^2 - B_{zi}^2 > 0$). On the other hand, if $B_{zi} > B_{ze}$, the growth rate for the $\alpha = 0$ mode is reduced compared to Eq. (4.19).

One should remember that it is undesirable to have an axial magnetic field enclosed by the shell, because then part of the energy of the imploding liner would be spent on the compression of this magnetic field. The other difficulty with imposing an axial magnetic field is that, in the time frame of the implosion, the axial magnetic field remains frozen into the conducting electrodes. Therefore strong distortions of the cylindrical symmetry, of the type shown in Fig. 7, are inevitable. One could reduce this effect by introducing radial cuts, but, as the skin depth is very small, the axial magnetic field would
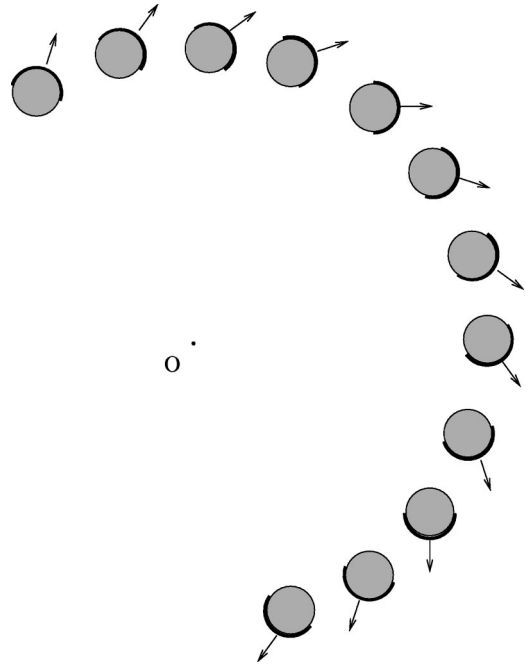


FIG. 24. Left-right asymmetric coating. Shown in heavier lines are the areas coated by material with a lower sublimation energy, which will ablate early in the pulse. The direction of the ablation flow is shown by arrows. Diameters of the wires are grossly exaggerated. Only part of the array is shown. Current flows into the paper.

remain frozen into the segments of the electrode between two neighboring cuts.

## C. Rotation

The possibility of using rotation of the shell for stabilization purposes has been discussed by Book and Winsor, 1974; Barcilon, Book, and Cooper, 1974; and Turchi *et al.*, 1976. The stabilizing effect comes from the centrifugal force that is directed opposite to the effective gravity force near the stagnation point. In the early works, it was supposed that rotation would be introduced by mechanical means. The concept of centrifugal stabilization was recently reconsidered by Rostoker, Peterson, and Tashiri (1995), who suggested using a cusp magnetic field to create an azimuthal torque that would appear because of the interaction of the $z$ component of the current and the $r$ component of the magnetic field. Hammer and Ryutov (1996) suggested using an ablative torque by producing a left-right asymmetric structure at the surface of the shell. One can also use left-right asymmetric coatings on the surfaces of wires (Fig. 24); an ablation of the coating early in the pulse would produce a torque acting on the wires and imparting an angular momentum to them.

To have an appreciable effect on the instability, the rotation should change the radial acceleration by a factor of the order of 1. This, in turn, means that, near the point of maximum compression, the rotation energy

should be comparable to the total implosion energy. This is the energy penalty associated with this method of stabilization.

A stability analysis of an imploding rotating liner compressing an axial magnetic field was carried out by Barcillon, Book, and Cooper (1974). The critical point in this system was the turning point of the radial motion of the rotating liner. Barcillon *et al.* concluded that it is difficult to achieve a strong stabilizing effect, especially in the case of a thin liner. Velikovich and Davis (1995) studied the stability of a steady-state configuration, $r$ =const, in which the centrifugal force was exactly balanced by the magnetic pressure (in the *Z*-pinch geometry). The stabilizing effect in this case was relatively modest. Although these results are somewhat discouraging, it is probably worth considering the stability of the *Z* pinch under realistic assumptions with regard to the time-history of the pinch radius $r(t)$. Although it is not very probable that rotation would entirely stabilize the system, it might reduce the growth rates of instabilities to an admissible level.

## D. Velocity shear

In principle, one can introduce an azimuthal shear flow instead of a solid-body rotation. The possible stabilizing effect of shear flow on the Rayleigh-Taylor instability was mentioned as early as 1961 by Chandrasekhar; in conjunction with fast *Z* pinches it was discussed by Hammer and Ryutov (1996) and Shumlak and Roderick (1998). To understand the role of the shear qualitatively, consider a slab geometry with a slab of an incompressible fluid supported from below by a massless fluid. Let the unperturbed flow velocity be directed along the *y* axis and be linearly dependent on *x*: $v_y = u(x/h)$. The shear flow will have the strongest effect on perturbations whose wave vector is directed along the direction of flow. For such perturbations, the shear flow will lead to stretching in the *y* direction and thereby to greatly changed eigenfunctions. One might hope that stretching of the "fingers" typical of a Rayleigh-Taylor instability would reduce their growth. The stretching time of the perturbation is of the order of $h/u$, independent of the scale of the perturbation, while the growth rate of a gravity-driven perturbation is of the order $(kg)^{1/2}$. Obviously, shear flow can have a significant effect on the development of perturbations if the condition $(h/u) \times (kg)^{1/2} < 1$ holds. For the most dangerous perturbations, with $k \sim 1/h$, one can rewrite this condition in terms of a so-called Froude number,

$$Fr \equiv \frac{u^2}{gh} > I. \tag{6.3}$$

Taking as an example $h = 0.1$ cm and $g = 3 \times 10^{15}$ cm/s², one finds that the velocity of the shear flow should be rather high, greater than $10^7$ cm/s. It is difficult to produce such a velocity directly. One can, however, expect an enhancement of the azimuthal velocity during implosion, owing to conservation of angular momentum. (For a "canonical" wire-array implosion, the viscous damping

of the shear flow is insignificant.) If the initial shear flow velocity is $10^6$ cm/s, the desired value will be reached at a convergence equal to 10. One can also speculate that the actual time required for perturbations to grow from an initial small level to a nonlinear phase constitutes at least several *e*-folding times $(kg)^{-1/2}$. Accordingly, one might hope to be able to write, on the right-hand side of inequality (6.3), some small number instead of 1. A numerical analysis by Shumlak and Roderick (1998) seems to point in this direction.

Unfortunately, shear flow does not have any effect on perturbations whose wave vectors are perpendicular to the direction of the flow. In other words, if the shear flow is in the azimuthal direction (the differential rotation), it does not affect azimuthally symmetric perturbations $(m=0)$. To stabilize these perturbations, one has to generate an axial shear flow, with $v_z$ varying with *x*. This type of shear motion cannot be enhanced by angular momentum conservation; therefore requirements stemming from inequality (6.3) become more stringent.

To generate shear flow, one can use a target consisting of two nested liners (Hammer and Ryutov, 1996). If the left-right asymmetric features are embedded into one of these liners, then ablation will cause its rotation; when the two liners collide, a differential rotation emerges. If up-down asymmetric features are created, then axial shear flow is formed. Shumlak and Roderick (1998) discussed the use of a conical gas puff to generate the axial shear.

Axial shear flow may have a stabilizing influence on quasiequilibrium *Z* pinches that can be formed near the stagnation point. This stabilization mechanism for equilibrium *Z* pinches was discussed by Shumlak and Hartman (1995). Their conclusion was that, if the initial profile is not very far from the marginally stable "Kadomtsev profile," then even a weak-velocity shear can produce considerable stabilization. On the other hand, Arber *et al.* (1995) have not found significant stabilization by the shear.

## E. Hourglass effect

Douglas, Deeney, and Roderick (1997) have discovered in numerical simulations that, by making the initial surface of a uniform-fill *Z* pinch concave (Fig. 25), one can suppress the growth of Rayleigh-Taylor perturbations. Because of the characteristic shape of the sheath, one can call this effect an "hourglass effect." Douglas, Deeney, and Roderick considered implosions of high-*Z* (strongly radiating) gas puffs (Ne, Xe), in which the transition layer between the magnetic piston and the shock front was thin (see Sec. II.B). For a sufficiently large initial curvature, the stabilizing effect is quite strong. The authors attribute this effect either to the advection of perturbations to the electrodes (there is tangential flow along the curved surface, in the direction of electrodes) or to the presence of axial shear flow. In principle, one could discriminate between these two possibilities by changing the sign of the curvature (making the surface convex instead of concave); the flow would
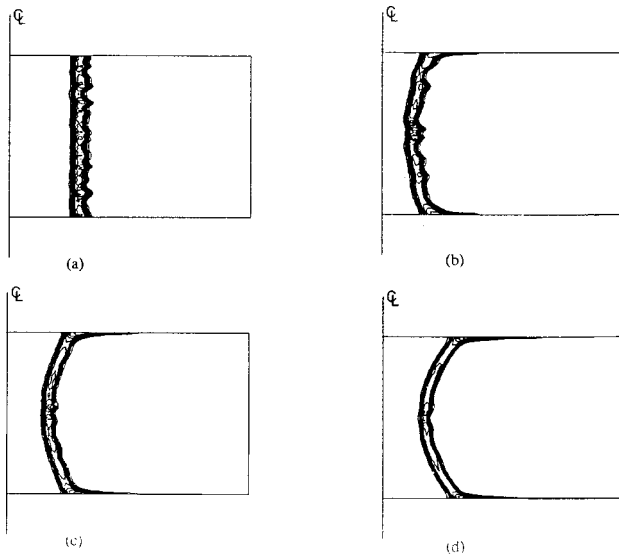
FIG. 25. Effect of a curved surface of a uniform-fill krypton *Z* pinch (from Douglas, Deeney, and Roderick, 1997, reprinted with kind permission of M. Douglas). Shown are density isocontours at the same time in the implosion for (a) a straight cylinder, (b) a 1.0-mm circular arc, (c) a 2.5-mm circular arc, and (d) a 5.0-mm circular arc.



FIG. 26. A corrugated wire array. The azimuthal mode number in this case is $m=6$. The thickness of the line in panel (a) corresponds to the local surface density of the liner material. The surface of a perfectly conducting liner coincides with one of the field lines. The adjacent field line is shown as a dashed line. Panel (b) shows a part of the initial array that can produce a structure similar to the one shown in panel (a): The array is assembled of the wires of two different diameters, $d_1$ and $d_2$.

change its sign and would advect perturbations to the equatorial plane, while the effect of shear should remain the same as for a concave surface.

## F. Deliberate violation of the azimuthal symmetry

As already mentioned in Sec. IV, the most dangerous small-*m* modes show a trend to strongly nonlinear development, with the fingerlike structures penetrating deep to the axis of the device (Fig. 22). Self-acceleration of the "fingertips" occurs because their mass density decreases, while the driving azimuthal magnetic field freely penetrates into this area through disklike slots—a characteristic feature of axisymmetric perturbations. Derzon, Nash, and Ryutov (1997) suggested reducing the growth rate of the axisymmetric perturbations by deliberate introduction of a periodic azimuthal asymmetry, as shown in Fig. 26, with a large enough amplitude and a large enough mode number *m* to destroy the azimuthal coherence of the fingerlike structure and to create conditions for short-circuiting (crow-barring) the disklike slots in many (*m*) points over the azimuth.

For this closure of the slots to occur at a moderately nonlinear stage in the growth of axisymmetric perturbations, when the peak-to-valley distance is of the order of their axial period λ, one has to produce azimuthal perturbations for which the amplitude, $\xi$, satisfies, roughly speaking, the condition: $\xi > \lambda/2$. One can conceive of several ways of creating azimuthal perturbations in a controlled manner. One way is to assemble the wire array with wires of azimuthally varying thickness (i.e., of varying mass), similar to what is shown in Fig. 26(b); the heavier wires will lag behind the lighter ones, thereby creating a corrugated structure. Another possibility is to
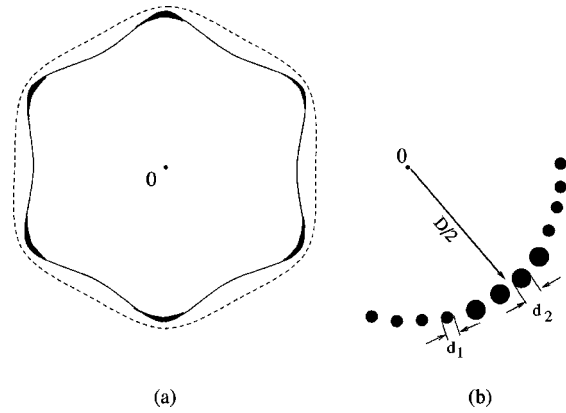
use wires of different materials (and, accordingly, of different mass). Still one more possibility is to use a kind of "imprinting" produced by the discrete structure of the return-current structure (which typically consists of ~10 separate posts; the gaps between the posts provide a necessary diagnostic access). At an early stage of the discharge, when the separation of the current sheath from the posts is comparable to the interpost distance, the radial driving force varies over the azimuth, giving rise to formation of a corrugated structure. Such a structure has been observed experimentally by Derzon, Nash, and Ryutov (1997).

In wire-array implosions, the axial period of the most dangerous modes is in the range of 1–1.5 mm. Therefore, according to the condition $\xi > \lambda/2a$, a relatively modest amplitude of corrugation (0.5–0.75 mm) could be sufficient to produce a considerable stabilizing effect. The mode number of the corrugation should be made large enough to provide many short-circuit channels over the azimuth. This is limited from above by the constraint that, at a given amplitude, the high-mode-number perturbation becomes nonlinearly stabilized by expulsion of the magnetic field from the tips of azimuthal perturbations [Fig. 21(b)]. The upper limit on the mode number set by this constraint is $m < r/2\xi \sim r/\lambda$. For a typical set of parameters of a wire-array implosion, the optimum mode number is ~15.

## G. Accretion

As mentioned in Secs. II and IV, in implosions of gas-puff loads one can, in principle, create an initial density distribution such that the sheath will converge on axis without any acceleration (Fig. 5). In its clearest form, this idea was expressed by Hammer (1995) and, later, by Hammer *et al.* (1996) and Velikovich, Cochran, and

Davis (1996). The energy penalty is associated with radiative losses of the accreted material. The stabilizing effects are caused merely by the absence of acceleration. The interface between the magnetic field and the plasma remains stable with respect to exponentially growing modes, even for very short wavelengths (shorter than the distance between the shock and the interface). Another source of stabilization is the presence of a detached shock, as discussed by Gol'berg and Velikovich (1993): because the shock front itself is stable with respect to the ripple perturbations, it extends its stabilizing influence over the whole area between the shock and magnetic piston.

One can think of a discrete version of the scheme proposed by Hammer *et al.* (1996) in which, instead of a continuous density distribution, one would create a set of nested wire arrays, with masses approximately following the desired density distribution. This would mean that the lightest arrays would be on the outside and that their mass would gradually grow towards the inside. Whether the improved stability would outweigh the added complexity is a question that can be answered only experimentally.

It has recently been discovered experimentally (Deeney, Douglas, *et al.*, 1998) that a considerable improvement in the quality of the implosion can be reached by using a two-shell wire array, with the inner shell situated at a half radius of the outer shell and having a mass smaller (not greater as in the aforementioned scheme) than the outer shell. The best result was reached with the inner mass as small as a quarter of the outer mass. It is not clear yet what specific mechanism is responsible for this improvement. One can speculate that strong heating during collision of the two shells causes a rapid viscous and thermal damping of perturbations developed in the outer shell by the time of the collision.

### H. Enhanced thermal dissipation

The suggestion has been made (Ryutov, 1996; Ryutov and Toor, 1998) that, to increase the rate of viscous and thermal dissipation, one should replace a uniform medium with a finely structured medium, with a scale $l$ of preexisting nonuniformities that is small compared to the scale $\lambda$ of the most dangerous perturbations. In the case of wire arrays, this could be done by replacing uniform wires with bundles of interwoven finer wires or by alternating the composition of the wires in the array. The hope is that the presence of the fine structures will introduce small-scale motions (and temperature variations) overlaid on the "averaged" motions (and temperature variations) on the larger scale of the most dangerous perturbations. Because the dissipation rate by both viscosity and thermal conductivity scales as $1/l^2$, one could expect that the growth rate of the instability would be substantially reduced. The effect of enhanced dissipation is certainly present, but in the examples studied so far it causes only a relatively small decrease in the linear growth rate (see also Sec. V B). A new element

that emerges in this picture is the appearance of oscillatory damping modes (in addition to the "standard" Rayleigh-Taylor modes). The presence of these modes may favorably affect the nonlinear stage of the instability. However, this issue has not been studied thus far.

### I. Finite Larmor-radius (FLR) effects

The ion gyroradius is small compared to a typical sheath thickness during the run-in phase. At this stage, the ion component can be well described by fluid equations. The situation changes dramatically after stagnation, when the ion thermal energy increases by orders of magnitude. Arber *et al.* (1995) studied the stability of an equilibrium pinch with an ion Larmor radius comparable to the pinch radius. They concluded that even if the $m=0$ mode is almost stable by virtue of reaching the Kadomtsev profile, the $m=1$ mode remains strongly unstable, despite finite Larmor-radius (FLR) effects. The growth rate is reduced by a factor of 2–3 with respect to an ideal MHD, but this is insufficient for a long-lasting steady-state equilibrium. Scheffel *et al.* (1997) have shown that a finite electron temperature has a destabilizing effect on a plasma with a finite Larmor radius.

Isichenko, Kulyabin, and Yan'kov (1989) considered a pinch column with a skin layer much thinner than the ion gyroradius so that ion motion in the interior of the pinch was unmagnetized. They found that the growth rate of short-wavelength perturbations, with $\lambda \ll r$, reached saturation at $\sim v_{Ti}/r$, i.e., became slower than in the MHD approximation, where it was $\sim(v_{Ti}/r) \times(r/\lambda)^{1/2}$. However, the most disruptive mode with $\lambda \sim r$ remained essentially as unstable as in the MHD approximation. Therefore the effects of a large Larmor radius do not provide sufficient stabilization in the stagnation phase. Velikovich (1991) came to a similar conclusion.

## VII. NON-MHD PHENOMENA

### A. Microturbulence and anomalous resistivity

A potential source of microinstabilities is the relative motion of electrons and ions. The velocity $u$ of this motion is directly related to the current density, $j=enu$, where $n$ is the electron density. In implosions of thin shells (like those formed in wire-arrays,) assuming that the current occupies the whole shell thickness, one can express $u$ in terms of the total pinch current $I$:

$$u(cm/s) \sim 10^4 \frac{AI(\text{MA})}{Z_{\text{eff}} \hat{m}(\text{mg/cm})}. \tag{7.1}$$

The assumption that the current flows through the whole thickness of the shell is quite plausible for the run-in phase of strongly radiating liners (Sec. II E).

In $Z$ pinches, the current is directed across the magnetic field; the electron temperature is comparable to or lower than the ion temperature. Under such circumstances, the most likely instability that could lead to the appearance of anomalous resistivity would be a lower-

hybrid instability, described by Krall and Liewer (1971) and Davidson and Gladd (1975). Early studies of this instability have been summarized in the survey by Davidson and Krall (1977). More recent results, specifically addressing the issues of nonlinear stabilization, can be found in analytical studies by Drake, Huba, and Gladd (1983) and by Drake, Guzdar, and Huba (1983) and in a numerical analysis by Brackbill *et al.* (1990). Possible effects of this instability on the Pease-Braginski current in a fiber pinch were studied by Robson (1991) and Chittenden (1995).

The ''natural'' frequency of lower-hybrid oscillations is (see, for example, Davidson and Krall, 1977)

$$\omega_{LH} = \omega_{ce}\sqrt{\frac{Z_{eff}m_e}{Am_p}}, \qquad (7.2)$$

where $m_p$ is the proton mass. Expression (7.2) for the lower-hybrid frequency pertains to the situation $\omega_{pe} > \omega_{ce}$, which is typical of Z pinches ($\omega_{pe}$ and $\omega_{ce}$ are electron-plasma and electron-cyclotron frequencies, respectively).

In an analysis of lower-hybrid instabilities, usually only perturbations with $k_{\parallel}=0$ are considered. In order for such perturbations to cause electron scattering and contribute to the anomalous resistivity, their transverse scale length should be comparable to or shorter than the electron gyroradius $\rho_e$. Otherwise, because the perturbations are slow, $\omega_{LH} \ll \omega_{ce}$, the electron magnetic moment will be conserved, and electrons will experience only adiabatic (reversible) variations of their velocity, thereby preventing the appearance of anomalous resistivity.

Another current-driven microinstability is the ion acoustic instability, which typically has a higher threshold in terms of the relative velocity of electrons and ions. Extensive studies of this instability are summarized in the surveys by Vedenov and Ryutov (1975) and Galeev and Sagdeev (1979). In a singly charged plasma this instability can be present only if the electron temperature is much higher than the ion temperature, $T_e \gg T_i$: at $T_e \sim T_i$ the ion sound speed is comparable to the thermal velocity of the ions, and acoustic waves experience a strong ion Landau damping. However, in a plasma with $Z_{eff} \gg 1$, this instability can be excited even at $T_i > T_e$. Indeed, the sound speed in a plasma with high-Z ions is equal to

$$\sqrt{\frac{Z_{eff}T_e+T_i}{m_i}}, \qquad (7.3)$$

while the ion thermal speed is $\sqrt{2T_i/m_i}$. Imposing a constraint that the sound speed exceed the ion thermal speed by a factor of 2, one finds the condition of weakly damped ion acoustic waves in a high-Z plasma:

$$T_e > 7T_i/Z_{eff}. \qquad (7.4)$$

One sees that, at $Z_{eff} \gg 1$, weakly damped ion acoustic modes can exist even at $T_i > T_e$. The critical current velocity for the onset of ion acoustic instability under such conditions is several ion thermal velocities,

$$u_{crit} = \zeta v_{Ti}, \qquad (7.5)$$

with $\zeta$ equal to 2–4. In the case of hydrogen-containing substances (for example, agar), the hydrogen ions, because of their high thermal velocities, can considerably increase the Landau damping and push the critical velocity to higher levels, approaching $u_{crit} \sim v_{T_e}$, typical of the Buneman instability.

If condition (7.4) is violated with a large enough margin (so that ion acoustic instability is not present), the relative electron-ion velocity $u$ may reach an electron thermal velocity, and a modified two-stream (or Buneman) instability may develop. Its growth rate is higher than that of an ion acoustic instability. However, reaching such high $u$'s for the typical parameters of dense pinches is not very probable (see Sec. IX).

The effect of microinstabilities on plasma resistivity is traditionally described in terms of the effective electron-scattering frequency $\nu_{eff}$, which should be added to the electron-ion collision frequency $1/\tau_{ei}$ in the expression for plasma resistivity,

$$\eta = \frac{m_e(\nu_{eff}+1/\tau_{ei})}{ne^2}. \qquad (7.6)$$

An estimate that is commonly used for the effective collision frequency produced by a lower hybrid instability is (Davidson and Gladd, 1975; Drake *et al.*, 1984)

$$\nu_{eff} = \zeta_1\omega_{LH}\left(\frac{u}{v_{Ti}}\right)^2, \qquad (7.7)$$

where $\zeta_1$ is a numerical factor of the order of 1.

At low plasma density and high pinch currents, when the current velocity $u$ reaches the threshold of ion acoustic instability, this latter instability becomes dominant because it usually results in a higher effective collision frequency approaching the ion-plasma frequency. Under the condition $\omega_{pe} > \omega_{ce}$, typical of a Z-pinch environment, the ion-plasma frequency is much higher than the lower hybrid frequency. Therefore, if the threshold for excitation of ion acoustic perturbations is reached at all, this instability takes over in establishing the anomalous resistivity. When the instability threshold $u = u_{crit}$ is reached, the effective scattering turns on so sharply that, in most cases of interest for Z pinches, it keeps the relative velocity just at the threshold level, so that the current density is

$$j = enu_{crit} \qquad (7.8)$$

with $u_{crit}$ as in Eq. (7.5). Equations (7.6)–(7.8) can serve as a basis for analyzing the effect of anomalous resistivity on the properties of Z pinches.

Microfluctuations produced by the plasma current, in addition to the anomalous resistivity, may cause acceleration of some of the plasma ions to suprathermal energies (see Sec. VII B). The anomalous resistivity, if present, affects the skin depth and therefore the Rayleigh-Taylor instability. The heating rate of the electrons during the implosion phase may grow considerably and therefore lead to enhancement of radiation losses compared to classical estimates. In the case of quasiequi-

librium pinches, the anomalous resistivity affects the Pease-Braginski current (Robson, 1991). We shall not attempt here to consider a completely self-consistent picture. Our discussion provides only a general framework for the analysis of the corresponding processes. As we shall see, in the fast-Z-pinch environment the velocity $u$ is typically smaller than or comparable to the ion thermal velocity. Therefore we concentrate our attention on the lower hybrid instability.

### 1. Run-in phase

To be specific, we begin this subsection with a discussion of wire arrays; later in this subsection we also mention gas puffs. The velocity $u$ of the relative motion of the electron and ion fluids is typically comparable to the ion thermal velocity. For a set of characteristic parameters of the run-in phase of tungsten wire-array implosions ($A \sim 180$, $T \sim 40$ eV, $Z_{\text{eff}} \sim 7$, $I = 10$ MA, $\hat{m} \sim 3$ mg/cm), one finds $u \sim 10^6$ cm/s, roughly equal to the ion thermal velocity $v_{Ti}$. For the "canonical" lower hybrid instability, $\omega_{\text{LH}}$ according to the paper by Davidson and Gladd (1975), the growth rate at $u < v_{Ti}$ scales as

$$(u/v_{Ti})^2 \omega_{\text{LH}}, \tag{7.9}$$

In the aforementioned numerical example, it is of the order of $\omega_{\text{LH}} \sim 1.5 \times 10^{11}\,\text{s}^{-1}$, i.e., the $e$-folding time for this instability is orders of magnitude shorter than the duration of the run-in phase. Accordingly, the instability reaches its nonlinear saturation.

There is a subtlety here: for the set of parameters chosen above and $n_i \sim 10^{19}\,\text{cm}^{-3}$, one finds that both the electron and ion magnetization products, $\omega_{\text{LH}}\tau_{ei}$ and $\omega_{\text{LH}}\tau_{ii}$, are considerably less than 1. This implies that the plasma is strongly collisional with respect to the lower hybrid modes. By itself, this does not necessarily mean that the instability is damped. Rather, it means that the theory presented in the aforementioned references should be reworked to include a hydrodynamic description of both electrons and ions (see, for example, Braginskii, 1965). The strongly collisional plasma also makes it very difficult for the instability to affect the plasma resistivity (because the anomalous collision frequency has to compete with classical collision frequency, which is very high).

In gas-puff implosions with a lower particle density, the role of the lower hybrid instability can be more important. However, the classical electron-ion collision time remains shorter than the expected anomalous collision time. Therefore, again, the current penetration should be determined by classical resistivity and/or by gross hydrodynamic instabilities. The anomalous resistivity may possibly play some role in the behavior of a very-low-density halo plasma that may surround the main discharge.

The effect of anomalous resistivity can, in principle, be used to reduce the current rise time in a wire array. The idea is to surround it by another, lower-density shell where the current would be sharply terminated by development of anomalous resistivity. Branitskii *et al.*

(1996) pursued this idea, studying implosions of gas puffs on a thin agar cylinder in the Angara-5 facility; Xe, Ar, and $C_3H_8$ (propane) were used as working gases. The annular jet had a radius of $r_0 = 1.6$ cm and a mass of 0.07 mg/cm; the maximum current was $\sim 3$ MA and the half-width of the current pulse was $\sim 100$ ns. The inner cylinder was made of agar, with a radius of $r_i = 0.5$–1 mm and a mass of 0.05–0.07 mg/cm. The switching of the current indeed occurred, but it did not have a sharp front. The authors concluded that the current disruption in the outer shell was probably caused by the Rayleigh-Taylor instability, although other factors may also have contributed.

Baksht *et al.* (1997) also studied a multiwire array surrounded by an outer gas shell. The dimensions were larger than in the previous work; the diameter of the gas jet was 8 cm and the diameter of the wire array was 3 cm, with wires 20 $\mu$m in diameter (68 $\mu$g/cm). Reproducibility of the current switching was not very good. To improve the symmetry of implosions, the authors plan to introduce preliminary ionization of the gaseous shell (see Sec. III of this paper). Note that another way of switching the current (not based on the phenomenon of anomalous resistance) is to use a light external wire array imploding on a smaller-diameter heavier wire array; the current through the inner array will be small until the outer array reaches it (Davis, Gondarenko and Velikovich, 1997).

### 2. The stagnation phase

In the stagnation phase, the temperatures of both plasma species are much higher, with the ion temperature considerably exceeding the electron temperature. On the other hand, the relative velocity $u$, according to Eq. (7.1), only decreases because of the increased $Z_{\text{eff}}$. Therefore the ratio $u/v_{Ti}$ should drop by a factor of $\sim 100$ compared to the run-in phase. This decrease more than compensates for the growth of the magnetic field caused by a reduced pinch radius, so that the growth rate (7.9) decreases to, roughly speaking, $10^8\,\text{s}^{-1}$. The corresponding $e$-folding time is long compared to the duration of the stagnation phase; this instability can hardly have a significant effect on the plasma resistivity during this phase.

It is interesting to note that, for the stagnation phase, the ratio of the relative velocity $u$ to the ion thermal velocity is equal to the ratio of the ion gyroradius to the pinch radius and can be expressed in terms of very few input parameters. One can show that, assuming that the current flows uniformly over the cross section of the stagnated plasma,

$$\frac{\rho_i}{r_{\text{min}}} \sim \frac{u}{v_{Ti}} \sim \frac{A}{Z_{\text{eff}}\sqrt{\ln C}}\sqrt{\frac{m_p}{r_{op}\hat{m}}} \sim 10^{-3}\frac{A}{Z_{\text{eff}}\sqrt{\hat{m}(\text{mg/cm})}}, \tag{7.10}$$

where $\rho_i$ is the ion gyroradius, $r_{op} = 1.6 \times 10^{-16}$ cm is the classical radius of a proton, and $C$ is the convergence (1.1). The estimate (7.10) corresponds to the ion temperature before equilibration with electrons begins, i.e.,

to an ion thermal velocity approximately equal to the liner velocity just before on-axis stagnation.

Of course, if the current is concentrated in a thin shell, or flows through a low-density plasma halo, the role of microinstabilities may become more important. The other place where anomalous resistivity may become important is the neck [Fig. 21(a)] formed as a result of the development of a sausage mode (we discuss this latter situation in Sec. VII.B). A discussion of the effects of anomalous resistance of the neck and some further references on this issue can be found in Sasorov (1992).

A study of the effects produced by anomalous resistivity in an equilibrium pinch can be found in Chittenden (1995). In equilibrium $Z$ pinches, where plasma density is typically lower than in fast $Z$ pinches, instability can become quite important because of a higher ratio $u/v_{Ti}$ and much lower frequency of Coulomb collisions.

## B. Generation of suprathermal particles and particle beams

As mentioned in Sec. IV, development of the Rayleigh-Taylor instability may lead to a situation in which one or several constrictions of the type shown in Fig. 21(a) are formed. Most commonly, the formation of high-energy particles in $Z$ pinches is related to formation of $m=0$ constrictions. Various theories concerning generation of nonthermal fast particles are discussed by Haines (1983), Trubnikov (1986), Vikhrev (1986), and Deutsch and Kies (1988). These papers also provide further bibliography. Experimental results from fast $Z$ pinches are essentially unavailable. For experiments pertaining to generation of high-energy particles in fiber pinches see Mitchell *et al.* (1998) and references therein.

One can distinguish three mechanisms that lead to the formation of high-energy particles in constrictions. First, there is a direct acceleration mechanism related to the generation of a high inductive voltage during current breakup after formation of the neck. This mechanism was the first to be suggested to explain generation of neutrons in the experiments of the early 1950s (see Vikhrev, 1986, and Deutsch and Kies, 1988, for references to experimental work). Second, there is a mechanism related to compressional heating of the substance situated in the neck, accompanied by ejection of hot material from the ends of the constriction. Third, if microturbulence is excited in the constriction (because of a high current density), stochastic acceleration of the tails of the ion distribution function may lead to generation of high-energy ions. It is quite conceivable that all three mechanisms for the formation of fast ions may act simultaneously. This is what makes the analysis of experiments on the generation of fast ions so difficult.

The chain of events that leads to inductive acceleration is as follows. After constriction develops, impedance grows, and the current through the neck diminishes, causing the generation of a large inductive voltage. The spatial and temporal evolution of the electric fields that can be generated in such an event have

been analyzed in great detail by Trubnikov (see a summary of these results in Trubnikov, 1986).

Trubnikov's analysis offers the following qualitative picture. Consider the motion of an individual ion in a time-varying electric field perpendicular to the azimuthal magnetic field. If the ion gyroradius is small compared to the neck radius $a$, and the electric field varies with a time scale exceeding $\omega_{Ci}^{-1}$, the electric field does not accelerate ions but rather causes drift motion, with the velocity proportional to the electric-field strength $E$. This is an adiabatic process in the sense that the drift velocity grows when the electric field (in the location of the ion) grows and decreases when the electric field decreases (either because of the temporal variation of the electric field, or because the ions leave the zone of the strong electric field near the neck). Therefore, to ensure an efficient nonadiabatic energy transfer to the ions, one has to assume that the electric field varies on a time scale short compared to the ion gyroperiod. Another possibility is that the ion accelerates near the axis of the discharge where the magnetic field is small. (An interesting question is what sets the lower limit for the pinch radius in the constriction. One surmises that this is the ion gyroradius; see the trajectory analysis in Haines, 1983.) To sustain the current through the neck with a rapidly growing resistance, an inductive electric field is generated directed along the pinch current. Accordingly, the ions should be accelerated predominantly in the direction of the pinch current at a time just before disruption. Collisions between beam and plasma ions would cause scattering of the beam. To reach the electrode, the beam must be formed at a distance not greater than a couple of mean free paths. The drag against plasma electrons in a cold plasma may also be substantial. An analysis of experimental measurements at Angara-5 from the viewpoint of their compatibility with the beam source of the neutrons is presented by Imshennik (1992).

We note in passing that it is conceivable that the currents present on the galactic scale form pinchlike structures and that development of the sausage instability gives rise to the generation of high-energy cosmic rays. This viewpoint was presented by Haines (1983) and Trubnikov (1990; see also further references in the latter paper). The arguments pointing out the presence of currents up to $10^{19}$ A in the galactic environment were presented by Peratt (1986, 1990). Figure 27 (Yusef-Zadeh, Morris, and Chance, 1984) depicts an object near the center of our galaxy where the presence of filaments may be a reflection of the pinch effect.

The second mechanism, most completely presented in the paper by Vikhrev (1986), attributes the generation of fast particles to an adiabatic compression of the plasma in the neck. This process is conceived as a gradual compression of the plasma along the sequence of Bennett equilibria, with a gradual decrease in linear particle density $N$ (the number of particles per unit length of the pinch) in the constriction by virtue of axial ion losses through the ends; the hot ions escape in both directions. The Bennet (1934) equilibrium condition,
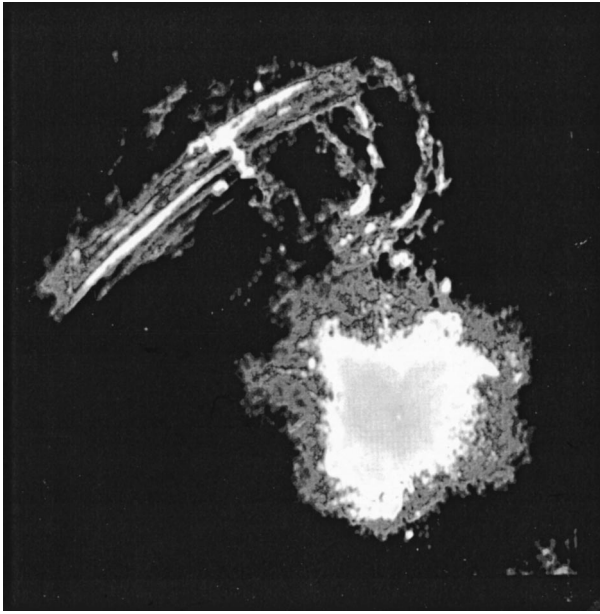
FIG. 27. The image of filaments near the center of our galaxy obtained at the wavelength 20 cm (courtesy of F. Yusef-Zadeh and the National Radio Astronomy Observatory, Charlottesville, Virginia). The length of the arcs is $\sim 30$ pc. According to Trubnikov (1990), they may be pinches.

$$T = \frac{\mu I^2}{4\pi \mathcal{N}}, \tag{7.11}$$

shows that the plasma temperature in the constriction must grow. If the constriction is short, with a radius $r$ comparable to its length $\ell$, the hot plasma will escape very rapidly through the ends, and no significant number of hot particles will be formed. However, if the length of the constriction is large, $\ell \gg r$, then the number of hot particles will increase, and conditions for generation of a considerable number of neutrons (in the case of a deuterium or a deuterium-tritium plasma) will be reached.

If the ion-ion collision frequency is high enough, then the ion distribution is almost isotropic, and therefore the neutron radiation generated in the constriction will also be isotropic. Still, if some hot ions do escape along the axis, an asymmetry in the number of ions reaching the anode and the cathode may appear (leading to asymmetry of neutron generation on the electrodes). The situation is illustrated in Fig. 28, which depicts two ion trajectories originating on the axis. If the initial ion velocity is slightly tilted to the axis and directed towards the cathode, the magnetic field produces a focusing force, and the ion rapidly moves along the axis towards the cathode. On the other hand, if the initial velocity is directed toward the anode, the magnetic force is defocusing, and the ion gets involved in a gyromotion with a slow drift towards the anode (see Haines, 1983). A collisionless version of ion acceleration by pinch "walls" converging on the axis was discussed by Deutsch and Kies (1988).

The third mechanism can be efficient in a plasma of relatively low density, where the plasma resistance is dominated by microfluctuations (Sec. VII.A). The ion
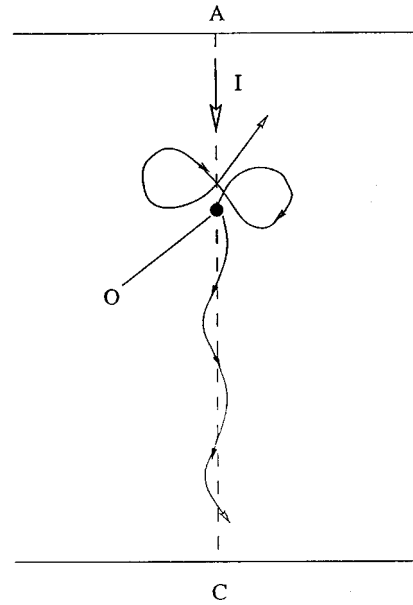


FIG. 28. Two ion trajectories originating in the same point "O" on the axis and forming initially the same small angle with the axis. If the initial velocity is directed towards the cathode, the ion trajectory remains close to the axis; if the initial velocity has an opposite direction, the ion trajectory acquires a peculiar character, with a much slower drift towards the anode.

scattering on microfluctuations usually leads to formation of a high-energy tail of the ion distribution function [Vedenov and Ryutov (1975) and Galeev and Sagdeev (1979)], whose evolution is governed by a Fokker-Planck-type equation,

$$\frac{\partial f}{\partial t} = \frac{1}{v^2} \frac{\partial}{\partial v} v^2 D(v) \frac{\partial f}{\partial v}, \tag{7.12}$$

with the diffusion coefficient proportional to the energy density of the fluctuations. The distribution function in Eq. (7.12) is normalized according to the relationship $dn = 4\pi f(v) v^2 dv$, where $dn$ is the number of ions per interval $dv$ of the ion velocities. For simplicity, we present Eq. (7.12) for the case of an isotropic spectrum of fluctuations. This equation describes the diffusive broadening of the high-energy tail of the ion distribution. The majority of the ions remain in the ion core dominated by Coulomb collisions. Despite the small number of ions in the tail, they may be responsible for nuclear reactions with a high energy threshold and may thereby be used for diagnostics purposes (to identify regimes where suprathermal particles are present).

Let us consider in greater detail the acceleration of an ion in the ion acoustic turbulence in a high-$Z$ plasma. Assuming approximately equal temperatures of the electrons and ions, one finds that the oscillations excited by this instability near its threshold, given in Eq. (7.5), have a wave number

$$k \sim \sqrt{Z_{\text{eff}}} \frac{\omega_{pe}}{v_{Te}}. \tag{7.13}$$

Based on the standard equations of the quasilinear theory, one finds that the diffusion coefficient in Eq.

(7.12) is directly related to the effective electron collision frequency $\nu_{\mathrm{eff}}$ that enters the expression for anomalous resistivity:

$$D \sim v^2 \nu_{\mathrm{eff}} Z_{\mathrm{eff}}^2 \sqrt{\frac{m_e}{m_i}} \left(\frac{T}{m_i v^2}\right)^{5/2}. \qquad (7.14)$$

The characteristic energy $W^*$ of the tail ions at time $t$ after the onset of anomalous resistivity will be

$$W^* \sim T(Z_{\mathrm{eff}}^2 \nu_{\mathrm{eff}} t)^{2/5} (m_e/m_i)^{1/5}. \qquad (7.15)$$

Equation (7.15) directly links the ion energy with $\nu_{\mathrm{eff}}$ and thereby with the anomalous resistivity (7.6) and provides a phenomenolgical link between the two effects—anomalous resistivity and the formation of an ion tail.

The maximum energy is limited by the duration of the turbulent state or by the residence time of the ion within the neck. An absolute upper limit is set by the condition that the ion gyroradius must become comparable to the neck size. This yields the following estimate for the maximum ion velocity $v_i$: $v_i m_i / Z_{\mathrm{eff}} e B \sim a$, where $a$ is the neck radius. As $B \sim \mu I / 2\pi a$, one finds that

$$\frac{v_i}{c} \sim \frac{Z_{\mathrm{eff}}}{A} \frac{I(\mathrm{MA})}{30}. \qquad (7.16)$$

At a current of ~20 MA, the protons, in principle, can be accelerated to subrelativistic energies [equation (7.16) corresponds to nonrelativistic energies; at higher currents it breaks down]. Of course, this is an estimate from above. Still, it shows the significance of the pinch current in providing conditions for generating high-energy particles.

So far we have been discussing the generation of fast ions. Fast-Z-pinch discharges often are accompanied by bursts of hard x rays, pointing to the presence of high-energy electrons. [An analogous situation might be the generation of multi-MeV electrons in high-altitude lightning (Fishman *et al.*, 1984).] Formation of electron beams is strongly suppressed by the presence of the transverse magnetic field of the pinch. One would not expect formation of an electric field exceeding $cB$, as this would require a complete current breakup within a time of the order of $r/c$. At $E < cB$, on the other hand, electrons cannot accelerate; they experience a slow nonrelativistic drift motion, with a velocity $E/B \ll c$. For this reason, models that attribute the formation of high-energy electrons to a mechanism of local adiabatic compression are of some interest. They predict the formation of hot (possibly relativistic) electrons near the necks (Vikhrev, 1986). These areas could then serve as sources of hard x rays. It is interesting to note that electron beams were detected in so-called $X$ pinches (a discharge through two or more crossed wires), in which they were generated near the intersection point (Ivanenkov *et al.*, 1996).

Formation of beams of runaway electrons is possible near the pinch axis where the magnetic field is weak and the condition $E > cB$ can be satisfied. At a given density and a given electric-field strength, there exists a group of electrons experiencing runaway. To be involved in a runaway process, the electron should have high enough initial energy that, before the first scattering, it doubles its energy. This condition, if expressed in terms of the effective collision frequency, reads as

$$\frac{eEv}{\nu_{\mathrm{eff}}(v)} > \frac{m_e v^2}{2}. \qquad (7.17)$$

We have explicitly included the dependence of the effective collision frequency on the electron velocity. Electrostatic fluctuations of the lower hybrid or ion acoustic type give rise to a dependence of $1/v^3$ in $\nu_{\mathrm{eff}}$, very much like that in a classical Coulomb collision. If classical collisions are important, $v_{\mathrm{eff}}$ should include them too. From Ohm's law, one finds that

$$u = \frac{eE}{m_e \nu_{\mathrm{eff}}(v_{Te})}. \qquad (7.18)$$

Because the current is carried by the main body of the electron distribution, the collision frequency that enters this equation corresponds to "thermal" electrons. For the $1/v^3$ dependence of the collision frequency, one finds from Eqs. (7.17) and (7.18) that the critical energy above which the runaway process begins is (Benford, 1978) $w_{\mathrm{crit}} = T v_{Te}/u$. The drift velocity $u$ usually does not exceed a few ion thermal velocities. Therefore only a small fraction of the total electron population can be involved in a runaway process. The spectrum of the runaway electrons can be found in Benford (1978).

The phenomena discussed in this section can be strongly affected by the presence of even a weak axial magnetic field. In particular, neck formation can be stopped because the axial field would grow inversely proportional to the square of the neck radius, while the azimuthal field would grow inversely proportional to the first power of the radius. On the other hand, an axial magnetic field considerably broadens the zone in which runaway electrons can be accelerated.

In the implosions of hollow shells (e.g., wire arrays), favorable conditions for runaway formation may be met inside the shell, where there is no magnetic field and the plasma density is low. An axial electric field may be present inside the shell if the skin depth exceeds the thickness of the shell (see Sec. II.E). A beam of accelerated electrons will be formed long before on-axis stagnation occurs. An early appearance of the beam (detected by x-ray radiation from the anode) can serve as an indicator of a great skin depth. At a high enough beam-to-plasma density ratio, the beam may experience a two-stream instability. A survey of the effects caused by this instability can be found in Breizman and Ryutov (1974).

In addition to acceleration mechanisms related to the formation of a neck, mechanisms based on ion acceleration through the sheaths near the electrodes have also been studied (see Haines, 1983, and Trubnikov, 1986, for further references).

## C. The Hall effect

When the electron gyrofrequency becomes greater than the electron collision frequency, the Lorenz force

in the electron momentum equation predominates over the electron-ion friction term. In a uniform plasma, the electron momentum equation should be written as

$$m_e \nu_{ei} \mathbf{u} = -e\mathbf{E} - e(\mathbf{u} + \mathbf{v}) \times \mathbf{B}. \qquad (7.19)$$

Here the electron-ion collision frequency includes, generally speaking, both Coulomb collisions and anomalous scattering; $\mathbf{v}$ is the ion velocity (which almost coincides with the velocity of the center of mass) and $\mathbf{u}$ is a relative electron-ion velocity. If $|\mathbf{u}|$ is greater than the characteristic velocity of the ion motion, then Eq. (7.19) shows that the magnetic field is convected together with the electron fluid (not with the plasma as a whole). In the limit of low collision frequency, the magnetic field is frozen into the electron fluid. It then becomes possible that the magnetic field will be redistributed over a time scale that is short compared to that for ion motion. Because the ion density within this short time scale remains constant, only those electron displacements are allowed that do not perturb the electron density. This type of motion is described by so-called "electron magnetohydrodynamics" (EMHD), or "Hall magnetohydrodynamics." The latter name is related to the analogy between the last term in Eq. (7.19) and the Hall term in the theory of current flow in solid conductors. A general survey of EMHD has been published by Gordeev, Kingsep, and Rudakov (1994). In a more recent paper, Kingsep and Rudakov (1995) present a set of criteria defining the parameter domain in which the effects of EMHD are important. Dissipative phenomena in EMHD were discussed by Sevast'yanov (1993). Roughly speaking, the effects of EMHD become important if the following two conditions are satisfied: $\omega_{Ce} > \nu_{ei}$ and $u > s, a$, where $s$ and $a$ are the sound and the Alfvén velocities, respectively.

The motions of an electron fluid become particularly interesting when the plasma density is nonuniform. If the plasma density varies in the $z$ direction, the skin effect becomes dependent on the direction of the current (see Gordeev, Kingsep, and Rudakov, 1994). Fast axisymmetric striations can be self-generated (Rudakov and Sevast'yanov, 1996). The streamlines of the current become wavy, with the axial wavelength of the order of the shell thickness. This happens within a time that is short compared to the time within which the ions would react to the field perturbation (the ion background is assumed to be steady).

An interesting and so far unresolved issue is that of the influence of these fast phenomena on the quality of the shell implosion and the development of slower instabilities involving ion motion (in particular, the Rayleigh-Taylor instability). In this respect, one should note that the current perturbations discussed by Rudakov and Sevast'yanov propagate along the axis with a velocity approximately equal to $u$; therefore, although the instantaneous force acting on the ions is strongly $z$ dependent, an averaging that occurs because of the traveling nature of these perturbations should make the average force $z$ independent and thus the possible seed for $m = 0$ hydrodynamic instability decreases.

For a flute-type mode, with the wave vector orthogonal to the magnetic field, even the presence of a strong Hall effect does not change the $k^{1/2}$ scaling of the growth rate (Gordeev, 1999a, 1999b).

The electron flow at the boundary between the electrode and the plasma is another important issue. At the electrode surface the tangential component of the electric field vanishes, and the electron flow becomes almost parallel to the wall. Weak collisions gradually shift electrons in the direction of the wall. Because this (axial) motion is slow (at weak collisions), the resistivity of the transition layer becomes anomalously high. More details on these issues can be found in the aforementioned survey of Gordeev, Kingsep, and Rudakov (1994). A 2D effect in electron magnetohydrodynamics may lead to increased plasma resistance (Esaulov and Sasorov, 1997).

## D. Spontaneous generation of a magnetic field

In implosions of uniform gas loads, where a shock wave propagates in front of the magnetic piston, there exists a zone of highly ionized plasma behind the shock but before the piston where the magnetic field is zero, at least in the ideal case in which no stray early-time breakdowns occur at the beginning of the shot. It turns out that, if the system does not possess perfect symmetry, a high magnetic field can be spontaneously generated in this zone. The mechanism we are referring to was identified a long time ago in conjunction with experiments on laser plasma heating and is associated with noncollinearity of the gradients of electron temperature and density (Stamper *et al.*, 1971). When $\nabla n$ and $\nabla T$ are not parallel, an electromotive force is generated in a plasma that drives the current and produces a magnetic field. This term should be added to the standard induction equation, which acquires the form (Stamper *et al.*, 1971)

$$\frac{\partial \mathbf{B}}{\partial t} = \nabla \times \mathbf{v} \times \mathbf{B} - \nabla \times (D_m \nabla \times \mathbf{B}) + \frac{\nabla n \times \nabla T}{en}. \qquad (7.20)$$

The first term on the right-hand side describes the convection of the magnetic field with a plasma flow (linetying), the second term describes joule dissipation (in the case of a uniform magnetic diffusivity, it reduces to a diffusion term $D_M \nabla^2 \mathbf{B}$), and the last term is the thermoelectromotive force. Noncollinearity of $\nabla n$ and $\nabla T$ in the problem under consideration may emerge from waviness of the piston caused, in turn, by the Rayleigh-Taylor instability.

Let us neglect for the moment the ohmic losses (this is equivalent to a statement that the skin depth is much smaller than the spatial scale of the perturbations). Then the maximum magnetic field is determined by balancing the first and the third terms on the right hand side of Eq. (7.20). Estimating the velocity of a plasma flow as a sound velocity $s$, we find that, to within an order of magnitude, $B \sim T/es\lambda$, where $\lambda$ is a spatial scale of nonuniformities. The magnetic field will vary (randomly, if the perturbations are random) at the scale $\lambda$. Assuming that one is dealing with an Ar plasma with a temperature of

100 eV and $Z_{\text{eff}} \sim 10$, one finds that for $\lambdabar \sim 0.5\,\text{mm}$, the magnetic field is $B \sim 10\,\text{T}$. Under typical $Z$-pinch conditions, this magnetic field does not lead to magnetization of electrons, and $\omega_{Be}\tau_{ei}$ remains less than 1. However, this field will be compressed at later stages of the implosion, when the shock wave has converged on the axis. This happens if the resistive dissipation time is longer than the compression time. In the opposite case, the magnitude of the magnetic field will be considerably decreased. Estimates for the conditions of a particular experiment can be made on the basis of Eq. (7.20). This mechanism of magnetic-field generation was possibly observed by Afonin and Murugov (1998).

Although this random field is usually small compared to the pinch magnetic field, it may play a significant role after the quasiequilibrium configuration is formed (Sec. II) and necks develop. In particular, this random field may prevent runaway electrons from being freely accelerated along the axis of the column (Sec. VII.B).

The other situation in which this mechanism for magnetic-field generation may play a role is a blow-off plasma filling the interior of the imploding shell. One expects that this plasma will be strongly nonuniform and that the conditions for the appearance of a thermal electromotive force will be thereby satisfied. The presence of a random magnetic field will affect transport properties of the blow-off plasma.

## VIII. APPLICATIONS OF FAST $Z$ PINCHES

### A. Radiation sources

#### 1. Hard x rays

One of the traditional applications of fast $Z$ pinches is generation of short pulses of intense kilo-electron-volt radiation, with the energy of the quanta up to 10 keV. For such applications, one can use a wire array made of some high-$Z$ material (say, nickel) or an annular gas puff of gases like Ar or Kr. If the parameters of the pinch are properly chosen, a plasma with an electron temperature of several hundred electron volts to over 1 keV can be formed, and excitation of the $L$ or $K$ shells becomes feasible. A survey of studies in this area prior to 1988 was published by Pereira and Davis (1988).

A rough optimization of the $Z$-pinch parameters for the highest yield in the desired $K$ or $L$ transition can be made based on the following arguments. The efficiency of converting the magnetic energy into the kinetic energy of the imploding shell is determined by the condition $\Pi = \Pi_{\text{opt}}$ where $\Pi$ is a dimensionless parameter defined by Eq. (2.4). As is clear from Eq. (2.4), for a given pulse-power generator, i.e., for given values of $I_{\text{max}}$ and $\tau$, the product $\hat{m} r_0^2$ must be kept constant. This means that the pinch mass $\hat{m}$ and the initial pinch radius $r_0$ can be varied only subject to the constraint

$$\hat{m} r_0^2 = \text{const}. \qquad (8.1)$$

The kinetic energy per ion scales as the implosion velocity squared, i.e., as $(r_0/\tau)^2$. The electrons acquire their
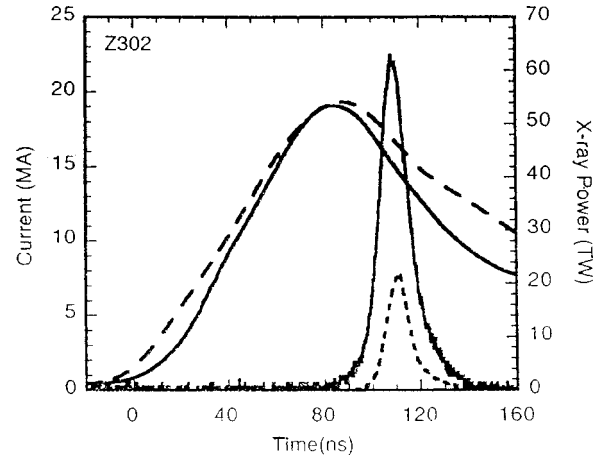


FIG. 29. The measured currents and x-ray powers from shot $Z302$, a 40-mm-diameter, 96-wire array with 20.3-$\mu$m-diameter titanium wires. The load (solid) and MITL (dashed) currents are shown, along with the total power (solid) and kilo-electron-volt (dashed) x-ray powers (from Deeney *et al.*, 1999a, reprinted with kind permission of C. Deeney).

energy from the ions, and the electron temperature therefore correlates with $(r_0/\tau)^2$. According to Eq. (8.1), the heavier liners have smaller initial radii, i.e., the electron temperature at stagnation decreases as the mass of the liner increases. Eventually the electron temperature becomes insufficient to excite a certain $K$ or $L$ transition. Conversely, for liners with less mass (larger initial radii), the kinetic energy per ion grows. At first sight, this would seem to mean that the lighter liners are better as sources of kilo-electron-volt x rays. However, if one goes too far in this direction, the radiation yield starts to decrease because the radiation power per unit volume scales as the density squared and, at small masses, decreases. Because of this, the pinch plasma begins to expand and cool down before any substantial fraction of the thermal energy gets converted into radiation. The slower energy exchange between electrons and ions at higher temperatures also acts in the same direction. These two opposite trends—decrease of the electron temperature at high masses, and decrease of the radiation power at low masses—determine the optimum mass of the imploding liner. At higher masses, self-absorption may reduce the $K$-shell radiation yield (Apruzese *et al.* 1998). A more detailed discussion of these issues, together with supporting experimental information, can be found in Pereira and Davis (1988), Thornhill, Whitney, and Davis (1990), Deeney, LePell *et al.* (1993, 1994), Deeney, McGurn, *et al.* (1997), Deeney, Nash *et al.*, 1998), and Whitney *et al.* (1990, 1994).

In recent experiments at the $Z$ facility (Deeney, Nash, *et al.*, 1997), the energy radiated in the $K$-shell transitions of Ti was well over a hundred kilojoules (Fig. 29). Deeney, Peterson *et al.* (1998) showed that reducing the height of the pinch from 2 to 0.75 cm did not change the total radiation power or the radiation energy. As the shortening of the pinch resulted in a decrease in the pinch inductance and some increase in the pinch current, the authors increased the mass per unit length to keep

the load match by keeping the parameter [Eq. (2.4)] more or less constant. The possibility of increasing implosion time from ~50 ns to ~170 ns by a proper increase of the initial array radius and mass has been demonstrated experimentally at the Saturn generator, with a favorable effect on the radiated power (Deeney *et al.*, 1999b).

In real life, although a considerable fraction of the kinetic energy can be converted to radiation upon stagnation, the plasma column still has sufficient pressure to expand somewhat and to be compressed again by the magnetic pressure. This process may explain the presence of a longer, lower-amplitude, and longer-wavelength radiation pulse that follows the main peak (Peterson *et al.*, 1997, 1999). Another phenomenon that may affect the final radiation yield is a short-circuiting of the transmission lines later in the pulse (Giuliani *et al.* 1990).

The stability of a $Z$-pinch implosion is important for efficient x-ray generation; it sets the minimum effective size to which the pinch can be compressed. A more stable implosion would allow one to increase the initial pinch radius and to reduce the mass while still having high density at stagnation (sufficient to radiate the thermal energy before the pinch rebounds).

To obtain harder x rays, in the range of tens of kilo electron volts, one could use an alternative approach based on adiabatic compression of a hydrogen plasma seeded with heavy impurities; the plasma temperature could possibly be made as high as 10 keV, allowing excitation of the $K$ lines of such elements as Xe. We discuss this possibility in more detail at the end of Sec. VIII.D.1.

### 2. Blackbody radiation

Fast $Z$ pinches with high-atomic-number materials are also used as a source of thermal radiation with a temperature from tens of electron volts to ~200 eV (and, in the future, over 300 eV). If the implosion occurs in the center of a closed cavity (sometimes called a "hohlraum"), the radiation from the pinch after several reflections from the walls, becomes almost blackbody radiation (Matzen, 1997). The wall (and the radiation) temperature can be roughly evaluated from the equation $P_{rad} = (1 - \alpha) A \sigma T^4$, where $P_{rad}$ is the power radiated by the pinch, $A$ is the surface area of the cavity, and $\alpha$ is the albedo of its walls. In experiments at the Saturn facility at Sandia, the radiation temperatures were in the range of 80 to 90 eV (Matzen, 1997; Matzen *et al.*, 1999). In experiments at the $Z$ facility, temperatures in the range of 120 to 140 eV (Porter, 1997) and, more recently, 155 $\pm 10$ eV (Matzen *et al.*, 1999) have been obtained.

### B. Studies of material properties under extreme conditions

Thermal radiation generated by the method just described can be used to drive shock waves in various materials. By studying the shock velocity, one can gain information about the equations of state of the materials
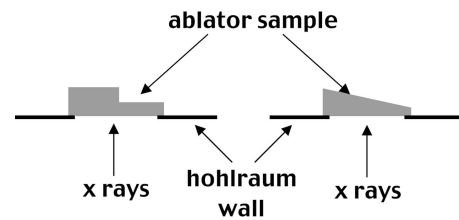


FIG. 30. Experimental arrangement used in 1997 studies of shock-wave propagation (from Olson *et al.*, 1997, reprinted with kind permission of R. Olson): (a) the average shock velocity measured by comparing the shock breakout times at two steps; (b) continuous measurements of the shock velocity made in a wedge sample.

under study. A typical geometry for such an experiment is shown in Fig. 30 (Olson *et al.*, 1997). Thermal radiation causes ablation of the material from the inner side of the sample, and the ablation pressure drives a shock whose velocity can be measured according to its time of arrival at the outer side of the sample. To be sure that the radiation spectrum is indeed close to the black-body spectrum [and therefore that the drive can be characterized by a single function $T(t)$], small cavities can be attached to the main one in such a way (Fig. 31) that the samples are protected from direct irradiation by the pinch, and only radiation from the walls of the cavity hits the surface of the sample (Matzen, 1997). Several configurations have been proposed that increase the uniformity of the radiation on the sample under study.

The hohlraum technique has been successfully used to study propagation of shocks in the materials that will be used in ICF capsules (Olson *et al.*, 1997) and to study equations of state of metals with pressures of ~3 Mbars (Branitskii *et al.*, 1996). The same technique is widely used in physics research with laser-driven hohlraums where it has reached a high degree of sophistication. A general survey of this approach can be found in Rosen
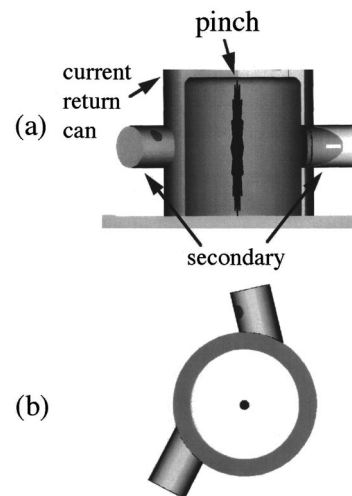


FIG. 31. Sideview (above) and end-on view (below) of a configuration with secondary hohlraums attached to the main one; this eliminates the effect of a direct irradiation of the sample by the pinch plasma.

(1996). It has been successfully used for studies of the structure of shock-compressed materials (Kalantar *et al.*, 1999), of hydrodynamic Rayleigh-Taylor and Richtmyer-Meshkov instabilities with controlled initial perturbations (Remington *et al.*, 1997a, of the effects of material strength on hydrodynamic phenomena (Kalantar *et al.*, 1997, Remington *et al.*, 1997a), and for astrophysical simulations (Remington *et al.*, 1997b). Two advantages of *Z*-pinch-driven hohlraums is their larger size and their considerably higher total radiation output (centimeters vs millimeters, and hundreds of kilojoules vs tens of kilojoules). This allows one to use thicker hydrodynamic packages, minimizing problems with radiation preheat. Larger sample sizes and longer times will also lead to better accuracy of the equation-of-state measurements. Gasilov *et al.* (1995) suggested generating multimegabar shocks in a central rod (~1 cm long) hit by an imploding liner. For yet larger experimental volumes, other techniques, based on magnetic compression driven by chemical explosives, are feasible (Hawke *et al.*, 1972).

## C. Generation of high magnetic fields

The use of an imploding cylindrical shell for generating high magnetic fields was suggested many years ago (Fowler *et al.*, 1960; Sakharov *et al.*, 1965). High fields are generated by compressing an initially modest axial field within an imploding, conducting cylindrical shell. Experiments with explosively driven systems were reported in the 1960s (Fowler *et al.*, 1960; Sakharov *et al.*, 1965), reaching magnetic fields as high as 20 MG. Implosions of metal shells in the *Z*-pinch geometry were studied by Alikhanov *et al.* (1981); a maximum magnetic field of 3.5 MG was obtained in a volume of a few tens of cubic centimeters.

We present a qualitative consideration of the magnetic-field compression in the *Z*-pinch setting, assuming that the thickness of the shell is negligibly small and that the shell has a high conductivity. The condition of conservation of the axial magnetic flux enclosed by this plasma shell is

$$B_z r^2 = B_{z0} r_0^2, \tag{8.2}$$

where $B_{z0}$ is the initial axial magnetic field. When the convergence ratio is high enough, the final axial magnetic field can be considerably greater than the initial one. Here we neglect edge effects of the type discussed in Sec. II.D. This is correct if the length of the pinch is greater than its radius.

The compression of the axial magnetic field can be analyzed in a particularly straightforward fashion in the reference case of a constant pinch current. In this case the energy conservation law shows that at the point of maximum compression, where the liner is at rest and its kinetic energy is zero, the following relationship holds:

$$\pi r^2 \frac{B_z^2}{2\mu} - \pi r_0^2 \frac{B_{z0}^2}{2\mu} = \pi r^2 \frac{B_\varphi^2}{2\mu} \left( 2 \ln \frac{r_0}{r} \right), \tag{8.3}$$

where $B_\varphi$ is the azimuthal magnetic field at the surface of the liner. At a convergence of $C \gg 1$, one can neglect the second term on the left-hand side of this equation. One then finds that, at the stagnation point, the (axial) magnetic field inside the liner is related to the (azimuthal) magnetic field of the pinch current by the equation

$$B_z = B_\varphi \sqrt{2 \ln C}. \tag{8.4}$$

Taking $C = 20$, one finds that the magnetic field inside the liner can be made approximately 2.5 times higher than the azimuthal *Z*-pinch field at the point of maximum compression. In other words, this scheme leads to relatively modest enhancement of the internal field compared to the external field that would be reached at the same convergence ratio. Still, this factor is non-negligible, especially because it is topologically more convenient to use the magnetic field inside the shell for studies of the interaction of superhigh fields with matter.

From Eqs. (8.2) and (8.4) one can see that the initial axial magnetic field required to reach this state is $B_{z0} = B_{\varphi 0} \sqrt{2 \ln C} / C$, where $B_{\varphi 0}$ is the initial azimuthal magnetic field. Taking as an example $B_{\varphi 0} = 0.5$ MG and a modest convergence of $C = 20$, one finds that the initial axial magnetic field should be ~60 kG, and the final axial magnetic field will be 25 MG. Accounting for the finite thickness of the imploding shell leads to somewhat smaller enhancement factors, because part of the implosion energy is spent on plasma heating and compression. These and other pertinent effects have been discussed by Felber, Liberman, and Velikovich (1985).

In experiments carried out during the last decade, annular gas puffs have been used to produce conducting imploding shells (Wessel *et al.*, 1986; Baksht *et al.*, 1987; Felber, Malley, *et al.*, 1988; Felber, Wessel, *et al.*, 1988). Magnetic fields in the range of 40 MG were reported by Felber, Malley *et al.* (1988). In summary, an axial implosion of the seed magnetic field is a proven way of reaching an axial magnetic field a few times higher than the azimuthal magnetic field at the stagnation point.

## D. Controlled thermonuclear fusion

There are two significantly different ways for using fast *Z* pinches for reaching controlled thermonucleus fusion (CTF). The first is based on the direct shock and/or adiabatic heating of an imploding DT plasma (possibly nested inside a liner made of a heavier material). The second is based on the generation of high-temperature blackbody radiation in a collision of the liner with some inner shell; the blackbody radiation then drives a spherical pellet in very much the same fashion as in the indirectly driven laser fusion systems (for a survey of those see Lindl, 1995). We discuss these two schemes in the next two subsections.

As was mentioned in the Introduction, quasiequilibrium pinches (not the fast pinches that are the subject of this survey) have also been considered as a potential candidate for fusion reactors, but we shall not discuss that approach here. Surveys of quasistatic pinches in

conjunction with fusion applications have been published by Haines (1982), Dangor (1986), and Robson (1989, 1994).

A well-known difficulty with using fast Z pinches in a future commercial fusion reactor is the considerable neutron and thermomechanical damage that would be suffered by the pulsed-power generator if the pinch were not separated from the generator by a large enough distance. A possible solution to this problem was suggested by Robson (1989), who envisaged using two long liquid-lithium jets that would serve as electrodes for the Z pinch. Drake *et al.* (1996) considered another technique that might be used if the energy to be delivered to the Z pinch were less than ~1 MJ per pulse. For this case one could conceive of dropping miniature diode assemblies, consisting of fusion targets and the necessary circuitry, into the reactor chamber and energizing them by a charged particle beam or even by a fast projectile (in this latter case, the assembly would have to carry a seed magnetic field that would be compressed by a fast projectile and drive the Z-pinch circuit).

The whole issue of standoff energy sources has not been explored in any detail. It would therefore be premature to write off Z pinches as a prototype for a fusion reactor solely on the basis of the absence of proven solutions for the power-supply problem. In addition, even if such solutions are not found, fast Z pinches can still be very useful for the fusion program; they could provide a relatively inexpensive demonstration of fusion ignition in a variety of pulsed-power fusion applications.

### 1. Plasma heating by implosion

Let us consider implosions of thin shells made of a DT mixture (see, for example, Nedoseev, 1991). Cryogenic DT fiber arrays can serve as such shells. The lifetime $\tau$ of the hot plasma column formed at the stagnation point will be of the order of $r_{min}/v_{Ti}$ where $r_{min}$ is the radius of the column [related to the initial radius of the shell by Eq. (1.1)], and $v_{Ti}$ is the ion thermal velocity corresponding to the temperature ~10 keV (i.e., $v_{Ti}$ ~$10^8$ cm/s). The Lawson criterion reads

$$n(\text{cm}^{-3})\tau(\text{s}) > Q \cdot 10^{14}, \tag{8.5}$$

where $n$ is the DT plasma density and $Q$ is the ratio of the fusion energy to the thermal energy of the imploded plasma (the gain factor). This condition can be rewritten as $W(\text{J/cm}) > 10^{31}Q^2/n(1/\text{cm}^3)$, where $W$ is the energy per unit length of the plasma column. Even with a relatively modest assumption with regard to the required gain, $Q \sim 10$, this condition means that one has to reach a density level of $\sim 10^{25}\,\text{cm}^{-3}$ to keep the energy of the plasma below $10^8$ J/cm. According to Eq. (2.9), to reach this energy, one would have to generate unrealistically high pinch currents, $\sim 10^9$ A. On the other hand, increasing the density in the imploded state above $10^{25}\,\text{cm}^{-3}$ would require unrealistically high convergence. A possible way of improving implosion stability and, thereby, axial convergence was analyzed by Golberg, Liberman, and Velikovich (1990), with the conclu-

sion that a break-even requires a radial convergence of ~30, with an energy release in the range of hundreds of megajoules/cm.

These observations point out the desirability of using a heavier shell to confine the DT plasma near the stagnation point. In this case, however, another difficulty surfaces: high electron thermal conductivity in the fusion plasma. Because the thermal capacity of a heavy shell is much greater than that of the fusion plasma it confines, there will be heat losses from the DT plasma to the confining shell. It turns out that this heat-loss mechanism leads to approximately the same energy limitations as discussed above and, for this reason, does not offer a more realistic alternative.

Potentially, very high densities can be achieved in 3D implosions with a linear convergence of ~30 (typical for laser-driven fusion). The whole concept then becomes similar to that of laser fusion, with the only difference being that the implosion of the capsule is driven by magnetic pressure. In principle, almost spherically symmetric implosions are feasible in the magnetic compression scheme, despite the fact that the magnetic pressure cannot be made spherically symmetric. This was demonstrated in a multimegajoule explosively driven experiment by Mokhov *et al.* (1979). More recently, quasispherical implosions in the Z-pinch geometry have been experimentally studied by Degnan *et al.* (1995). A linear convergence ratio of ~6–7 was reached. It remains, unclear however, whether the very fast, high-convergence implosions needed to ignite the fuel in the center of the capsule are actually feasible. This issue requires further analysis.

One more school of thought (see, for example, Yan'kov, 1991) pursues the detonation wave approach, in which the nuclear burn wave would be ignited at some point in a cylindrical column and would propagate along the axis. The detonation could be ignited in a "neck" that could be deliberately produced at a certain axial location. Linhart *et al.* (1994) considered even the possibility of detonating a column of pure deuterium (not a DT mixture) by imploding a short section filled with DT. These schemes would give rise to very large energy release per pulse, in the range of 1 GJ (approximately equivalent to 250 kg of high explosives). Strong heating of a CH fiber plasma in the zone of a deliberately created constriction was observed by Aranchuk *et al.* (1997). Numerical simulations by Lindemuth (1990) have shown spontaneous formation of hot spots as a result of the development of a sausage instability in cryogenic deuterium fibers. Alikhanov *et al.* (1984) observed a spontaneous formation of 10 $\mu$m diameter necks in gas-puff pinches with an initial radius of a few centimeters. Some degree of control over the location of hot spots has been demonstrated by Afonin *et al.* (1999) in a single-wire pinch with axially varying initial composition.

Very high densities of DT fuel can be reached in the so-called staged pinch (Rahman *et al.*, 1995), where a liner would implode onto a DT fiber situated near the liner axis and carrying an initial axial current. Compres-

sion of the azimuthal magnetic field has an interesting feature; growth rate of the field becomes very high when the outer liner comes close to the inner fiber. This is a result of the fact that, when the gap between the fiber and the liner is much greater than the fiber radius, the fiber inductance depends on the gap only logarithmically, whereas with gaps smaller than the fiber radius, the dependence is linear. Therefore the current in the fiber experiences a very sharp rise, compresses the fiber, and ignites the fusion fuel. Numerical examples presented by Rahman et al. (1995) show that the fiber density may reach values of $\sim 10^{25}$ cm$^{-3}$ even at a relatively modest current of 2 MA in an imploding liner with an initial radius of 2 cm. However, this optimistic conclusion is based on the assumption that the inner surface of the liner remains cylindrical to within an accuracy of a few micrometers at the time of maximum compression. This does not seem easily achievable.

Probably the most straightforward approach, to break-even if not to ignition is based on adiabatic compression of a magnetized plasma. It has been understood for many years that, to suppress heat losses from the fusion plasma to the walls of the imploding liner, one can use a relatively weak magnetic field, such that its pressure is small compared to the plasma pressure, i.e.,

$$\beta \equiv \frac{2\mu p}{B^2} \gg 1 \qquad (8.6)$$

is satisfied. This condition is, in fact, almost mandatory because, if the inequality (8.6) reverses its sign, the liner implosion becomes inefficient; the liner works predominantly against the magnetic pressure, and the liner energy is converted predominantly to the energy of the compressed magnetic field, not the thermal energy of a plasma.

As was pointed out by Drake et al. (1996), a 3D implosion of the liner is preferable to a purely cylindrical implosion. This can be understood in the following way: the z component of the magnetic field inside the shell scales as the square of the instantaneous convergence $C^2$; in other words, the magnetic pressure scales as $C^4$:

$$p_M = p_{M0} C^4, \qquad (8.7)$$

where $p_{M0}$ is the magnetic pressure of the axial magnetic field at the beginning of the implosion. The pressure $p$ of a fully ionized hydrogen plasma scales as a volume to the power $(-\frac{5}{3})$, or $p = p_0 C^{10/3}$ for a purely cylindrical implosion. Clearly, the magnetic pressure grows faster than the plasma pressure, and, at the high convergence ratios that are of interest in this problem, becomes greater than the plasma pressure. On the other hand, for a 3D implosion, the scaling for the magnetic pressure remains unchanged [Eq. (8.7)], while the plasma pressure now scales as $C^5$ and grows faster than the magnetic pressure.

Plasma confinement under condition (8.6) was discussed many years ago by Budker and his co-workers (see Alikhanov et al. 1967; Budker, 1973). In the context of a laser-heated plasma it was discussed by Pashinin and Prokhorov (1971). Since then, it has been studied in
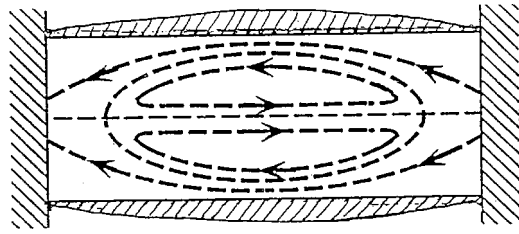


FIG. 32. A field-reversed configuration nested inside the liner with axially varying thickness of the walls.

great detail both theoretically and numerically (see, for example, Vekshtein, 1990). The general conclusion was that, because the plasma pressure is almost constant over the radius, the plasma density becomes very high near the cold walls. The magnetic field is convected to this high-density region from the plasma core, and a "cushion" of very high magnetic field is formed near the walls. At moderate plasma betas [see Eq. (8.6) for the definition of beta], below 10–20, the resulting confinement of the hot plasma core proves to be quite satisfactory; the confinement time exceeds tens of the Bohm confinement time. At the high densities typical of the system under consideration, this confinement time does not substantially limit the plasma gain (see Drake et al., 1996, for more details). This concept is sometimes referred to as magnetized target fusion (MTF; Lindemuth and Kirkpatrick, 1983). A high-energy (many tens of megajoules) variant of this system is the MAGO device under study at Los Alamos National Laboratory and the All-Russian Scientific Research Institute of Experimental Physics (Lindemuth et al., 1996).

Among magnetic configurations that could be imploded are the field-reversed configuration (FRC), the spheromak, and the diffuse Z pinch. Figure 32 shows an FRC nested inside the liner. To make the implosion three dimensional, it was suggested that the liner mass density vary over the length, with a maximum density near the equatorial plane (see Alikhanov et al., 1977). The liner would then be squeezed near the ends faster than near the equator, and the FRC would be compressed both axially and radially. What is yet to be proven in this approach is the formation of a field-reversed configuration suitable for the subsequent compression. Experience here is limited to relatively large (tens of centimeters in diameter) FRC's with a plasma with a density of $\sim 10^{15}$ cm$^{-3}$. Preliminary scaling analysis (Ryutov, 1997) shows that creation of a much smaller (1–2 cm diameter) FRC with a plasma density $\sim 10^{18}$ cm$^{-3}$ and temperature $\sim 100$ eV is feasible.

In Drake et al. (1996) this scheme has been analyzed for relatively slow (1–2 $\mu$s implosions of heavy (at least a few grams) liners that could be driven by relatively simple condenser banks. The conclusion was reached that a 10-keV DT plasma under break-even conditions could be formed at as low a plasma energy content as $\sim 100$ kJ. No analyses have been made with regard to the potentials of this scheme with much lighter liners and faster drivers, like those used in the Z facility.
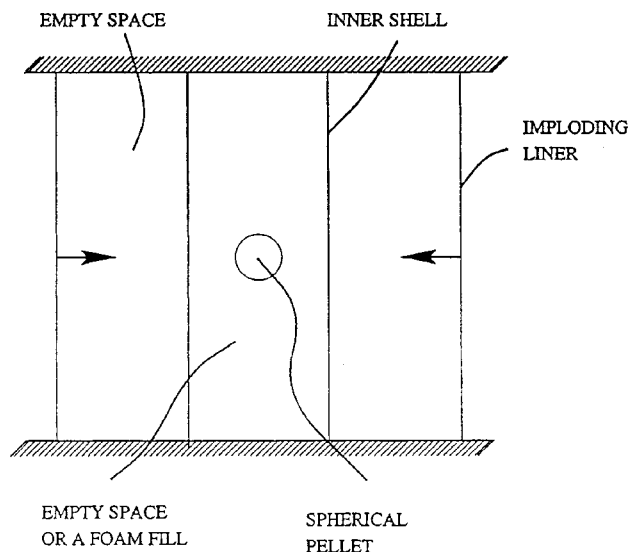
Note that, if seeded with heavier impurities, this

FIG. 33. Schematic of a dynamic hohlraum experiment.

plasma could serve as a high-power source of hard x rays. If the atomic number of the impurities is chosen in such a way that they are completely stripped at 10 keV, one can generate a smooth bremsstrahlung spectrum, corresponding to a temperature of ~10 keV. If the impurities are heavy (like Xe), then a considerable fraction of energy could be radiated in $K$-shell lines with energies ~20 keV and higher (Toor and Ryutov, 1997).

#### 2. Generation of blackbody radiation to drive a fusion capsule

A very different way of using $Z$ pinches for fusion (Smirnov, 1991; Matzen, 1997; and also earlier unpublished reports from both Sandia and Troitsk) resembles indirect-drive laser inertial confinement fusion (ICF); a nice qualitative discussion of this application of fast $Z$ pinches has recently been published by G. Yonas (1998). When an imploding liner collides with an inner shell situated near the axis, the impact energy is converted into thermal energy in both shells. If the imploding plasma shell is sufficiently thick, it will trap the radiation produced by the stagnation (Fig. 33). In analogy with the terminology used in laser fusion, the interior of a shell filled with (almost) blackbody radiation is called a "hohlraum." To emphasize the fact that the walls of the hohlraum continue to implode after the impact between the two shells, the term "flying radiation case" or "dynamic hohlraum" is often used (Matzen, 1997; Brownell et al. 1998, Matzen et al., 1999). A spherically symmetric capsule filled with DT fuel is situated in the center of the dynamic hohlraum. Thermal radiation causes the ablation and implosion of the surface layers of the capsule. We shall not discuss here issues of the capsule's design and its implosion physics (see Olson et al., 1999, and Hammer et al., 1999, for capsule designs). Instead we shall focus on some issues related to $Z$-pinch-driven hohlraums.

The radiation temperatures required for ignition of an indirect-drive DT capsule are around 250 eV for designs similar to ICF capsules driven by lasers (Lindl, 1995). The temperatures currently reached in $Z$-pinch experiments are in the range of 130 to 180 eV (see, for example, Nash et al. 1997b, 1999; Leeper et al. 1998). These ICF-ignition and high-yield capsules also require precise pulse shaping and a high degree of radiation symmetry.

The temporal dependence of the radiation flux can be controlled by adjusting the shape of the inner and/or outer shells. For example, the configuration shown in Fig. 34(a) will produce a long "pedestal" caused by the interaction of the ends of the two shells, followed by a sharp pulse produced during the impact of the central, almost parallel, parts of the shells. The minimum attainable duration of the impact (and, accordingly, the maximum possible radiation flux) is determined by the thickness of the two shells at the time of impact. In the overall context of pulse shaping and radiation symmetry, the importance of eliminating gross hydrodynamic instabilities becomes quite clear.

For these ICF capsules to reach ignition, the radiation field at the location of the capsule ablating surface should be spherically symmetric to within an accuracy of ~1% in the lower azimuthal modes. Because the $Z$-pinch geometry does not possess this symmetry, the size of the capsule should be a small fraction of the size of the radius of the dynamic hohlraum. One method of isolating the radiation source from the capsule is to fill the dynamic hohlraum with a low-atomic-number, low-density material that creates a large plasma pressure but is relatively thin to the radiation produced by stagnation of the imploding plasma. A more radical solution of this problem is an overall spherical symmetrization of the implosion, as shown in Fig. 34(b). Although the problem of irradiation symmetry is difficult, it does not appear to be insurmountable. Detailed studies of laser-driven hohlraums have shown that one can reach quite satisfactory results by a proper shaping of the hohlraum, by using optimally placed passive screens, and by reducing the pellet diameter to approximately one third of the diameter of the hohlraum.

An attractive feature of $Z$-pinch-driven dynamic hohlraums is the relatively low cost of the pulsed-power generator and the high total impact energies (in the range of a few hundred kilojoules to a few megajoules) available in the existing devices like $Z$, Saturn, or Angara-5.

In addition to radiation temperature, pulse shaping, and symmetry, several other issues should be considered in the design of dynamic hohlraums. We mention some of them here without attempting serious analysis:

(1) The ablation surface of the capsule must be isolated from the imploding liners and the shocks that they generate; if the hohlraum is filled with a foam, the shock wave excited in the foam by the impact with the liner must not interact with the ablation surface of the capsule before the capsule implodes. In the case of an empty hohlraum, low-density ejecta can be of some concern if they reach the capsule before the ablation process is well established.
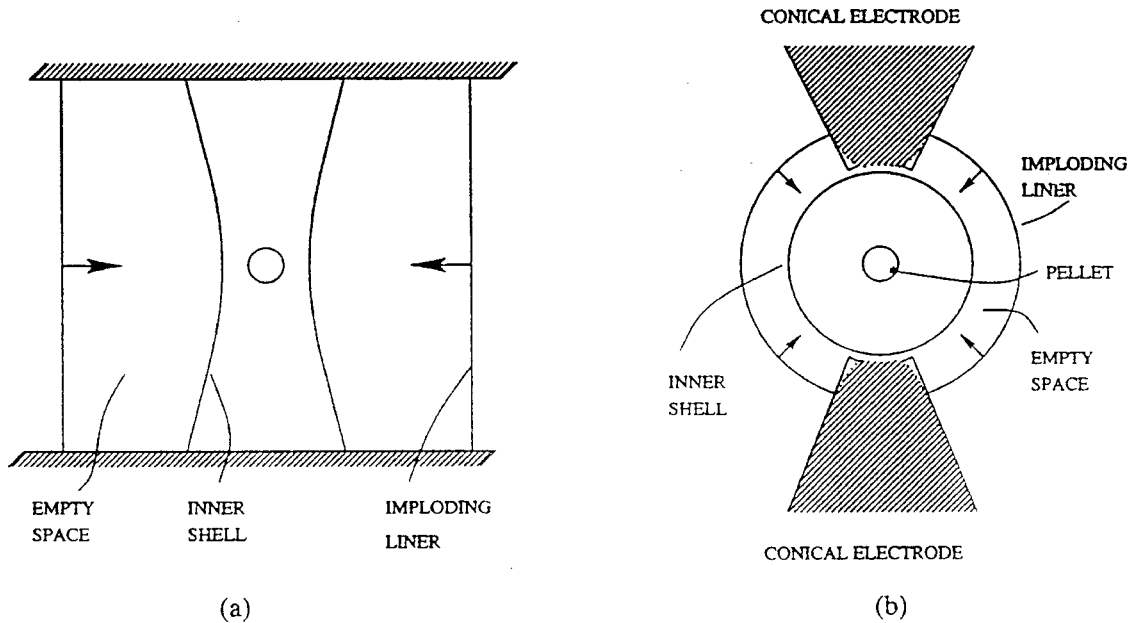
FIG. 34. Configurations of the dynamic hohlraum: (a) A configuration with a shaped inner shell. A hyperboloid-of-revolution shape can be made from straight wires, by tilting them by the same angle with respect to the axis of revolution. (b) A quasispherical implosion. This type of implosion can also be generated from the initially cylindrical wire array with axially varying linear mass density. The axial variation of the mass can be reached by a controlled surface-deposition technique; the substrate will be an initially uniform wire array.

(2) Some low-density blow-off plasma will almost certainly be present inside of an empty hohlraum during the early phase of the $Z$-pinch implosion (its source can be the radiation preheat during the run-in phase or inductive splitting of the drive current). By itself, because of its low density, it will probably have no significant effect on the pellet. However, if the axial electric field penetrates through the liner, it could generate particle beams in this low-density plasma, which might then cause considerable preheating of the pellet and violate its spherical symmetry.

(3) A magnetic field may be generated inside the plasma filling the hohlraum, which may affect pellet performance.

All these issues are in a relatively early stage of assessment. On the other hand, none of them seems to pose insurmountable problems for the dynamic-hohlraum concept in general. In particular, one could eliminate most of the problems by using geometries of the type shown in Fig. 35, in which the $Z$-pinch implosions occur at the ends of the main hohlraum (Matzen, 1997).

### E. Other possible applications

In some modes of operation, especially if the neck formation could be triggered in a controlled way, $Z$ pinches could serve as sources of high-energy, high-intensity beams of charged particles, in particular, protons and deuterons. Such beams could then be used for the generation of short-lived isotopes. The proton-rich isotopes required for positron emission tomography for

medical purposes could possibly be produced (see Dawson, 1993, for a discussion of a different method of producing these isotopes). The beam could also be used for measuring nuclear cross sections of very short-lived isotopes.

Rudakov et al. (1991) and Kingsep et al. (1997) have discussed the possibility of creating a very-high-power flux to the electrodes by adiabatic compression of a plasma by an imploding liner. The heat losses to the liner would be suppressed by an axial magnetic field. Amplification of the flux to the electrodes would occur because of a very strong dependence of the electron thermal diffusivity on the electron temperature ($\chi_e \propto T_e^{5/2}$; see Huba, 1994).

The fact that a $Z$ pinch produces high-intensity radiation with a spectrum that is at least crudely controllable
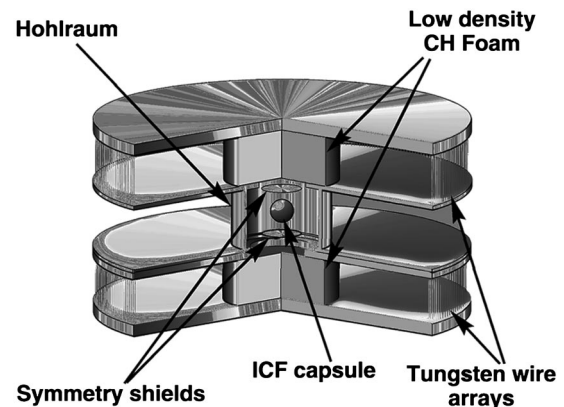


FIG. 35. A static hohlraum with two $Z$-pinch radiation sources situated at the ends.

can be used for generating population inversion in various active media. Porter, Spielman, Matzen, *et al.* (1992), and Porter, Spielman, Vargas, and Matzen (1992) have successfully used the radiation of a sodium wire array to pump a Ne gas cell and create a population inversion for transitions with wavelengths near 11 Å.

$Z$ pinches have already been used for collecting information that could be of interest in astrophysics. Very encouraging results have been achieved in studies of the opacities of iron plasma (Springer *et al.* 1997). Interesting possibilities exist for simulating various high-energy-density astrophysical phenomena—for example, the formation of high-energy intergalactic jets. For this purpose, jets of the type shown in Fig. 8 could be made, and their propagation detected through the gas or plasma filling the space beyond the anode surface.

## IX. SUMMARY AND A GLANCE TO THE FUTURE

The fast $Z$ pinch is a fascinating object, whose behavior is determined by a variety of processes of magnetohydrodynamics, radiative transport, atomic physics, plasma microinstabilities, and beam physics. A particular "shot" is formed by a chain of inseparable stages, from the current initiation and fast early-time instabilities, through the run-in phase where hydrodynamic instabilities distort and broaden the imploding shell, to a final on-axis stagnation, accompanied by a burst of intense radiation, possible formation of a transitional quasiequilibrium configuration, and, sometimes, disruption of the plasma column and the generation of fast particles. The $Z$ pinch is to a high degree a self-organized object, for which a change of a single input parameter may trigger a long chain of tightly interwoven processes occuring on various temporal and spatial scales and leading to an outcome very different from simple "mechanistic" predictions.

We believe that all the pieces of physics that are important for $Z$-pinch performance have been identified in this survey. Theory and simulations correctly describe many aspects of these phenomena. In particular, the gross dynamics of implosions of wire arrays is nicely predicted by one-dimensional hydrodynamic simulations, which provide a correct value for the time of a pinch collapse on axis (or on the inner cylinder). On the other hand, it is still difficult to predict, based on first principles, the temporal evolution of the thickness of the shell and the experimentally observed shape of the radiation pulse (although, by playing with a few adjustable parameters, one can reach a reasonable agreement). In addition, experimental information on the development of hydrodynamic perturbations during the run-in phase is relatively sparse. Although the key physics phenomena have probably already been identified, their sometimes subtle interplay still requires a much better understanding.

One area where experimental information is almost nonexistent is the direct detection of microturbulence that may be responsible for the anomalous resistance and other effects. Any measurements of this kind are particularly difficult at large facilities, where the huge energy release in the diode region requires heavy shielding and forces one to locate the diagnostics equipment at large distances from the pinch area. In such a situation, indirect information can probably be used to detect anomalous plasma resistance. If it is actually present, then one can expect a considerable axial electric field to exist inside the empty imploding shell, leading to generation of electron beams early in the pulse. Another way of making indirect measurements is to change the composition of the pinch material. For instance, varying the relative amount of a light (say, deuterium) component may considerably affect microturbulence and may interfere with the phenomena of electron magnetohydrodynamics. The effects of electron magnetohydrodynamics can be controlled to certain extent by a weak axial magnetic field that would lift the restriction associated with current flow across the field lines in the outer part of the pinch. The present survey contains some information and references necessary for the planning of such dedicated experiments, which seem to be quite important. They would allow one to define the parameter domain in which fast $Z$ pinches are governed by standard MHD equations, and would establish the significance (or insignificance) of the anomalies outside that domain. Smaller university-scale facilities (of the type described by Bauer *et al.*, 1997 and Haines, 1997), where one can study specific phenomena in a more benign environment, can also be of great help.

Previous advances in fast-$Z$-pinch physics were made in direct correlation with progress in pulsed-power technology; a higher pinch current has always led to a considerable increase in the maximum kinetic energy of the imploding liner and maximum radiation power. A good recent example is the progress made in the transition from the Saturn facility to the $Z$ facility. The current pulsewidth was increased by over a factor of 2 (from $\sim 50$ to $\sim 110$ ns) and the current was increased by a factor of $\sim 2.5$ (from approximately 7 to approximately 18 MA), resulting in an increase in the radiated energy of a factor of $\sim 5$ and an x-ray power increase of a factor of $\sim 3$ (see Matzen, 1997). Therefore it is interesting to conjecture what one can expect from a further increase in the pinch current if new facilities become available (see for example, the discussion of a 60-MA generator $X$-1 by Leeper *et al.*, 1998 and of a 50-MA-range facility based on inductive energy storage by Azizov *et al.*, 1998). In the discussion that follows, we assume that the current can be represented as

$$I = I_{max} f(t/\tau), \tag{9.1}$$

where $f$ is some given bell-shaped function with a maximum equal to 1; in other words, we assume that the shape of the current wave form does not change, but only scaling factors over the horizontal ($\tau$) and vertical ($I_{max}$) axes, where $\tau$ is a pulse width. For discharges with similar current wave forms, the optimum set of parameters is related by Eq. (2.4):

$$\frac{\mu I_{\max}^2 \tau^2}{4\pi \hat{m} r_0^2} = \Pi = \text{const.} \tag{9.2}$$

Provided the parameter $\Pi$ is kept constant, the time-histories of the pinch radius are similar for similar current wave forms [i.e., for the same function $f$ in Eq. (9.1)]. One expects that, if the shell thickness $h$ is determined by the hydrodynamic instability, then the thicknesses of two shells with the same value of the parameter $\Pi$ will also have similar time-histories, i.e., the shell thickness will be proportional to $r_0$ times some function $g(t/\tau)$, identical for two systems with similar current wave forms. This would also mean that, in two implosions with the same function $f$ and the same $\Pi$, the attainable convergence $C_{\max}$ will be the same.

The velocity of the shell scales as $r_0/\tau$:

$$v \sim r_0/\tau. \tag{9.3}$$

According to Eq. (9.2), this means that the kinetic energy of the shell (per unit length) at the instant of on-axis collapse scales as $I_{\max}^2$:

$$W_{\text{kin}} \propto I_{\max}^2. \tag{9.4}$$

Remarkably, the radius, mass, and implosion time do not enter this relationship. The maximum power $Q$ (per unit length) that can be released in the stagnation is of the order of

$$Q \sim W_{\text{kin}}(v/h) \tag{9.5}$$

where $h$ is a shell thickness at the instant of stagnation. For similar implosions, $h$ scales as $r_0$. Therefore, according to Eq. (9.3),

$$Q \propto I_{\max}^2/\tau. \tag{9.6}$$

The initial radius of the pinch and the mass $\hat{m}$ do not enter this equation (provided the parameter $\Pi$ is kept constant). Equations (9.4) and (9.6) provide a rationale for increasing the current in the generators used to feed the pinch discharge; both the maximum attainable implosion energy and the maximum power scale as $I_{\max}^2$. They also show that the maximum power is inversely proportional to the current pulse width.

Some additional constraints on the parameters of systems with a higher current may stem from the possible breakdown of the applicability conditions of the hydrodynamic description of the system. In particular, at higher currents one may enter the parameter domain in which the relative velocity of electrons and ions considerably exceeds the ion thermal velocity, triggering the onset of anomalous resistivity and increasing Ohmic losses during the implosion phase. The relative velocity $u$ of electrons and ions scales (for the liners made of the same material) as $I_0/\hat{m}$ [see Eq. (7.1)]. The plasma temperature during the implosion of liners of heavy materials is not sensitive to the other parameters of the system and is in the range of 30 to 40 eV (i.e., the ion thermal speed is essentially constant). For a tungsten liner with $T=40$ eV and $Z_{\text{eff}}=6$, one finds that the constraint $u < 4v_{Ti}$ [Eq. (7.5)] can be rewritten as

$$\frac{I_{\max}(\text{MA})}{\hat{m}(\text{mg/cm})} < 10. \tag{9.7}$$

The electron magnetization parameter $\omega_{Ce}\tau_{ei}$ at a constant temperature (characteristic of the run-in phase), and for liners made of the same material, scales as $I_0 r_0/\hat{m}$. In implosions of tungsten wire arrays at the Z facility ($I_{\max}=20$ MA, $\hat{m}=2$ mg/cm, $r_0=2$ cm), the magnetization parameter is $\sim$0.5. Accordingly, the condition that this parameter remains less than 1 can be presented as

$$\frac{I_{\max}(\text{MA})r_0(\text{cm})}{\hat{m}(\text{mg/cm})} < 40. \tag{9.8}$$

It is not obvious that violation of conditions (9.7) and (9.8) will necessarily lead to any catastrophic consequences. Still, to remain in the domain where a relatively simple hydrodynamic description is valid and where successful experiments at the existing devices $Z$ and Saturn have been carried out, it is probably reasonable, in the planning of future experiments, to take into account constraints (9.7) and (9.8). Figure 36 shows the split of the parameter domain by these constraints for $I_{\max}=20$ MA, $\tau=100$ ms [Fig. 36(a)] and $I_{\max}=60$ MA, $\tau=150$ ns [Fig. 36(b)].

At higher currents, constraints on the dimensions of the diode assembly may become important. If the magnitude of the surface current in a magnetically insulated transmission line (MITL) is too high, an explosion of the skin layer in the line may occur within the pulse duration, resulting in greater Joule heating losses in the line. The surface current in an MITL scales as the current divided by the diode radius. To keep this current below its critical value, one would have to increase the diode radius proportionally to the current. An increase in the radius of the return current conductor should be accompanied by a proportional increase in the initial pinch radius (to maintain the parasitic inductances at a low level). Therefore one concludes that the parameter $I_{\max}/r_0$ should remain below some critical level. Taking this value from the current experiment at the $Z$ facility, we obtain one more constraint on the parameters of an experiment with a higher current:

$$\frac{I_{\max}(\text{MA})}{r_0(\text{cm})} < 15. \tag{9.9}$$

An inspection of Fig. 36(b) reveals that there is a broad area in the parameter space in which a $Z$ pinch with a current several times higher than the currently attained level of 20 MA can operate with the high efficiency characteristic of the existing experiments. Taking as an example an operational point $\hat{m}=10$ mg/cm in Fig. 36(b), one finds that the optimum radius is approximately 4 cm. With the assumed pulse width of 150 ns, this would give an implosion velocity only 30% higher than in the current experiments. This is beneficial in the sense that collisional relaxation times will remain short and no further deviations from local thermodynamic equilibrium than in current experiments will occur. At
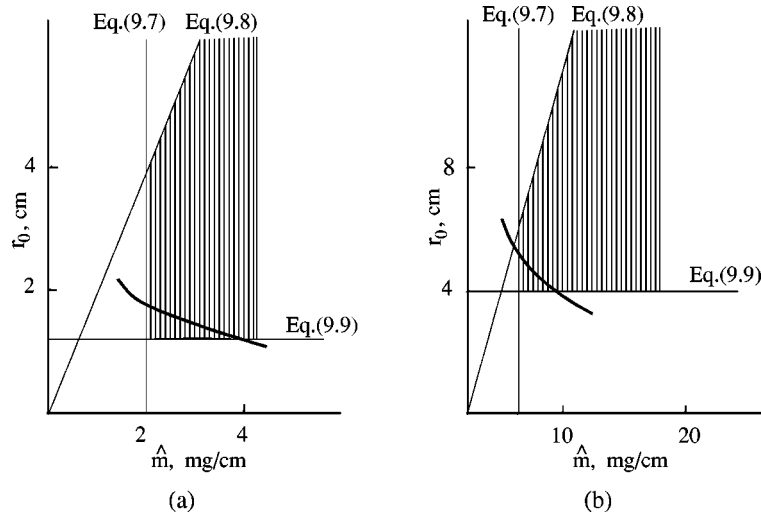
FIG. 36. Parameter space for fast *Z* pinches: (a) $I_{max}=20$ MA, $\tau=100$ ns; (b) $I_{max}=60$ MA, $\tau=150$ ns. Shaded area represents the domain where conditions (9.7)–(9.9) are satisfied. The bold line corresponds to Eq. (9.2) with $[I_{max}(\mathrm{MA})]^2[\tau(\mathrm{ns})]^2/\hat{m}(\mathrm{mg/cm})[r_0(\mathrm{cm})]^2=5\times10^5$ (a typical value for the current experiments).

the same time, the total liner energy will increase by a factor of 9, and the power will increase by a factor of 6.

Reaching a higher current may be interesting not only as a means for generating higher radiation power or a higher temperature in a dynamic hohlraum but also for a range of problems of more general interest. In particular, it is worth noting that the currently achieved current is only several times less than the so-called proton Alfvén current,

$$I_{pA} \equiv \frac{2\pi m_p c}{e\mu} = 30 \ \ \mathrm{MA}. \tag{9.10}$$

At currents exceeding $I_{pA}$, the gyroradius of a subrelativistic proton becomes smaller than the radius of the current channel. The attainment of this current may bring about some interesting new phenomena in the generation of high-energy ion beams at the stagnation phase (Sec. VII.B). This may be of great value for better understanding the mechanism of the generation of cosmic rays.

In summary, during the past decade, the physics of fast *Z* pinches has made significant progress, both in terms of pinch parameters attained in experiments at large facilities and in the identification of key physics issues governing pinch phenomena. In the coming years, one can expect further progress related to (1) development of diagnostic instrumentation; (2) dedicated experiments at smaller, university-scale facilities; (3) advances in computer simulations; and (4) development of schemes for mitigation of the most dangerous instabilities. Fast *Z* pinches will continue to play an important role as the sources of kilo-electron-volt radiation, as drivers for fusion-related experiments, and as sources of information on material properties at extreme conditions. With the development of better means of control of the neck formation at the point of a maximum compression, new possibilities can open for generating high-

current beams of heavy ions. Fast *Z* pinches may also provide important insights into the mechanisms of astrophysical phenomena.

## REFERENCES

Afonin, V. I., 1995, Plasma Phys. Rep. **21**, 250.
Afonin, V. I., 1999, Plasma Phys. Rep. **25**, 620.
Afonin, V. I., D. N. Litvin, V. A. Podgornov, and A. V. Senik, 1999, Plasma Phys. Rep. **25**, 728.
Afonin, V. I., and V. M. Murugov, 1998, Plasma Phys. Rep. **24**, 332.
Aivazov, I. K., V. D. Vikharev, G. S. Volkov, L. B. Nikandrov, V. P. Smirnov, and V. Ya. Tsarfin, 1988, Sov. J. Plasma Phys. **14**, 110.
Al'bikov, V. A., *et al.*, 1990, Sov. At. Energy **68**, #1, 34.
Aliaga-Rossel, R., *et al.*, 1998, IEEE Trans. Plasma Sci. **26**, 1101.

Alikhanov, S. G., V. P. Bakhtin, V. I. Vasil'ev, I. S. Glushkov, A. D. Muzychenko, V. P. Novikov, A. G. Olejnik, and Da. Toporkov, 1981, *Plasma Physics and Controlled Nuclear Fusion Research* (Proceedings of the 8th International Conference, Vienna, International Atomic Energy Agency), Vol. 2, p. 699.

Alikhanov, S. G., V. G. Belan, G. I. Budker, A. I. Ivanchenko, and G. N. Kichigin, 1967, Sov. At. Energy **22**, 1307.

Alikhanov, S. G., *et al.*, 1977, *Plasma Physics and Controlled Nuclear Fusion Research* (Proceedigs of the 6th International Conference, Vienna, International Atomic Energy Agency), Vol. 3, pp. 517.

Alikhanov, S. G., V. I. Vasil'ev, E. Ya. Kononov, K. N. Koshelev, Yu. Y. Sidel'nikov, and D. A. Toporkov, 1984, Sov. J. Plasma Phys. **10**, 605.

Antolak, A. J., *et al.*, 1997, Rev. Sci. Instrum. **68**, 848.

Apruzese, J. P., *et al.*, 1998, Phys. Plasmas **5**, 4476.

Aranchuk, L. E., S. L. Bogolyubski, and O. V. Tel'kovskaya, 1985, Sov. Phys. Tech. Phys. **30**, 1312.

Aranchuk, L. E., *et al.*, 1986, Sov. J. Plasma Phys. **12**, 765.

Aranchuk, L. E., S. A. Dan'ko, A. V. Kopchikov, V. D. Korolev, A. S. Chuvatin, and V. V. Yan'kov, 1997, Plasma Phys. Rep. **23**, 194.

Aranson, I., B. Meerson, and P. Sasorov, 1993, Phys. Rev. E **47**, 4337.

Arber, T. D., P. G. F. Russel, M. Coppins, and J. Scheffel, 1995, Phys. Rev. Lett. **74**, 2698.

Atchinson, W. L., R. J. Fael, V. Morgan, and R. E. Reynovsky, 1997, "Examination of Instability Growth in Solid Liner Surfaces Using Comparison of Two Dimensional MHD and Measured Data," Paper C204 presented at Conference on High-Density *Z* Pinches, Vancouver, Canada (unpublished).

Averkiev, V. V., A. N. Dolgov, V. K. Lyapidevskii, A. S. Savelov, and G. Kh. Shalakhutdinov, 1992, Sov. J. Plasma Phys. **18**, 374.

Azizov, E. A., *et al.*, 1998, Paper CN-69/IF/2 presented at the 17th IAEA Fusion Energy Conference, Yokohama, Japan.

Bailey, J., Y. Ettinger, A. Fisher, and N. Rostoker, 1982, Appl. Phys. Lett. **40**, 460.

Baker, W. L., M. C. Clark, J. H. Degnan, G. F. Kiuttu, C. R. McClenahan, and R. E. Reinovsky, 1978, J. Appl. Phys. **49**, 4694.

Baker, L., and J. R. Freeman, 1981, J. Appl. Phys. **52**, 655.

Baksht, R. B., *et al.*, 1995, Plasma Phys. Rep. **21**, 907.

Baksht, R. B., *et al.*, 1997, Plasma Phys. Rep. **23**, 135.

Baksht, R. B., A. G. Russkikh, and A. A. Chagin, 1997, Plasma Phys. Rep. **23**, 175.

Baksht, R. B., A. G. Russkikh, and A. V. Fedyunin, 1995, Tech. Phys. **40**, 1224.

Baksht, R. B., A. Z. Velikovich, B. A. Kablambaev, M. A. Liberman, A. V. Luchinskii, and N. A. Ratakhin, 1987, Sov. Phys. Tech. **32**, 145.

Barak, G., and N. Rostoker, 1982, Appl. Phys. Lett. **41**, 918.

Barcilon, A., D. L. Book, and A. L. Cooper, 1974, Phys. Fluids **17**, 1707.

Barnier, J-N., J-M. Chevalier, B. D. Dubroca, and J. Rouch, 1998, IEEE Trans. Plasma Sci. **26**, 1094.

Bartnik, A., G. V. Ivanenkov, L. Karpinski, A. R. Mingaleev, S. A. Pikus, V. M. Romanova, W. Stepniewski, T. A. Shelkovenko, and K. Jach, 1994, Quantum Electron. **24**, 169.

Bartnik, A., G. V. Ivanenkov, L. Karpinski, S. A. Pikuz, and T. A. Shelkovenko, 1990, Sov. J. Plasma Phys. **16**, 857.

Bashilov, Yu. A., and S. V. Pokrovskii, 1976, JETP Lett. **23**, 421.

Basko, M. M., 1994, Phys. Plasmas **1**, 1270.

Bateman, G., 1980, *MHD Instabilities* (MIT, Cambridge, MA).

Bauer, B., *et al.*, 1997, in *Dense Z-pinches*, AIP Conf. Proc. No. 409, edited by N. R. Pereira, J. Davis, and P. E. Pulsiter (AIP, Woodbury, NY), p. 153.

Beg, F. N., A. E. Dangor, P. Lee, M. Tatarakis, S. L. Nittikeer, and M. G. Haines, 1997, Plasma Phys. Controlled Fusion **39**, 1.

Benattar, R., S. V. Zakharov, A. F. Nikiforov, V. G. Novikov, V. P. Gasilov, A. Yu. Krukovskii, and V. S. Zakharov, 1999, Phys. Plasmas **6**, 175.

Benford, G., 1978, Appl. Phys. Lett. **33**, 983.

Bennett, W. H., 1934, Phys. Rev. **45**, 890.

Bernstein, I. B., and D. L. Book, 1983, Phys. Fluids **26**, 453.

Bishop, A., 1958, *Project Sherwood (The US Program in Controlled Fusion)* (Addison-Wesley, Reading, MA).

Bobrova, N. A., T. L. Razinkova, and V. P. Sasorov, 1992, Sov. J. Plasma Phys. **18**, 269.

Book, D. L., 1996, Phys. Plasmas **3**, 354.

Book, D. L., E. Ott, and M. Lampe, 1976, Phys. Fluids **19**, 1982.

Book, D. L., and N. K. Winsor, 1974, Phys. Fluids **17**, 662.

Brackbill, J. U., D. W. Forslund, K. B. Quest, and D. Winske, 1984, Phys. Fluids **27**, 2682.

Braginski, S. I., 1958, Sov. Phys. JETP **6**, 494.

Braginski, S. I., 1965, in *Reviews of Plasma Physics*, edited by M. A. Leontovich (Consultants Bureau, New York), Vol. 1, p. 205.

Branitskii, A. V., *et al.*, 1991, Sov. J. Plasma Phys. **17**, 311.

Branitskii, A. V., *et al.*, 1996, Plasma Phys. Rep. **22**, 277.

Branitskii, A. V., *et al.*, 1997, in *Proceedings of the 11th International Conference on High-Power Particle Beams*, Prague, Czech Rep., 1996 (Czech Academy of Science, Prague), v. 1, p. 292.

Branitskii, A. V., V. D. Vikharev, A. G. Kasimov, S. L. Nedoscev, A. A. Rupasov, G. S. Sarkisov, V. P. Smirnov, V. Ya. Tsarfin, and A. S. Shikanov, 1992a, Sov. J. Plasma Phys. **18**, 129.

Branitskii, A. V., V. D. Vikharev, A. G. Kasimov, S. L. Nedoseev, A. A. Rupasov, G. S. Sarkisov, V. P. Smirnov, V. Ya. Tsarfin, and A. S. Shhikanov, 1992b, Sov. J. Plasma Phys. **18**, 588.

Breizman, B. N., and D. D. Ryutov, 1974, Nucl. Fusion **14**, 873.

Brownell, J. H., R. L. Bowers, K. D. McLenithan, and D. L. Peterson, 1998, Phys. Plasmas **5**, 2071.

Budker, G. I., 1973, in *Proceedings of the 6th European Conference on Controlled Fusion and Plasma Physics*, Moscow, USSR, July 30–Aug. 4, 1973 (Joint Institute for Nuclear Research, Dubna, Moscow Region), Vol. 2, p. 136.

Bud'ko, A. B., and M. A. Liberman, 1992, Phys. Fluids B **4**, 3499.

Bud'ko, A. B., M. A. Liberman, and F. F. Kamenets, 1990, Plasma Phys. Controlled Fusion **32**, 309.

Bud'ko, A. B., M. A. Liberman, A. L. Velikovich, and F. S. Felber, 1990, Phys. Fluids B **2**, 1159.

Bud'ko, A. B., A. L. Velikovich, M. A. Liberman, and F. S. Felber, 1989, Sov. Phys. JETP **69**, 76.

Burkhalter, P. G., G. J. Shiloh, A. Fisher, and R. D. Cowan, 1979, J. Appl. Phys. **50**, 4532.

Bychkov, V. V., M. A. Liberman, and A. L. Velikovich, 1990, Phys. Rev. A **42**, 5031.

Camarcat, N., J. Delvaux, B. Etlicher, *et al.*, 1985, Laser Part. Beams **3**, 415.

Catto, P. J., 1978, Phys. Fluids **21**, 30.

Chandrasekhar, S., 1961, *Hydrodynamic and Hydromagnetic Stability* (Clarendon, Oxford).

Chen, C. J., and P. S. Lykoudis, 1972, Sol. Phys. **25**, 380.

Chittenden, J. P., 1995, Phys. Plasmas **2**, 1242.

Chittenden, J. P., and M. G. Haines, 1990, Phys. Fluids B **2**, 1889.

Chittenden, J. P., S. V. Lebedev, A. R. Bell, R. Aliaga-Rossel, S. N. Bland, and M. G. Haines, 1999, Phys. Rev. Lett. **83**, 100.

Chittenden, J. P., R. A. Rossel, S. V. Lebedev, I. H. Mitchell, M. Tatarakis, A. R. Ball, and M. G. Haines, 1997, Phys. Plasmas **4**, 4309.

Choi, P., and C. Dumitrescu-Zoita, 1997, in *Dense Z-pinches*, AIP Conf. Proc. No. 409, edited by N.-R. Pereira, J. Davis, and P. E. Pulsifer (AIP, Woodbury, NY), p. 51.

Chukbar, K. V., 1993a, Plasma Phys. Rep. **19**, 783.

Chukbar, K. V., 1993b, Plasma Phys. Rep. **19**, 785.

Clark, R. W., J. Davis, and F. L. Cochran, 1986, Phys. Fluids **29**, 1971.

Clark, R. W., R. Richardson, J. Brannon, M. Wilkinson, and J. Katzenstein, 1982, J. Appl. Phys. **53**, 5552.

Cochran, F. L., J. Davis, and A. L. Velikovich, 1995, Phys. Plasmas **2**, 1.

Coppins, M., I. D. Culverwell, and M. G. Haines, 1988, Phys. Fluids **31**, 2688.

Dangor, A. E., 1986, Plasma Phys. Controlled Fusion **28**, 1931.

Davidson, R. C., and N. T. Gladd, 1975, Phys. Fluids **18**, 1327.

Davidson, R. C., and N. A. Krall, 1977, Nucl. Fusion **17**, 1313.

Davis, J., N. A. Gondarenko, and A. L. Velikovich, 1997, Appl. Phys. Lett. **70**, 170.

Dawson, J. M., 1993, in *Proceedings of the 2nd Wisconsin Symposium on ³He and Fusion Power* (University of Wisconsin, WSCAR-TR-AR3-9307-3, J. Santarius, compiler), p. 127.

Deeney, C., C. A. Coverdale, *et al.*, 1999a, Phys. Plasmas **6**, 2081.

Deeney, C., C. A. Coverdale, *et al.*, 1999b, Phys. Plasmas **6**, 3576.

Deeney, C., M. R. Douglas, R. B. Spielman, T. J. Nash, D. L. Peterson, P. L'Eplattenier, G. A. Chandler, J. F. Seamen, and K. W. Struve, 1998, Phys. Rev. Lett. **81**, 4883.

Deeney, C., P. D. LePell, F. L. Cochran, M. C. Coulter, K. G. Whitney, and J. Davis, 1993, Phys. Fluids B **5**, 992.

Deeney, C., P. D. LePell, B. H. Failor, J. S. Meachum, S. Wong, J. W. Thornhill, K. G. Whitney, and M. C. Coulter, 1994, J. Appl. Phys. **75**, 2781.

Deeney, C., J. McGurn, *et al.*, 1997, Rev. Sci. Instrum. **68**, 653.

Deeney, C., T. J. Nash, *et al.*, 1997, Phys. Rev. E **56**, 5945.

Deeney, C., T. J. Nash, *et al.*, 1998, Phys. Plasmas **5**, 2431.

Deeney, C., D. L. Peterson, R. B. Spielman, K. W. Struve, and G. A. Chandler, 1998, Phys. Plasmas **5**, 2605.

Degnan, J. H., *et al.*, 1995, Phys. Rev. Lett. **74**, 98.

DeGroot, J. S., *et al.*, 1997a, in *Dense Z-Pinches*, AIP Conf. Proc. No. 409, edited by N.-R. Pereira, J. Davis, and P. E. Pulsifer (AIP, Woodbury, NY), p. 157.

DeGroot, J. S., A. Toor, S. M. Golberg, and M. A. Liberman, 1997b, Phys. Plasmas **4**, 737.

Derzon, M. S., *et al.*, 1996, Phys. Rev. Lett. **76**, 435.

Derzon, M. S., *et al.*, 1997a, Rev. Sci. Instrum. **68**, 848.

Derzon, M. S., *et al.*, 1997b, Bull. Am. Phys. Soc. **42**, 1994.

Derzon, M. S., T. J. Nash, and D. D. Ryutov, 1997, Bull. Am. Phys. Soc. **42**, 2069.

Desjarlais, M., and B. Marder, 1999, Phys. Plasmas **6**, 2057.

Deutsch, R., and W. Kies, 1988, Plasma Phys. Controlled Fusion **30**, 921.

Douglas, M. R., C. Deeney, and N. F. Roderick, 1997, Phys. Rev. Lett. **78**, 4577.

Douglas, M. R., C. Deeney, and N. Roderick, 1998, Phys. Plasmas **5**, 4183.

Drake, J. F., P. N. Guzdar, A. B. Hassam, and J. D. Huba, 1984, Phys. Fluids **27**, 1148.

Drake, J. F., P. N. Guzdar, and J. D. Huba, 1983, Phys. Fluids **26**, 601.

Drake, J. F., J. D. Huba, and N. T. Gladd, 1983, Phys. Fluids **26**, 2247.

Drake, R. P., J. H. Hammer, C. W. Hartman, L. J. Perkins, and D. D. Ryutov, 1996, Fusion Technol. **30**, 310.

Esaulov, A. A., and P. V. Sasorov, 1997, Plasma Phys. Rep. **23**, 1997.

Felber, F. S., 1982, Phys. Fluids **25**, 643.

Felber, F. S., M. A. Liberman, and A. L. Velikovich, 1985, Appl. Phys. Lett. **46**, 1042.

Felber, F. S., M. M. Malley, F. J. Wessel, M. K. Matzen, M. A. Palmer, R. B. Spielman, M. A. Liberman, and A. L. Velikovich, 1988, Phys. Fluids **31**, 2053.

Felber, F. S., and N. Rostoker, 1981, Phys. Fluids **24**, 1049.

Felber, F. S., F. J. Wessel, N. C. Wild, H. D. Rahman, A. Fisher, M. A. Liberman, and A. L. Velikovich, 1988, J. Appl. Phys. **64**, 3831.

Fishman, G. J., *et al.*, 1984, Science **264**, 1313.

Fowler, C. M., W. B. Garn, and R. S. Caird, 1960, J. Appl. Phys. **31**, 588.

Freidberg, J. P., 1982, Rev. Mod. Phys. **54**, 801.

Galeev, A. A., and R. Z. Sagdeev, 1979, in *Reviews of Plasma Physics*, edited by M. A. Leontovich (Consultants Bureau, New York), Vol. 7, p. 1

Gasilov, V. A., S. V. Zakharov, A. Yu. Krukowskii, and K. V. Skorovarov, 1995, Plasma Phys. Rep. **21**, 399.

Gasque, A. M., *et al.*, 1996, in *Proceedings of the 11th International Conference on High-Power Particle Beams*, Prague, Czech Rep., June 1996 (Czech Academy of Sciences, Prague), Vol. 1, p. 550.

Giuliani, Jr., J. L., *et al.*, 1990, J. Quant. Spectrosc. Radiat. Transf. **44**, 471.

Golberg, S. M., M. A. Liberman, and A. L. Velikovich, 1990, Plasma Phys. Controlled Fusion **32**, 319.

Gol'berg, S. M., and A. L. Velikovich, 1993, Phys. Fluids B **5**, 1164.

Gonzalez, A. G., and J. Gratton, 1990, Plasma Phys. Controlled Fusion **32**, 3.

Gordeev, A. V., 1987, Sov. J. Plasma Phys. **13**, 713.

Gordeev, A. V., 1999a, Plasma Phys. Rep. **25**, 70.

Gordeev, A. V., 1999b, Plasma Phys. Rep. **25**, 227.

Gordeev, A. V., A. S. Kingsep, and L. I. Rudakov, 1994, Phys. Rep. **243**, 215.

Gordeev, E. M., *et al.*, 1998, Plasma Phys. Rep. **24**, 916.

Gratton, J., F. T. Gratton, and A. G. Gonzalez, 1988, Plasma Phys. Controlled Fusion **30**, 435.

Grigor'ev, S. F., and S. V. Zakharov, 1987, Sov. Tech. Phys. Lett. **13**, 254.

Guderley, G., 1942, Luftfahrtforschung **19**, 301.

Haines, M. G., 1960, Proc. R. Soc. London, Ser. A **77**, 643.

Haines, M. G., 1974, J. Plasma Phys. **12**, 1.

Haines, M. G., 1982, Phys. Scr. **T2/2**, 380.

Haines, M. G., 1983, Nucl. Instrum. Methods Phys. Res. **207**, 179.

Haines, M. G., 1989, Plasma Phys. Controlled Fusion **31**, 759.

Haines, M. G., 1997, in *Dense Z-Pinches*, AIP Conf. Proc. No. 409, edited by N.-R. Pereira, J. Davis, and P. E. Pulsifer (AIP Woodbury, NY), p. 27.

Haines, M. G., 1998, IEEE Trans. Plasma Sci. **26**, 1275.

Haines, M. G., and M. Coppins, 1991, Phys. Rev. Lett. **66**, 1462.

Haines, M. G., *et al.*, 1996, Laser Part. Beams **14**, 261.

Hammel, B. A., *et al.*, 1994, Phys. Plasmas **1**, 1662.

Hammel, J. E., 1989, in *Dense Z-Pinches*, AIP Conf. Proc. No. 195, edited by N. Pereira, J. Davis, and N. Rostoker (AIP Woodbury, NY), p. 303.

Hammer, J. H., 1995, Bull. Am. Phys. Soc. **40**, 1863.

Hammer, J. H., *et al.*, 1996, Phys. Plasmas **3**, 2063.

Hammer, J. H., and D. D. Ryutov, 1996, in *Proceedings of the 11th International Conference on High-Power Particle Beams*, Prague, Czech Rep., June 1996 (Czech Academy of Sciences, Prague), Vol. 1, p. 178.

Hammer, J. H., and D. D. Ryutov, 1999, Phys. Plasmas **6**, 3302.

Hammer, J. H., M. Tabak, S. C. Wilks, J. D. Lindl, D. S. Bailey, P. W. Rambo, A. Toor, G. B. Zimmerman, and J. L. Porter, Jr., 1999, Phys. Plasmas **6**, 2129.

Harris, E. G., 1962, Phys. Fluids **5**, 1057.

Hawke, R. S., D. E. Duerre, J. G. Huebel, H. Klapper, D. J. Steinberg, and R. N. Keeler, 1972, J. Appl. Phys. **43**, 2734.

Hsing, W. W., C. W. Barnes, J. B. Beck, *et al.*, 1997, Phys. Plasmas **4**, 1832.

Hsing, W. W., and N. M. Hoffman, 1997, Phys. Rev. Lett. **78**, 3876.

Huba, J. D., 1994, NRL Plasma Formulary, NRL/PU/6790-94-265.

Hussey, T. W., M. K. Matzen, and N. F. Roderick, 1986, J. Appl. Phys. **59**, 2677.

Hussey, T. W., and N. F. Roderick, 1981, Phys. Fluids **24**, 1384.

Hussey, T. W., N. F. Roderick, and D. A. Kloc, 1980, J. Appl. Phys. **51**, 1452.

Hussey, T. W., N. F. Roderick, U. Schumlak, R. B. Spielman, and C. Deeney, 1995, Phys. Plasmas **2**, 2055.

Imshennik, V. S., 1992, Sov. J. Plasma Phys. **18**, 349.

Imshennik, V. S., and V. V. Neudachin, 1987, Sov. J. Plasma Phys. **13**, 707.

Imshennik, V. S., and V. V. Neudachin, 1988, Sov. J. Plasma Phys. **14**, 393.

Inogamov, N. A., 1985, J. Appl. Mech. Tech. Phys. **26**, 702.

Isichenko, M. B., K. L. Kulyabin, and V. V. Yan'kov, 1989, Sov. J. Plasma Phys. **15**, 617.

Ivanenkov, G. V., A. R. Mingaleev, S. A. Pikuz, V. M. Romanova, and T. A. Shelkovenko, 1996, Plasma Phys. Rep. **22**, 363.

Kadomtsev, B. B., 1966, in *Reviews of Plasma Physics*, edited by M. A. Leontovich (Consultants Bureau, New York), Vol. 2, p. 153.

Kalantar, D. H., *et al.*, 1999, Rev. Sci. Instrum. **70**, 629.

Kalantar, D., and D. Hammer, 1993, Phys. Rev. Lett. **71**, 3806.

Kalantar, D. H., *et al.*, 1997, Bull. Am. Phys. Soc. **42**, 1953.

Katzenstein, J., 1981, J. Appl. Phys. **52**, 676.

Kilkenny, J. D., S. G. Glendinning, S. W. Haan, B. A. Hammel, J. D. Lindl, D. Munro, B. A. Remington, S. V. Weber, J. P. Knauer, and C. P. Verdon, 1994, Phys. Plasmas **1**, 1379.

Kingsep, A. S., V. I. Kosarev, A. I. Lobanov, and A. A. Sevast'yanov, 1997, Plasma Phys. Rep. **23**, 953.

Kingsep, A. S., and L. I. Rudakov, 1995, Plasma Phys. Rep. **21**, 576.

Kleev, A. I., and A. L. Velikovich, 1990, Plasma Phys. Controlled Fusion **32**, 763.

Kloc, D. N., N. F. Roderick, and T. W. Hussey, 1982, J. Appl. Phys. **53**, 6706.

Kolb, A. S., 1960, Rev. Mod. Phys. **32**, 74.

Krall, N. A., and P. C. Liewer, 1971, Phys. Rev. A **4**, 2094.

Kull, H. J., 1991, Phys. Rep. **206**, 197.

Landau, L. D., and E. M. Lifshitz, 1987, *Fluid Mechanics* (Pergamon, New York).

Lazier, S. E., T. L. Barber, M. S. Derzon, and J. W. Kellogg, 1997, Rev. Sci. Instrum. **68**, 660.

Lebedev, S. V., R. Aliaga-Rossel, J. P. Chittenden, I. H. Mitchell, A. E. Dangor, M. G. Haines, and J. F. Worley, 1998a, Phys. Plasmas **5**, 3366.

Lebedev, S. V., I. H. Mitchell, R. Aliaga-Rossel, S. N. Bland, J. P. Chittenden, A. E. Dangor, and M. G. Haines, 1998b, Phys. Rev. Lett. **81**, 4152.

Lebedev, S. V., R. Aliaga-Rossel, S. N. Bland, J. P. Chittenden, A. E. Dangor, M. G. Haines, and I. H. Mitchell, 1999, Phys. Plasmas **6**, 2016.

Leeper, R. J., *et al.*, 1997, Rev. Sci. Instrum. **68**, 868.

Leeper, R. J., *et al.*, 1998, Paper CN-69/OV3/4 presented at the 17th IAEA Fusion Energy Conference, Yokohama, Japan.

Lezzi, A. M., and A. Prosperetti, 1989, Phys. Fluids A **1**, 1784.

Lindemuth, I. R., 1990, Phys. Rev. Lett. **65**, 179.

Lindemuth, I. R., *et al.*, 1996, *Plasma Physics and Controlled Nuclear Fusion Research* (Proceedings of the 16th International Conference, Vienna, IAEA), Vol. 2, p. 723.

Lindemuth, I. R., and R. C. Kirkpatrick, 1983, Nucl. Fusion **23**, 263.

Lindl, J., 1995, Phys. Plasmas **2**, 3933.

Linhart, J. G., 1994, in *Dense Z-Pinches*, AIP Conf. Proc. No. 299, edited by M. Haines and A. Knight (AIP, Woodbury, NY), p. 664.

Lisitsyn, I. V., S. Katsuki, and H. Akiyama, 1999, Phys. Plasmas **6**, 1389.

MacFarlane, J. J., P. Wang, T. J. Nash, M. S. Derzon, G. A. Allshouse, and C. Deeney, 1997, Rev. Sci. Instrum. **68**, 1069.

Manheimer, W., D. Colombant, and E. Ott, 1984, Phys. Fluids **27**, 2164.

Matuska, W., R. L. Bowers, J. H. Brownell, H. Lee, C. M. Lund, D. L. Peterson, and F. Roderick, 1996, Phys. Plasmas **3**, 1415.

Matzen, M. K., 1997, Phys. Plasmas **4**, 1519.

Matzen, M. K., *et al.*, 1999, Plasma Phys. Controlled Fusion **41**, A175.

Maxon, S., *et al.*, 1996, Phys. Plasmas **3**, 1737.

Meek, J. M., and J. D. Craggs, 1978, *Electric Breakdown of Gases* (Wiley, New York).

Meierovich, B. E., 1986, Sov. Phys. Usp. **29**, 506.

Meierovich, B. E., and S. T. Sukhorukov, 1991, Sov. J. Plasma Phys. **17**, 598.

Mikaelian, K. O., 1996, Phys. Rev. E **54**, 3676.

Mitchell, I. H., R. Aliaga-Rossel, J. P. Chittenden, A. Robledo, H. Schmidt, and M. G. Haines, 1998, IEEE Trans. Plasma Sci. **26**, 1267.

Miyamoto, T., 1984, Nucl. Fusion **24**, 337.

Mokhov, V. N., V. K. Chernyshev, V. B. Yakubov, M. S. Protasov, V. M. Danor, and E. I. Zharinov, 1979, Sov. Phys. Dokl. **24**, 557.

Mosher, D., and D. Colombant, 1992, Phys. Rev. Lett. **68**, 2600.

Mosher, D., *et al.*, 1998, Bull. Am. Phys. Soc. **43**, B1F3.

Munro, D. H., 1988, Phys. Rev. A **38**, 1433.

Muron, D. J., M. J. Hurst, and M. S. Derzon, 1997, Rev. Sci. Instrum. **68**, 656.

Nash, T. J., M. S. Derzon, G. Allshouse, C. Deeney, D. Jobe, J. Seaman, T. Gilliland, J. McGurn, J. J. MacFarlane, and P. Wang, 1997a, Rev. Sci. Instrum. **68**, 1083.

Nash, T. J., *et al.*, 1997b, in *Dense Z-Pinches*, AIP Conf. Proc. No. 409, edited by N.-R. Pereira, J. Davis, and P. E. Pulsifer (AIP, Woodbury, NY), p. 175.

Nash, T. J., *et al.*, 1999, Phys. Plasmas **6**, 2023.

Nedoseev, S. L., 1991, in *Physics of Alternative Magn. Conf. Schemes* (Proceedings of the International School of Plasma Physics ''Piero Caldirola,'' Editrice Compositori, Bologna), p. 575.

Neudatchin, V. V., and P. V. Sasorov, 1991, Nucl. Fusion **31**, 1053.

Olson, R. E., *et al.*, 1997, Phys. Plasmas **4**, 1818.

Olson, R. E., *et al.*, 1999, Fusion Technol. **35**, 260.

Ott, E., 1972, Phys. Rev. Lett. **29**, 1429.

Pashinin, P. P., and A. M. Prokhorov, 1971, Sov. Phys. JETP **60**, 1630.

Parks, D. E., 1983, Phys. Fluids **26**, 448.

Pease, R. S., 1956, Proc. R. Soc. London, Ser. A **70**, 11.

Peratt, A. L., 1986, IEEE Trans. Plasma Sci. **PS-14**, 639.

Peratt, A. L., 1990, IEEE Trans. Plasma Sci. **PS-18**, 26.

Pereira, N. R., 1990, Phys. Fluids B **2**, 677.

Pereira, N. R., and J. Davis, 1988, J. Appl. Phys. **64**, R1.

Pereira, N.-R, J. Davis, and P. E. Pulsifer, 1997, Eds., *Dense Z-Pinches*, AIP Conference Series No. 409 (AIP, Woodbury, NY).

Pereira, N. R., N. Rostoker, and J. S. Pearlman, 1984, J. Appl. Phys. **55**, 704.

Peterson, D. L., R. L. Bowers, J. H. Brownell, A. E. Greene, K. D. McLenithan, T. A. Oliphant, N. F. Roderigue, and A. J. Scannapieco, 1996, Phys. Plasmas **3**, 368.

Peterson, D. L., *et al.*, 1997, in *Dense Z-Pinches*, AIP Conf. Proc. No. 409, edited by N.-R. Pereira, J. Davis, and P. E. Pulsifer (AIP, Woodbury, NY), p. 201.

Peterson, D. L., *et al.*, 1998, Phys. Plasmas **5**, 3302.

Peterson, D. L., *et al.*, 1999, Phys. Plasmas **6**, 2178.

Phillips, J. A., 1987, in *McGraw-Hill Encyclopedia of Science and Technology* (McGraw-Hill, New York), Vol. 13, p. 521.

Pikuz, S. A., *et al.*, 1997, in *Dense Z-Pinches*, AIP Conf. Proc. No. 409, edited by N.-R. Pereira, J. Davis, and P. E. Pulsifer (AIP, Woodbury, NY), p. 429.

Porter, J. L., 1997, Bull. Am. Phys. Soc. **42**, 1948.

Porter, J. L., R. B. Spielman, M. K. Matzen, E. J. McGuire, L. E. Ruggles, M. F. Vargos, J. P. Appruzese, R. W. Clark, and J. Davis, 1992a, Phys. Rev. Lett. **68**, 796.

Porter, J. L., R. B. Spielman, M. F. Vargas, and M. K. Matzen, 1992, Rev. Sci. Instrum. **63**, 5703.

Potter, D., 1978, Nucl. Fusion **18**, 813.

Rahman, H. U., P. Amendt, and N. Rostoker, 1985, Phys. Fluids **28**, 1528.

Rahman, H. U., F. J. Wessel, and N. Rostoker, 1995, Phys. Rev. Lett. **74**, 714.

Raizer, Yu. P., 1991, *Gas Discharge Physics* (Springer, Berlin/ Heidelberg).

Remington, B. A., *et al.*, 1997a, Bull. Am. Phys. Soc. **42**, 1840.

Remington, B. A., *et al.*, 1997b, Phys. Plasmas **4**, 1994.

Robson, A. E., 1989, in *Dense Z-Pinches*, AIP Conf. Proc. No. 195, edited by N. R. Pereira, J. Davis, and N. Rostoker (AIP, Woodbury, NY), p. 362.

Robson, A. E., 1991, Phys. Fluids B **3**, 1461.

Robson, A. E., 1994, in *Dense Z-Pinches*, AIP Conf. Proc. No. 299, edited by M. Haines and A. Knight (AIP, Woodbury, NY), p. 707.

Roderick, N. F., 1986, J. Appl. Phys. **60**, 1269.

Roderick, N. F., R. E. Peterkin, Jr., T. W. Hussey, R. B. Spielman, M. R. Douglas, and C. Deeney, 1998, Phys. Plasmas **5**, 1477.

Roderick, N. F., and T. W. Hussey, 1984, J. Appl. Phys. **56**, 1387.

Roderick, N. F., and T. W. Hussey, 1986, J. Appl. Phys. **59**, 662.

Rosen, M. D., 1996, Phys. Plasmas **3**, 1803.

Rosenau, P., R. A. Nebel, and H. R. Lewis, 1988, Phys. Fluids B **1**, 1233.

Rostoker, N., G. G. Peterson, and H. Tahsiri, 1995, Comments Plasma Phys. Control. Fusion **16**, 129.

Rousskikh, A. G., R. B. Baksht, A. Yu. Labetsky, A. V. Shishlov, and A. V. Fedyunin, 1999, Plasma Phys. Rep. **25**, 527.

Rudakov, L. I., K. A. Baigarin, Y. G. Kalinin, V. D. Korolev, and M. A. Kumachov, 1991, Phys. Fluids B **3**, 2414.

Rudakov, L. I., and A. A. Sevastyanov, 1996, Plasma Phys. Rep. **22**, 1095.

Ruden, E. L., and D. E. Bell, 1997, J. Appl. Phys. **82**, 163.

Ruden, E., H. U. Rahman, A. Fisher, and N. Rostoker, 1987, J. Appl. Phys. **61**, 1311.

Ryutov, D. D., 1996, Phys. Plasmas **4**, 4376.

Ryutov, D. D., 1997, *2nd Symposium on Current Trends in International Fusion Research*, Washington, DC, March 1997 (NRC Research, Ottawa), p. 44.

Ryutov, D. D., and A. Toor, 1998, Phys. Plasmas **5**, 22.

Sakharov, A. D., *et al.*, 1965, Sov. Phys. Dokl. **10**, 1045.

Samokhin, A. A., 1988, J. Appl. Mech. Tech. Phys. **29**, 243.

Sanford, T. W. L., *et al.*, 1996, Phys. Rev. Lett. **77**, 5063.

Sanford, T. W. L., T. J. Nash, R. C. Mock, R. B. Spielman, K. W. Struve, J. H. Hammer, J. S. De-Groot, K. G. Whitney, and J. P. Apruzese, 1997a, Phys. Plasmas **4**, 2188.

Sanford, T. W. L., T. J. Nash, *et al.*, 1997b, Rev. Sci. Instrum. **68**, 852.

Sanford, T. W. L., R. C. Mock, R. B. Spielman, D. L. Peterson, D. Mosher, and N. F. Roderick, 1998a, Phys. Plasmas **5**, 3737.

Sanford, T. W. L., R. L. Mock, R. B. Spielman, D. L. Peterson, D. Mosher, and N. F. Roderick, 1998b, Phys. Plasmas **5**, 3755.

Sanford, T. W. L., R. C. Mock, T. J. Nash, K. G. Whitney, P. E. Pulsifer, J. P. Apruzese, D. Mosher, D. L. Peterson, and M. G. Haines, 1999a, Phys. Plasmas **6**, 1270.

Sanford, T. W. L., and R. C. Mock, *et al.*, 1999b, Phys. Plasmas **6**, 2030.

Sarkisov, G. S., A. S. Shikanov, B. Etlicher, S. Attelan, and C. Rouille, 1995a, JETP Lett. **61**, 485.

Sarkisov, G. S., A. S. Shikanov, B. Etlicher, S. Attelan, C. Rouille, and V. V. Yan'kov, 1995b, JETP **81**, 743.

Sarkisov, G. S., and B. Etlicher, 1995, JETP Lett. **61**, 797.

Sarkisov, G. S., B. Etlicher, S. Attelan, and C. Rouille, 1995, JETP Lett. **61**, 555.

Sasorov, P. V., 1991, Sov. J. Plasma Phys. **17**, 874.

Sasorov, P. V., 1992, Sov. J. Plasma Phys. **18**, 143.

Scheffel, J., T. D. Arber, M. Coppins, and P. G. F. Russel, 1997, Plasma Phys. Controlled Fusion **39**, 559.

Sethian, J. D., A. E. Robson, K. A. Gerber, and A. W. DeSilva, 1987, Phys. Rev. Lett. **59**, 892.

Sevast'yanov, A. A., 1993, Plasma Phys. Rep. **19**, 227.

Sharp, D. H., 1984, Physica D **12**, 3.

Shiloh, J., A. Fisher, and N. Rostoker, 1978, Phys. Rev. Lett. **40**, 515.

Shiloh, J., A. Fisher, and E. Bar-Avraham, 1979, Appl. Phys. Lett. **35**, 390.

Shumlak, U., and C. Hartman, 1995, Phys. Rev. Lett. **75**, 3285.

Shumlak, U., and N. R. Roderick, 1998, Phys. Plasmas **5**, 2384.

Skowronek, M., and P. Romeas, 1985, J. Appl. Phys. **57**, 2519.

Smirnov, V. P., 1991, Plasma Phys. Controlled Fusion **33**, 1697.

Smith, R. S., and W. O. Doggett, 1985, Appl. Phys. Lett. **46**, 1128.

Spielman, R. B., D. L. Hanson, M. A. Palmer, M. K. Matzen, T. W. Hussey, and J. M. Peek, 1985, J. Appl. Phys. **57**, 830.

Spielman, R. B., M. K. Matzen, M. A. Palmer, P. B. Rand, T. W. Hussey, and D. H. McDaniel, 1985, Appl. Phys. Lett. **47**, 229.

Spielman, R. B., *et al.*, 1989, in *Proceedings of the 7th IEEE Pulsed Power Conference*, Monterey, CA (Institute of Electrical and Electronic Engineers, New York), p. 445.

Spielman, R. B., *et al.*, 1996, in *Proceedings of the 11th International Conference on High-Power Particle Beams*, Prague, Czech Rep., 1996 (Czech Academy of Sciences, Prague), Vol. 1, p. 150.

Spielman, R. B., C. Deeney, *et al.*, 1997, in *Dense Z-Pinches*, AIP Conf. Proc. No. 409, edited by N.-R. Pereira, J. Davis, and P. E. Pulsifer (AIP, Woodbury, NY), p. 101.

Spielman, R. B., C. Deeney, *et al.*, 1998, Phys. Plasmas **5**, 2105.

Springer, P. T., *et al.*, 1997, J. Quant. Spectrosc. Radiat. Transf. **58**, 927.

Stallings, C., K. Childers, I. Roth, and R. Schneider, 1979, Appl. Phys. Lett. **35**, 524.

Stamper, J. A., K. Papadopoulos, R. N. Sudan, S. O. Dean, and E. A. McLean, 1971, Phys. Rev. Lett. **26**, 1012.

Struve, K. W., *et al.*, 1997, in *Proceedings of the 11th IEEE International Pulsed Power Conference*, Baltimore, MD, June 29–July 2, 1997, edited by G. Cooperstein and I. Vitkovitsy (Institute of Electrical and Electronics Engineers, NY), p. 162.

Stygar, W. A., *et al.*, 1997, in *Proceedings of the 11th IEEE International Pulsed Power Conference*, Baltimore, MD, June 29–July 2, 1997, edited by G. Cooperstein and I. Vitkovitsy (Institute of Electrical and Electronics Engineers, NY), p. 1258.

Suydam, B. R., 1958, *Proceedings of the 2nd International Conference on the Peaceful Uses of Atomic Energy*, Geneva, Switzerland (United Nations, New York), Vol. 31, p. 157.

Thornhill, J. W., J. Davis, J. P. Apruzese, K. G. Whitney, and F. L. Cochran, 1997, in *Dense Z-Pinches*, AIP Conf. Proc. No. 409, edited by N.-R. Pereira, J. Davis, and P. E. Pulsifer (AIP, Woodbury, NY), p. 193.

Thornhill, J. W., K. G. Whitney, and J. Davis, 1990, J. Quant. Spectrosc. Radiat. Transf. **44**, 251.

Tonks, L., 1937, Trans. Electrochem. Soc. **72**, 167.

Tonks, L., 1939, Phys. Rev. **56**, 360.

Toor, A., and D. Ryutov, 1997, Bull. Am. Phys. Soc. **42**, 2053.

Trubnikov, B. A., 1986, Sov. J. Plasma Phys. **12**, 271.

Trubnikov, B. A., 1990, Sov. Phys. Usp. **33**, 1061.

Turchi, P. J., and W. L. Baker, 1973, J. Appl. Phys. **44**, 4936.

Turchi, P. J., A. L. Cooper, R. Ford, and D. J. Jenkins, 1976, Phys. Rev. Lett. **36**, 1546.

Uman, M. A., 1986, *All about Lightning* (Dover, New York).

Vedenov, A. A., and D. D. Ryutov, 1975, in *Reviews of Plasma Physics*, edited by M. A. Leontovich (Consultants Bureau, New York), Vol. 6, p. 1.

Vekshtein, G. E., 1990, in *Reviews of Plasma Physics*, edited by B. B. Kadomtsev (Consultants Bureau, New York), Vol. 15, p. 1.

Velikhov, E. P., I. V. Novobrantsev, V. D. Pis'mennyi, A. T. Rakhimov, and A. N. Starostin, 1972, Sov. Phys. Dokl. **17**, 772.

Velikovich, A. L., 1991, Sov. Phys. Tech. Phys. **36**, 210.

Velikovich, A. L., F. L. Cochran, and J. Davis, 1996, Phys. Rev. Lett. **77**, 853.

Velikovich, A. L., and J. Davis, 1995, Phys. Plasmas **2**, 4513.

Veretennikov, V. A., M. O. Koshevoi, N. V. Panferov, V. V. Pikalov, A. A. Rupasov, O. G. Semenov, and A. S. Shikanov, 1992, Sov. J. Plasma Phys. **18**, 131.

Vikhrev, V. V., 1986, Sov. J. Plasma Phys. **12**, 262.

Vikhrev, V. V., and S. I. Braginski, 1986, in *Reviews of Plasma Physics*, edited by M. A. Leontovich (Consultants Bureau, New York), Vol. 10, p. 425.

Vishniac, E. T., 1983, Astrophys. J. **274**, 152.

Volkov, G. S., S. A. Dan'ko, P. Zehnter, V. I. Zaitsev, V. O. Mishenskii, M. V. Fedulov, A. Chuvatin, and B. Etlicher, 1999, Plasma Phys. Rep. **25**, 34.

Volkov, G. S., E. G. Utyugov, and I. N. Frolov, 1993, Plasma Phys. Rep. **19**, 579.

Wessel, F. J., F. S. Felber, N. C. Wild, H. Yu. Rahman, A. Fisher, and E. Ruden, 1986, Appl. Phys. Lett. **48**, 1119.

Whitham, G. B., 1974, *Linear and Nonlinear Waves* (Wiley, New York).

Whitney, K. G., J. W. Thornhill, *et al.*, 1994, Phys. Rev. E **50**, 2166.

Whitney, K. G., J. W. Thornhill, J. P. Apruzese, and J. Davis, 1990, J. Appl. Phys. **67**, 1725.

Wong, K. L., P. T. Springer, J. H. Hammer, C. A. Iglesias, A. L. Osterheld, M. E. Foord, H. C. Bruns, J. A. Emig, and C. Deeney, 1998, Phys. Rev. Lett. **80**, 2334.

Yan'kov, V. V., 1991, Sov. J. Plasma Phys. **17**, 305.

Yonas, G., 1998, Sci. Am. **279**, 40.

Youngs, D. L., 1991, Phys. Fluids A **3**, 1312.

Yusef-Zadeh, F., M. Morris, and D. Chance, 1984, Nature (London) **310**, 557.

Zel'dovich, Ya. B., and Yu. P. Raizer, 1967, *Physics of Shock Waves and High-Temperature Hydrodynamic Phenomena* (Academic, New York, London).